Nicholas M. Patrikalakis
George A. Kriezis

Three-Dimensional Non-Linear Dynamics of Compliant Risers

MIT Sea Grant
College Program

Massachusetts
Institute of Technology
Cambridge, MA 02139

MITSG 87-11
July 1987

THREE-DIMENSIONAL NON-LINEAR DYNAMICS OF COMPLIANT RISERS

by

Nicholas M. Patrikalakis

George A. Kriezis

MIT Sea Grant
College Program

Massachusetts Institute
of Technology
77 Massachusetts Ave.
Cambridge, MA 02139

MITSG 87-11
July 1987
NA84AA-D-00046
RT 20 $6.00

Table of Contents

List of Figures

List of Tables

ABSTRACT

A mathematical model is presented for the three-dimensional non-linear static and frequency domain dynamic analysis of non-rotationally uniform single leg multitube compliant risers with torsion in the presence of

- unidirectional monochromatic surface gravity waves traveling at an arbitrary angle,
- arbitrary monochromatic motions and rotations of the upper and lower ends, of the same frequency as the waves, and
- arbitrary currents.

The effects of riser-ocean bottom interaction, present in some catenary configurations, and of non-linear hydrodynamic drag are taken into account, using an equivalent harmonic linearization technique. The governing non-linear ordinary differential equations are subsequently solved using an adaptive non-uniform grid finite difference method, an embedding technique and Newton's iteration. Good initial approximations of the solution are also provided allowing fast convergence of the iterative scheme.

The proposed riser analysis methodology is compared with a cable dynamic analysis and two time domain finite element analyses of compliant risers. Three riser configurations are used for these comparisons; a riser configuration idealized as a cable, a catenary riser configuration and a steep wave riser configuration.

Additional numerical examples are also presented to examine the effects of various excitation conditions on the performance of different types of risers. The riser configurations examined, include a shallow water buoyant riser, a shallow water catenary riser under the presence of two-dimensional and three-dimensional excitation and a deep water catenary riser experiencing riser-ocean bottom interaction.

ACKNOWLEDGEMENTS

Funding for this research was obtained from the M.I.T. Sea Grant College Program, the U.S. Minerals Management Service, Chevron, Bridgestone Corporation and Furukawa Electric Co. of Japan. The authors are indebted to Professor M.S. Triantafyllou and to Dr H.Shin for assisting in the comparison of the compliant riser programs with cable idealizations. Dr D.Y.Yoon and Mr. T.Maekawa assisted us in the derivation or verification of many of the new equations needed in this work. P. McSweeney prepared part of the typed manuscript.

RELATED SEA GRANT REPORTS

1. A Mathematical Model for Compliant Risers. By N. M. Patrikalakis and C. Chryssostomidis. Cambridge, Mass.: MIT Sea Grant Report No. 85-17, 1985.
2. Non-Linear Statics of Non-Rotationally Uniform Rods with Torsion. By N. M. Patrikalakis and C. Chryssostomidis. Cambridge, Mass.: MIT Sea Grant Report No. 85-18, 1985.
3. Linear Dynamics of Compliant Risers. By N. M. Patrikalakis and C. Chryssostomidis. Cambridge, Mass.: MIT Sea Grant Report No. 85-19, 1985.

1. INTRODUCTION AND OUTLINE

Compliant risers are assemblages of pipes with very small overall bending rigidity used to convey oil from the ocean floor or a subsurface buoy to a surface platform. A compliant riser is permitted to acquire large static deformations because of its small bending rigidity and readjusts its configuration in response to large slow motions of the supporting platforms, to which it is rigidly connected, without excessive stressing. Compliant risers have been used successfully in protected waters in buoy loading stations for tankers. Extensions of shallow water concepts have been recently proposed as alternatives to conventional production risers, because they simplify the overall production system.

The purpose of this work is to:

- Present a mathematical model for the three-dimensional non-linear static and frequency domain dynamic analysis of non-rotationally uniform compliant risers with torsion in the presence of unidirectional monochromatic waves travelling at an arbitrary angle, arbitrary monochromatic motions and rotations of the upper and lower ends of the riser, of the same frequency as the waves, and arbitrary currents.
- Study the effects of riser-ocean bottom interaction, present in some catenary configurations, and the effects of non-linear drag due to separation and wake formation, using a harmonic equivalent linearization technique
- Present a solution technique to solve the general three-dimensional non-linear static and dynamic compliant riser problem in the presence of the above mentioned excitations.
- Provide comparisons of the proposed methodology, with other related cable or riser dynamic analyses
- Present some examples from the static and dynamic analysis of buoyant and catenary risers in a two-dimensional or three-dimensional configuration possibly under the presence of riser-ocean bottom interaction.

This work is organized as follows:

- Chapter 2 provides a complete formulation of the three-dimensional static and dynamic riser problem. This Chapter provides the governing equations and boundary conditions for the problem. In addition it presents in detail the equivalent linearization techniques employed to approximate the non-linear drag forces due to separation and wake formation and the forces due to riser-ocean bottom interaction.
- Chapter 3 provides the numerical solution algorithm for the solution of the static and dynamic riser problem using an embedding technique.
- Chapter 4 provides comparisons of the proposed methodology with a cable dynamic analysis methodology and two finite element methodologies for the analysis of compliant risers, using a riser configuration idealized as a cable, a catenary riser and a steep wave riser configuration.
- Chapter 5 provides some additional numerical results for a shallow water buoyant riser, a shallow water catenary riser and a deep water catenary riser experiencing riser-ocean bottom interaction.
- Chapter 6 presents brief conclusions from the present work and recommendations for additional research in this area.

2. PROBLEM FORMULATION

2.1 INTRODUCTION

A mathematical model for the non-linear global static and dynamic behavior of an assemblage of tubes modelled as a non-rotationally uniform slender elastic rod with space varying torque can be found in [1] and [2]. Efficient numerical solutions of the non-linear three-dimensional static problem of a compliant riser in the presence of a steady current can be found in [2] and [3]. The numerical solution scheme employs a novel embedding technique which starts by using two-dimensional solutions as initial approximations. Numerical techniques to determine the two-dimensional solutions using embedding can be found in [3] to [5]. References [3] and [4] provide such techniques for buoyant risers in a current while reference [5] provides a technique for catenary risers without ocean bottom interaction. The initial approximations of the solution of the corresponding two-dimensional static problems are analytical and are derived using asymptotic techniques. These analytical solutions correctly account for all major external and restoring forces for each case and, therefore, provide excellent initial approximations of the solution of the non-linear static problem. For this reason, fast convergence of the embedding sequence and the associated Newton-Raphson iterations employed in the numerical solution of the non-linear problem is observed in [2] to [5] as opposed to the more usual incremental loading method.

Efficient solutions of the linear unforced and undamped dynamic problem of a compliant riser around a non-linear static configuration to determine natural modes and frequencies using a combination of embedding and asymptotic techniques can be found in [6] and [7]. The asymptotic solutions of the linear eigenproblem for compliant risers are based on [8].

In this work we extend the theory developed in [1] to [7] to allow three-dimensional non-linear static and dynamic analysis of non-rotationally uniform compliant risers with torsion in the presence of

- unidirectional monochromatic surface gravity waves traveling at an arbitrary angle,
- arbitrary monochromatic motions and rotations of the upper and lower ends, of the same frequency as the waves, and
- arbitrary currents.

In this work, the effects of riser-ocean bottom interaction, present in some catenary configurations, and of non-linear drag primarily due to separation and wake formation are taken into account.

Our solution approach is iterative and involves the following steps:

1. Solution of the non-linear static problem in the presence of mean forces and moments due to the currents and waves (possibly involving static riser-ocean bottom interaction).
2. Linearization of the structural part of the non-linear dynamic equations around the static configuration for small dynamic motions and angles.

3. Equivalent linearization of the non-linear riser-ocean bottom interaction forces.
4. Equivalent linearization of the non-linear drag force and moment assuming monochromatic three-dimensional excitation and response.
5. Solution of the resulting non-linear boundary value problem modeling compliant riser dynamics, possibly involving riser-ocean bottom interaction, in the frequency domain.
6. Determination of mean forces and moments due to currents, waves and riser motion.

Once these mean forces and moments are obtained, we iterate starting from step 1 until we reach a convergent solution.

This process provides

- The static configuration and the associated static tension and bending moments.
- The dynamic motion amplitude and phase and the associated dynamic tension and bending moments for a general three-dimensional monochromatic excitation and response.
- The total static and dynamic tension and bending moments.

2.2 RISER-OCEAN BOTTOM INTERACTION

2.2.1 STATIC RISER-OCEAN BOTTOM INTERACTION

The mathematical model developed in [1] is modified below to account for the non-linear riser-ocean bottom interaction. In this analysis we neglect the lateral dimensions of the riser tubes and we assume that the ocean bottom can be adequately represented by the planar surface y=0. Figure 2-1 illustrates a riser cross-section interacting with the ocean bottom. The system $U_o'' = [\vec{\zeta}_o, \vec{\xi}_o, \vec{\eta}_o]^T$ is the body fixed system used in [1] to [5] for static analysis.

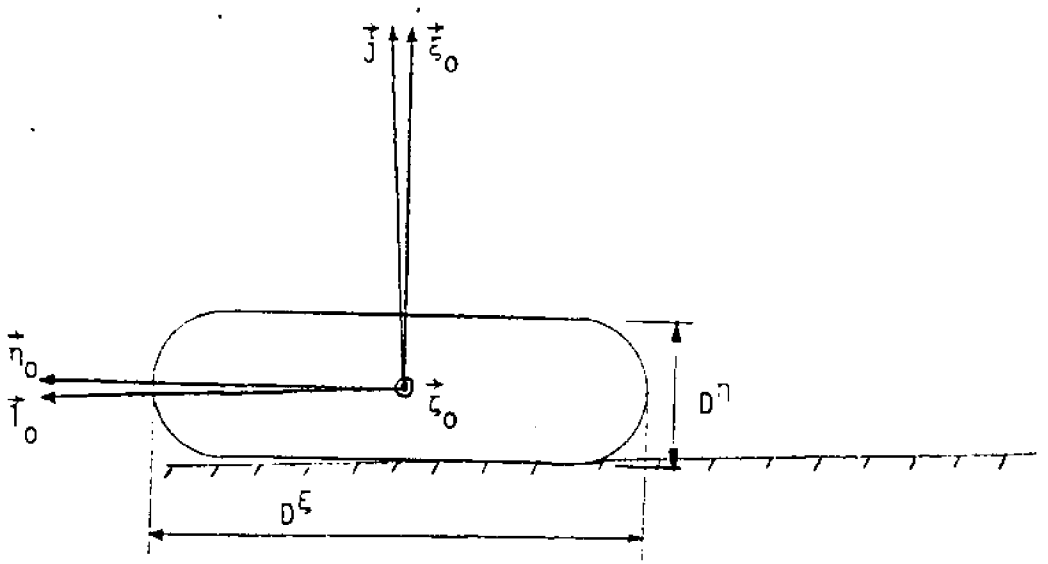

Figure 2-1: Riser-Ocean Bottom Interaction

U_o'' is related to $U = [\vec{i}, \vec{j}, \vec{k}]^T$ by

$$U_o'' = C_o \cdot U \qquad (2.1)$$

where $C_o = [c_{ij}^o]$ is a 3x3 rotation matrix derived in [3] in terms of the Euler angles ϕ_o, θ_o and ψ_o. In analyzing the interaction forces and moments, we assume that $\vec{\zeta}_o$ is roughly horizontal, which is a good approximation because, as we will see, the ocean bottom is very stiff. Therefore, $\vec{\zeta}_o \cdot \vec{j} = c_{12}^o = 0$ and from [3] we obtain $\phi_o \approx 0$. In Figure 2-1, define $\vec{\tau}_o = \vec{\zeta}_o \times \vec{j}$, which can be expressed as

$$\vec{\tau}_o = [-c_{13}^o, 0, c_{11}^o] \cdot U \qquad (2.2)$$

or using (2.1) and the property $C_o^{-1} = C_o^T$, see [9], as

$$\vec{l}_o = [0, c^o_{11}c^o_{23} - c^o_{13}c^o_{21}, c^o_{11}c^o_{33} - c^o_{13}c^o_{31}] \cdot U''_o \qquad (2.3)$$

Using $\phi_o = 0$ and [3], we also have

$$\vec{l}_o = [\sin\theta_o, 0, \cos\theta_o] \cdot U = [0, \sin\psi_o, \cos\psi_o] \cdot U''_o \qquad (2.4)$$

as can be also seen in Figure 2-2, where the assumption $\phi_o = 0$ is made.

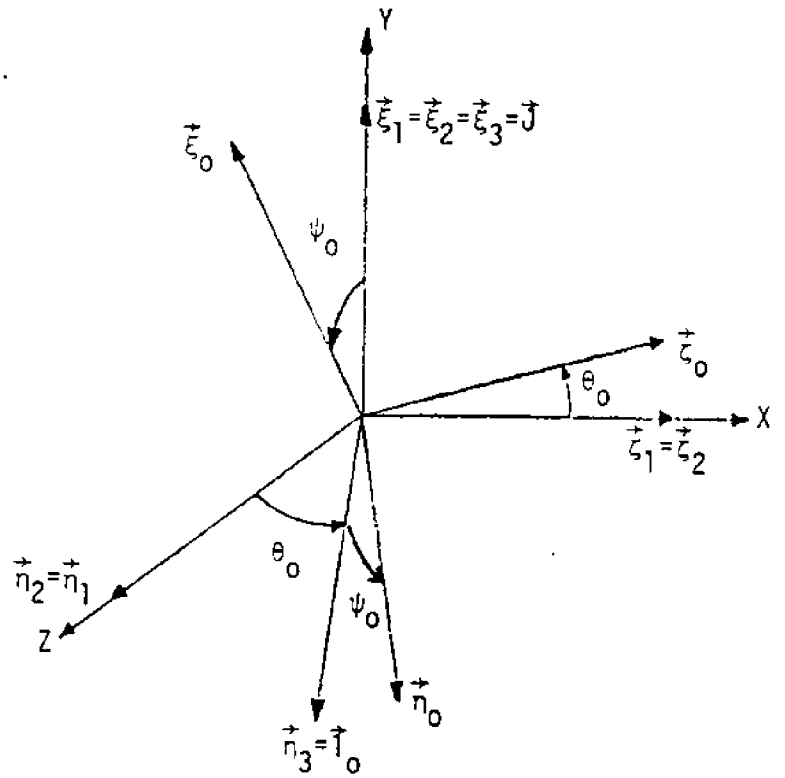

Figure 2-2: Euler Angles at the Riser-Ocean Bottom Interface

Following [10], the following assumptions for the static interaction force $\vec{F}_{Bo}$ and moment $\vec{M}_{Bo}$ per unit length are made, valid for $y_o < 0$, i.e. when the riser penetrates the soil

$$\vec{F}_{Bo} = -k^y \, y_o \, \vec{j} \qquad (2.5)$$

$$\vec{M}_{Bo} = -k^\psi \, \psi_o \, \vec{\zeta}_o \qquad (2.6)$$

where k^y and k^ψ are the vertical and rocking spring constants per unit length of the soil. If $y_o > 0$, we have $\vec{F}_{Bo} = \vec{M}_{Bo} = 0$. In our static analysis, we neglect interaction force per unit length components along $\vec{\zeta}_o$ and $\vec{l}_o$ because no reliable model is available to account for these components for large riser displacements away from a

previous static equilibrium position. In addition, we neglect static interaction moments per unit length about $\vec{\xi}_o$ and $\vec{l}_o$ because of the strip theory approximation followed in this work.

If the riser tube is assumed rigid, the spring coefficients k^y and k^ψ depend on the geometric form of the contact area and on the soil shear modulus G^B and Poisson's ratio ν^B, see [10]. For contact areas which are rectangular of width 2d and length 2c, the above coefficients are given by

$$k^y = \frac{G^B}{1-\nu^B}\,\beta^y\,\sqrt{\frac{d}{c}} \tag{2.7}$$

$$k^\psi = \frac{G^B}{1-\nu^B}\,\beta^\psi\,4d^2 \tag{2.8}$$

where β^y and β^ψ are functions of d/c. For $d/c \ll 1$, which is the usual case, $\beta^y \approx 2.2$ and $\beta^\psi \approx 0.37$. If we assume that the contact geometry is rectangular, we may choose

$$d \approx D^\xi/2 \tag{2.8.1}$$

$$c = l_b/2 \tag{2.8.2}$$

where l_b is the riser length on the bottom. Equation (2.8.1) is, of course, very approximate, particularly if $D^\xi = D^\eta$, but is used here for order of magnitude estimates. Reference [10] provides a discussion of how to obtain reasonable estimates of G^B and ν^B. Typically the values of ν^B vary between 0.25 and 0.45, while the values of G^B show a much larger variation between 30 MPa to 350 MPa or even higher. For example, using $\nu^B = 0.45$, $G^B = 350$MPa, $D^\xi = 0.31$m, $l_b = 200$m, we find that $k^y = 55$MPa and $k^\psi = 23$MPa. If the effective weight of the riser is $W_e = 250$N/m, the resulting penetration is of the order of 5×10^{-6}m, i.e. negligible. The above analysis indicates that by assuming a perfectly rigid ocean bottom, no significant errors in the vertical static position of the riser will result. However, due to equation (2.5), no similar statement can be made about the horizontal position of the riser on the ocean floor for three-dimensional configurations. It is expected that this horizontal position greatly depends on the method of deployment of riser for catenary and lazy S configurations. If the method of deployment leads to a nearly straight static configuration on the ocean floor, equation (2.5) indicates that the riser position will continue to be nearly straight, as the overall riser configuration becomes genuinely three-dimensional, except near the lower support point due to the effect of a clamped rod boundary condition. If a reasonable method of deployment for catenary and lazy S configurations is followed, it is expected that due to its high flexibility no significant static bending stresses will result in the portion of the riser on the ocean floor. This, of course, assumes that the ocean floor is practically flat or that existing protrusions do not significantly impede motions of the riser.

2.2.2 DYNAMIC RISER-OCEAN BOTTOM INTERACTION

In this section we provide a mathematical model for the riser-ocean bottom interaction forces and moments for small dynamic motions and angles around a static configuration. Following [10], the following assumptions are made for the total static and dynamic force and moment per unit length on the riser, valid for $y=y_o+y_1 < 0$, i.e. when the riser penetrates the soil

$$\vec{F}_{B1} = -[k^y y + c^y y_t]\vec{J} - [k^l l_1 + c^l l_{1t}]\vec{l}_o \qquad (2.9)$$

$$\vec{M}_{B1} = -[k^\psi \psi + c^\psi \psi_t]\vec{\zeta}_o \qquad (2.10)$$

where k^y, k^l and k^ψ are vertical, horizontal and rocking spring constants per unit unit length; c^y, c^l and c^ψ are the corresponding damping coefficients; $l_1 = \sin\psi_o\, q + \cos\psi_o\, r$ is a small dynamic displacement along $\vec{l}_o$ and subscript t denotes partial derivative with respect to time. If $y = y_o + y_1 \geq 0$, we have $\vec{F}_{B1} = \vec{M}_{B1} = 0$.

If the tube is assumed rigid, the above spring coefficients depend on the geometric form of the contact area, the soil shear modulus G^B, Poisson's ratio ν^B, while the damping coefficients also depend upon density ρ^B and to a lesser extent upon the frequency of excitation [10]. If the assumptions made in equations (2.7) and (2.8) are also followed here, then

$$k^l = 2(1+\nu^B)G^B\beta^l\sqrt{\frac{d}{c}} \qquad (2.11)$$

where β^l is a function of d/c. For $d/c \ll 1$, which is the usual case, $\beta^l \approx 1.1$. Using results for circular footings and the procedure suggested in [10], an order of magnitude estimate of c^y and c^l for rectangular contact areas of width 2d can be obtained from:

$$c^y \simeq 6.8\,\frac{d}{\pi}\,\frac{\sqrt{\rho^B G^B}}{1-\nu^B} \qquad (2.12)$$

$$c^l \simeq 36.8\,\frac{d}{\pi}\,\frac{1-\nu^B}{7-8\nu^B}\,\sqrt{\rho^B G^B} \qquad (2.13)$$

Using a similar process for c^ψ appears to be even more approximate due to the different geometries involved but may be used for rough estimates:

$$c^\psi \simeq 1.6\,\frac{d^3}{\pi}\,\frac{\sqrt{\rho^B G^B}}{(1-\nu^B)(1+\beta^\psi)} \qquad (2.14)$$

where

$$B^{\psi} = \frac{3(1-\upsilon^{B})\pi}{16} \frac{J^{\zeta\zeta}}{\rho^{B} d^{4}} \qquad (2.15)$$

where $J^{\zeta\zeta}$ is the mass moment of inertia per unit length around the tangential axis to the centerline. It should also be stressed again that the above expressions are all very approximate if $D^{\xi} = D^{\eta}$.

If the tube is not assumed rigid, then the above expressions should also involve stiffness and damping contributions due to lateral shell deformations of the tubes primarily due to the vertical component of the interaction force. If the spring coefficient k^{T} of the tube in this shell deformation mode is comparable or much smaller than k^{y} of equation (2.7), then k^{y} in equation (2.9) should be replaced by

$$k_{e}^{y} = \frac{k^{y} \cdot k^{T}}{k^{T} + k^{y}} \qquad (2.16)$$

which effectively reduces the spring interaction force. The damping coefficients should also be replaced by new effective damping coefficients which also take into account energy losses in the riser due to the above mode of deformation.

2.2.3 FINAL EXPRESSIONS FOR RISER-OCEAN BOTTOM INTERACTION FORCES AND MOMENTS

Based on the above discussion and because of the very approximate way in which the results of [10] for rectangular or circular foundation footings need to be extrapolated to provide estimates of the interaction forces and moments for risers on the ocean floor, our expressions for the interaction loads were simplified to only capture the major relevant effects. For practically flat bottoms, for which horizontal motions of a riser are essentially unhindered, the major effects of this interaction are expected to be adequately modelled by only taking into account vertical interaction forces and neglecting rocking moments altogether ($\vec{M}^{B} = 0$). Therefore, using (2.9) we obtain

$$\vec{F}_{B} = \begin{cases} -[k_{e}^{y} y + c_{e}^{y} y_{t}]\vec{j} & y < 0 \\ 0 & y \geq 0 \end{cases} \qquad (2.17)$$

for the overall static and dynamic interaction force, where k_{e}^{y} and c_{e}^{y} are effective spring and damping constants obtained as discussed in previous sections. Equation (2.17) is similar to the equation used in [8] for mooring line time simulations.

For reasons of generality, we will assume now that the ocean floor is at $y = h_{B}$ as in Figure 2-3 in which case equation (2.17) needs to be rewritten as

$$\vec{F}_B = \begin{cases} -[k_e^y(y-h_B) + c_e^y y_t]\cdot\vec{j} & y - h_B < 0 \\ 0 & y - h_B \geq 0 \end{cases} \qquad (2.18)$$

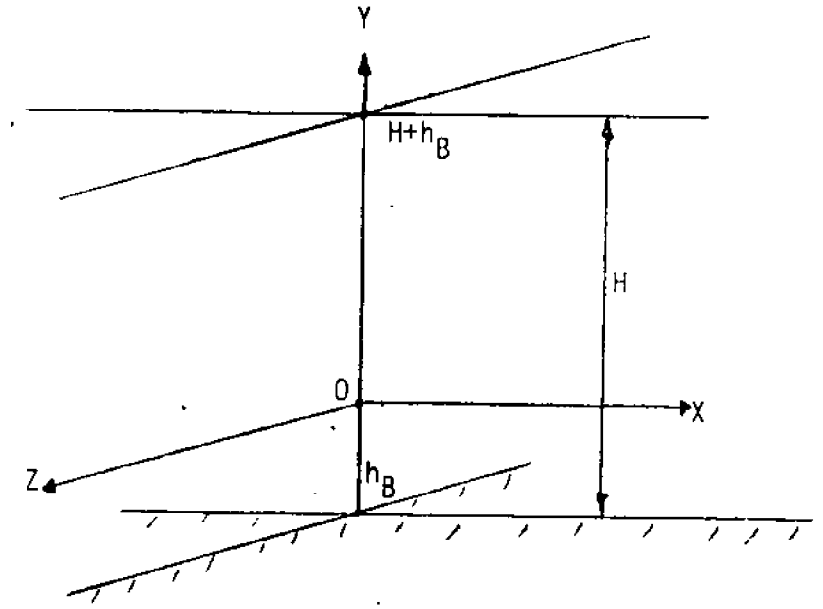

Figure 2-3: Axis System

The riser-ocean bottom interaction modelled using (2.18) is a non-linear mechanism which can be properly studied using a time domain approach. Due to the very high stiffness of the soil implied in (2.18), significant impact phenomena may exist, in particular if very large riser velocities close to the touch down point are present [11]. If, however, the top end excitation has decayed significantly and the velocity of the touch down point is small, the interaction can be considered smooth and quasi-static [11]. Reference [11] also provides an estimate of when impact phenomena are expected for the case of a two-dimensional taut cable on a perfectly rigid ocean floor. Such impact phenomena are possible when the speed of the touch down point is larger than the phase velocity, c_f, of an equivalent taut string, $c_f = (T_o/M)^{1/2}$, where T_o is the local effective tension and M the mass plus added mass of the cable in the normal direction. An estimate of the expected velocity of the touch down point can be made by multiplying the frequency of excitation times its quasi-static motion determined by imposing the dynamic motion of the top end as a quasi-static offset on top of a particular static offset. The adequacy of such procedures needs to be verified using a time domain solution.

If no significant impact phenomena are expected, equivalent linearization is, however, expected to be adequate. This is the approach implemented in this work.

2.3 NON-LINEAR HYDRODYNAMIC LOADS

The prediction of the external loads $\vec{F}_H$ and $\vec{M}_H$ is, perhaps, one of the more important factors in a successful analysis of the static and dynamic behavior of compliant risers. Until rational methods allow the prediction of these loads in separated flows, approximate estimates based on strip theory and experimental two-dimensional flow models may be used for design purposes, see [12] to [14]. At local amplitudes of oscillation large compared to the diameter in the presence or absence of current, the drag component of the hydrodynamic force dissipates energy given to the system from external excitation, such as the oscillation of the support points of the riser [12]. When the local amplitude of oscillation in the presence of a current is less than about one diameter, the drag component of the force may actually provide energy to the system for certain ranges of the reduced velocity, see [12] to [14]. This situation is likely to occur in many compliant riser applications involving an external current or large slow drift oscillations of the supporting platforms (effectively acting as currents for most of the cycle). However, as the results of [12] and [13] indicate, the limiting amplitude, at least for constant currents, of the mode excited, is only slightly above one diameter, which unless the mode excited is sufficiently high, is not expected to be a driving factor. However, vortex induced lift response leads to an increase of the mean drag coefficient parallel to the current (or slow large amplitude oscillation) which may in turn have a significant effect on the response parallel to the current.

In this work, we will concentrate on the dissipative effects of quadratic drag either in the presence or absence of current. Quadratic drag acts differently than linear drag in that it reduces large amplitudes faster and allows smaller amplitudes to persist for larger distances from the excitation point. Linear drag would, of course, induce a uniform exponential decay of the amplitude away from the excitation point.

In this work, we adopt the following procedure based on [15] to estimate the external hydrodynamic force and moment per unit length on the riser. A similar procedure was used in [2] to [5] to estimate the external static force and moment due to a current.

We assume first that the external current velocity is a given function of y and of the following form:

$$\vec{V}_c(y) = [V_c^x(y), 0, V_c^z(y)] \cdot U \qquad (2.19)$$

Next we assume the presence of monochromatic travelling surface gravity waves of the form

$$\eta = A_w \exp[-ik\,(x\cos\theta_w + z\sin\theta_w) + i\omega t] \qquad (2.20)$$

where A_w, k, ω, θ_w are the wave amplitude, wave number, circular frequency and angle of the direction of propagation with respect to the +x axis and i the imaginary unit. The real part needs to be taken in (2.20) and the

associated equations to follow. The corresponding wave potential is

$$\Phi = +i \frac{gA_w}{\omega} \frac{\cosh[k(y-h_B)]}{\cosh(kH)} \exp[-ik(x\cos\theta_w + z\sin\theta_w)+i\omega t] \qquad (2.21)$$

where H is the water depth, $y = h_B$ is the equation of the ocean floor and k, H and ω are related by the dispersion relation

$$\omega^2 = gk \tanh(kH) \qquad (2.22)$$

The associated particle wave velocities are obtained by taking the partial derivatives of Φ with respect to x, y and z:

$$V^x = \omega A_w \frac{\cosh[k(y-h_B)]}{\sinh(kH)} \cos\theta_w \exp[-ik(x\cos\theta_w + z\sin\theta_w)+i\omega t] \qquad (2.23)$$

$$V^y = i\omega A_w \frac{\sinh[k(y-h_B)]}{\sinh(kH)} \exp[-ik(x\cos\theta_w + z\sin\theta_w)+i\omega t] \qquad (2.24)$$

$$V^z = \omega A_w \frac{\cosh[k(y-h_B)]}{\sinh(kH)} \sin\theta_w \exp[-ik(x\cos\theta_w + z\sin\theta_w)+i\omega t] \qquad (2.25)$$

The corresponding particle wave accelerations are

$$V_t^x = i\omega^2 A_w \frac{\cosh[k(y-h_B)]}{\sinh(kH)} \cos\theta_w \exp[-ik(x\cos\theta_w + z\sin\theta_w)+i\omega t] \qquad (2.26)$$

$$V_t^y = -\omega^2 A_w \frac{\sinh[k(y-h_B)]}{\sinh(kH)} \exp[-ik(x\cos\theta_w + z\sin\theta_w)+i\omega t] \qquad (2.27)$$

$$V_t^z = i\omega^2 A_w \frac{\cosh[k(y-h_B)]}{\sinh(kH)} \sin\theta_w \exp[-ik(x\cos\theta_w + z\sin\theta_w)+i\omega t] \qquad (2.28)$$

Next we present expressions for the hydrodynamic forces and moments per unit length on the riser appropriate for determining the solution of the non-linear static and linearized dynamic problem for small dynamic deflections and angles around the static configuration. Here, as in [6] and [7], the linearized dynamic equilibrium equations are expressed in the local static U_o^* system and, therefore, we will provide expressions for the components of the total external hydrodynamic loads in this system, consistent with the range of validity of the problem addressed here.

The total tangential hydrodynamic force is modelled as:

$$F_H^{\zeta_o}(s,t) = [\rho_w(A_b - A_o) + m_a^{\zeta}]V_t^{\zeta_o} - m_a^{\zeta}p_{tt} + 0.5\rho_w P_e^{\xi\eta} C_f V_{rel}^{\zeta_o} | V_{rel}^{\zeta_o} | \qquad (2.29)$$

where

- ρ_w is the salt water density
- A_o is the riser tubes outer cross-sectional area
- A_b is the riser tubes and buoyancy modules outer cross-sectional area
- p is a small dynamic displacement along ζ_o
- m_a^{ζ} is the added mass per unit length of the buoyancy modules in the ζ direction and $m_a^{\zeta} = 0$ for all bare riser sections
- C_f a frictional coefficient, and
- $P_e^{\xi\eta}$ is an "equivalent" wetted perimeter of the cross-section derived in [3] which accounts for frictional and separation effects and is given by

$$P_e^{\xi\eta}(s) = P^{\xi\eta}(s) + \frac{C_D'(A_b - A_o)}{C_f L_b} \qquad (2.30)$$

- $P^{\xi\eta}(s)$ is the overall wetted perimeter of the cross-section
- C_D' is a separation and wake formation drag coefficient for the buoyancy modules for flow parallel to ζ
- L_b is the buoyancy module length

Within the bare part of the riser, we set $A_b = A_o$ and therefore $P_e^{\xi\eta} = P^{\xi\eta}$, as expected. Within the part of the riser covered by buoyancy modules, (2.29) allows representation of a uniformly distributed force due to separation and wake formation.

Using (2.1), we can determine $V_t^{\xi_o}$, the particle wave acceleration in the $\vec{\zeta}_o$ direction and $V_{rel}^{\xi_o}$, the relative velocity of the fluid particles due to wave and current motion with respect to the riser in the $\vec{\zeta}_o$ direction. In these estimates, all velocities and accelerations of the external flow are evaluated at the static position (x_o, y_o, z_o) of the riser. This is an acceptable approximation because the dynamic displacements are small with respect to the length scales of the external flows, i.e. $\lambda_c = |V_c| / (d|V_c|/dy)$ for the current and $\lambda = 2\pi / k$ for the wave.

Next we express the drag component of the hydrodynamic force orthogonal to $\vec{\zeta}_o$ as

$$\vec{F}_{drag}^{\xi_o\eta_o} = 0.5\,\rho_w D_f C_D\, \vec{V}_{rel}^{\xi_o\eta_o} | \vec{V}_{rel}^{\xi_o\eta_o} | \qquad (2.31)$$

where D_f is the maximum frontal dimension of the cross-section orthogonal to $\vec{V}_{rel}^{\xi_o\eta_o}$, C_D is a drag coefficient primarily due to separation and wake formation and

$$\vec{V}_{rel}^{\xi_o\eta_o} = [0, V_{rel}^{\xi_o}, V_{rel}^{\eta_o}] \cdot U_o'' \qquad (2.32)$$

and $V_{rel}^{\xi_o}$ and $V_{rel}^{\eta_o}$ are the relative velocities of the fluid particles due to wave and current motion with respect to the riser in the $\vec{\xi}_o$ and $\vec{\eta}_o$ directions. As in reference [3], the cross sections modelled in this work are of the form shown in Figure 2-4.

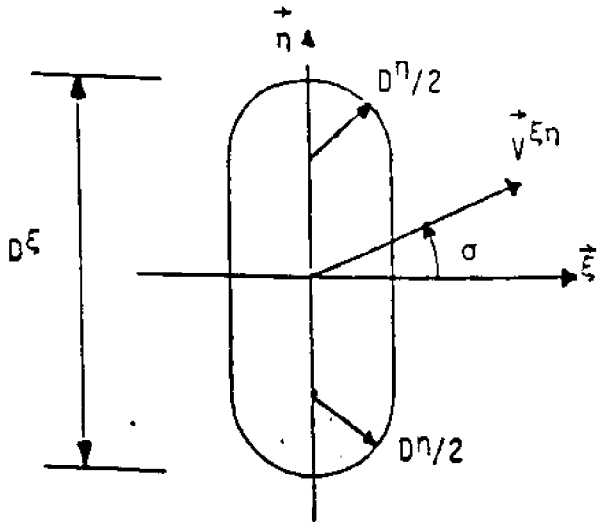

Figure 2-4: Cross-Section Idealization

For such cases

$$D_f = (D^{\xi} - D^{\eta})|\cos\sigma| + D^{\eta} \qquad (2.33)$$

where

$$|\cos\sigma| = |V_{rel}^{\xi_o}| / |\vec{V}_{rel}^{\xi_o\eta_o}| \qquad (2.34)$$

Now introducing the inertial part of the hydrodynamic forces in the $\vec{\xi}_o$ and $\vec{\eta}_o$ directions, analyzing (2.31) in these directions and using (2.32) to (2.34), we obtain for the total hydrodynamic forces along $\vec{\xi}_o$ and $\vec{\eta}_o$:

$$F_H^{\xi_o}(s,t) = [\rho_w A_b + m_a^{\xi}] V_t^{\xi_o} - m_a^{\xi} q_{tt} + 0.5\rho_w C_D V_{rel}^{\xi_o} [(D^{\xi} - D^{\eta})|V_{rel}^{\xi_o}| + D^{\eta}|\vec{V}_{rel}^{\xi_o\eta_o}|] \qquad (2.35)$$

$$F_H^{\eta_o}(s,t)=[\rho_w A_b+m_a^{\eta}]V_t^{\eta_o} - m_a^{\eta} r_{tt} + 0.5\rho_w C_D V_{rel}^{\eta_o}[(D^{\xi}-D^{\eta})|V_{rel}^{\xi_o}|+D^{\eta}|\vec{V}_{rel}^{\xi_o\eta_o}|] \qquad (2.36)$$

where

- m_a^{ξ} and m_a^{η} are added masses per unit length in the $\vec{\xi}$ and $\vec{\eta}$ directions,
- q, r are small dynamic displacements along $\vec{\xi}_o$ and $\vec{\eta}_o$, and

$$|\vec{V}_{rel}^{\xi_o\eta_o}| = [(V_{rel}^{\xi_o})^2 + (V_{rel}^{\eta_o})^2]^{1/2} \qquad (2.37)$$

The fluid acceleration and relative velocity terms needed in equations (2.29), (2.35) and (2.36) are defined by

$$[V_t^{\zeta_o}, V_t^{\xi_o}, V_t^{\eta_o}]^T = C_o \cdot [V_t^x, V_t^y, V_t^z]^T \qquad (2.38)$$

$$[V_{rel}^{\zeta_o}, V_{rel}^{\xi_o}, V_{rel}^{\eta_o}]^T = C_o \cdot [V_c^x+V^x, V^y, V_c^z+V^z]^T - [p_t, q_t, r_t]^T \qquad (2.39)$$

For the reasons mentioned earlier, all fluid velocities and accelerations are evaluated at the static position (x_o,y_o,z_o) of the riser.

In our estimates of the hydrodynamic forces, equations (2.29), (2.35) and (2.36), lift forces orthogonal to $\vec{\zeta}_o$ and $\vec{V}^{\xi_o\eta_o}$ are neglected in accordance with the arguments concerning the maximum vortex induced lift response made at the beginning of this section. However, the magnitude of C_D may significantly increase if such lift motion exists, see [13] and [14]. In this work, constant values of C_D along the length are used for simplicity. Procedures to obtain estimates of C_D and of the added mass coefficients used to determine sectional added mass for circular cylinders and a number of idealized excitation conditions in terms of the flow and response parameters using rigid cylinder experiments can be found in [12] to [14].

Finally, we need to provide estimates for the external hydrodynamic moment $\vec{M}_H$. Due to the strip theory approximation used in this work, the only component which is considered non-zero is the moment around the tangent to the centerline [16]. Within ideal flow theory, the presence of $M_H^{\zeta_o}$ can be explained because the cross-section is not, in general, symmetrical about an axis orthogonal to $\vec{V}_{rel}^{\xi_o\eta_o}$ on the $\vec{\xi}_o$, $\vec{\eta}_o$ plane [16]. Due to lack of data for real flow conditions, we estimate the external torque per unit length using potential theory and adding a quadratic frictional component:

$$M_H^{\zeta_o} = (m_a^{\xi} - m_a^{\eta}) V_{rel}^{\xi_o} V_{rel}^{\eta_o} - J_a^{\zeta\zeta} \omega_t^{\zeta} - \frac{1}{2} \rho_w C_f^{\xi} \rho^{\xi\eta} r^3 \omega^{\zeta} |\omega^{\zeta}| \tag{2.40}$$

where r can be approximately taken as

$$r \simeq (D^{\xi} + D^{\eta})/4 \tag{2.41}$$

and C_f^{ζ} is a frictional coefficient for oscillatory torsional motions.

2.4 GOVERNING EQUATIONS

2.4.1 NON-LINEAR STATIC EQUATIONS

As indicated earlier, the first step in the solution process followed in this work is the solution of the non-linear static problem in the presence of mean forces and moments due to currents and waves possibly involving static riser ocean bottom interaction. This is followed by the solution of the linearized dynamic equations for small motions around the static configuration and the determination of more accurate mean forces and moments also including the effects of riser motion.

For reasons of completeness, the general static equilibrium equations, obtained from [1] by including riser-ocean bottom interaction forces $\vec{F}_B$, replacing the external hydrodynamic loads $\vec{F}_H$ and $\vec{M}_H$ by their mean values and setting all velocities and angular velocities equal to zero, are given below

$$T_{os} = \mu c^o_{12} + Q^\xi_o \Omega^\eta_o - Q^\eta_o \Omega^\xi_o - F^\xi_{Ho} - F^\xi_{Bo} \tag{2.42}$$

$$Q^\xi_{os} = \mu c^o_{22} + Q^\eta_o \Omega^\zeta_o - T_o \Omega^\eta_o - F^\xi_{Ho} - F^\xi_{Bo} \tag{2.43}$$

$$Q^\eta_{os} = \mu c^o_{32} + T_o \Omega^\xi_o - Q^\xi_o \Omega^\zeta_o - F^\eta_{Ho} - F^\eta_{Bo} \tag{2.44}$$

$$\Omega^\zeta_{os} = -\beta^p_e [M^\zeta_{Ho} + (1/\beta^\eta_e - 1/\beta^\xi_e)\Omega^\eta_o \Omega^\xi_o + (1/\beta^p_e)_s \Omega^\zeta_o] \tag{2.45}$$

$$\Omega^\xi_{os} = \beta^\xi_e [Q^\eta_o - (1/\beta^p_e - 1/\beta^\eta_e)\Omega^\zeta_o \Omega^\eta_o - (1/\beta^\xi_e)_s \Omega^\xi_o] \tag{2.46}$$

$$\Omega^\eta_{os} = -\beta^\eta_e [Q^\xi_o - (1/\beta^p_e - 1/\beta^\xi_e)\Omega^\xi_o \Omega^\zeta_o + (1/\beta^\eta_e)_s \Omega^\eta_o] \tag{2.47}$$

$$\phi_{os} = (\Omega^\xi_o \sin\psi_o + \Omega^\eta_o \cos\psi_o)/\cos\theta_o \tag{2.48}$$

$$\theta_{os} = \Omega^\xi_o \cos\psi_o - \Omega^\eta_o \sin\psi_o \tag{2.49}$$

$$\psi_{os} = \Omega^\zeta_o + \tan\theta_o [\Omega^\xi_o \sin\psi_o + \Omega^\eta_o \cos\psi_o] \tag{2.50}$$

$$x_{os} = (1+\gamma T_o) c^o_{11} \tag{2.51}$$

$$y_{os} = (1+\gamma T_o) c^o_{12} \tag{2.52}$$

$$z_{os} = (1+\gamma T_o) c^o_{13} \tag{2.53}$$

$$s^*_{os} = 1+\gamma T_o \tag{2.54}$$

where

$$\beta_e^p(s) = W_a L^3/GI_e^p(s) \tag{2.55.1}$$

$$\beta_e^\xi(s) = W_a L^3/EI_e^{\xi\xi}(s) \tag{2.55.2}$$

$$\beta_e^\eta(s) = W_a L^3/EI_e^{\eta\eta}(s) \tag{2.55.3}$$

$$\gamma(s) = W_a L/EA(s) \tag{2.55.4}$$

$$\mu(s,y_o) = W(s,y_o)/W_a \tag{2.55.5}$$

The above governing equations (2.42) to (2.54) are non-dimensional. Forces are non-dimensionalized by $W_a L$, where W_a is the average effective weight per unit length of the riser in water, and lengths by L, the unstretched riser length. In addition, the elements c_{ij}^o of the static transformation matrix C_o can be expressed in terms of the static Euler angles, see [3].

Thirteen boundary conditions are, in addition, required to complete the statement of the static problem. In this work, single leg multitube riser configurations with a fixed and clamped lower end and prescribed static offsets and angles at the upper end are studied. The corresponding boundary conditions are

$$x_o(0)=y_o(0)=z_o(0) = s_o^*(0) = 0 \tag{2.56}$$

$$\theta_o(0) = \psi_o(0) = 0,\ \phi_o(0) = \phi_B \tag{2.57}$$

$$x_o(1)=x_T;\ y_o(1)=y_T;\ z_o(1)=z_T \tag{2.58}$$

$$\phi_o(1)=\phi_T;\ \theta_o(1)=\theta_T;\ \psi_o(1)=\psi_T \tag{2.59}$$

Equations (2.42) to (2.54) and (2.56) to (2.59) are of the following symbolic form

$$\vec{w}_{os} = \vec{f}_o(s,\vec{w}_o) \qquad \vec{g}(\vec{w}_o(0),\vec{w}_o(1))=0 \tag{2.60}$$

where $\vec{w}_o(s)$ is the solution vector and $\vec{f}_o$ is a non-linear function of s and $\vec{w}_o$. For the general three-dimensional static problem we choose

$$\vec{w}_o=[T_o,Q_o^\xi,Q_o^\eta;\Omega_o^\zeta,\Omega_o^\xi,\Omega_o^\eta;\phi_o,\theta_o,\psi_o;x_o,y_o,z_o;s_o^*]^T \tag{2.61}$$

with $N_o = 13$ unknown scalar variables. The first twelve variables are coupled in the governing equations while s_o^* can be determined from (2.54) once the computation of T_o is completed.

The mean external loads $\vec{F}_{Bo}$, $\vec{F}_{Ho}$ and $\vec{M}_{Ho}$ required in the solution of (2.57) will be determined for the general case in Section 2.4.2. For the initial solution of the static problem the hydrodynamic loads are computed by assuming zero dynamic motion, i.e. only taking into account the effects of effective weight, current, surface waves, ocean-bottom interaction and boundary conditions. For subsequent iterations, they are computed without making this assumption, i.e. by also including the effect of dynamic motion.

2.4.2 EQUIVALENT LINEARIZATION OF NON-LINEAR LOADS FOR MONOCHROMATIC RESPONSE

For overdamped systems, as a compliant riser operating at large amplitudes in comparison to its diameter, and in the absence of significant impact phenomena, it is well known that the equivalent linearization of the non-linear external loads allows us to replicate the results of time domain codes with accuracy usually sufficient for preliminary design, see [11], [17] and [18]. This occurs because higher frequency components introduced by the external load non-linearities are filtered out. In this work equivalent linearization of the non-linear external loads is performed assuming monochromatic excitation and response of given circular frequency ω. Our equivalent linearization procedure is based on [17] and minimizes the mean square error over a period of oscillation between each non-linear component of the load and its monochromatic approximation.

As stated above, the dynamic solutions studied in this work are of the form

$$\vec{w}_1(s,t) = \mathrm{Re}[\vec{w}_1(s)\exp(i\omega t)] \tag{2.62}$$

where $\vec{w}_1(s,t)$ is the solution vector, $\vec{w}_1(s)$ is a complex function of the arc length, subscript 1 denotes dynamic quantities, ω is the given circular frequency of oscillation and t is the time. As in reference [6], we find it convenient to choose

$$\vec{w}_1(s) = [T_1, Q_1^{\xi}, Q_1^{\eta}; \Omega_1^{\zeta}, \Omega_1^{\xi}, \Omega_1^{\eta}; \beta_{23}, \beta_{13}, \beta_{12}; p, q, r]^T \tag{2.63}$$

and we will express the governing dynamic equations in terms of these unknowns, separated into real and imaginary parts

$$\vec{w}_1(s) = \vec{w}_{1R}(s) + i\,\vec{w}_{1I}(s) \tag{2.64}$$

where i is the imaginary unit.

2.4.2.1 EQUIVALENT LINEARIZATION OF RISER-OCEAN BOTTOM INTERACTION FORCES

The approach taken in this work, as explained above, is to use an equivalent linearization of the distributed interaction force (2.18) in the solution of the dynamic problem assuming monochromatic excitation and response. An alternative approach, used in mooring dynamics [8], which replaces the part of the cable on the ocean floor with boundary conditions at the touchdown point, although attractive in two-dimensional configurations, does not extend easily to three-dimensional configurations present in compliant risers where the part of the riser on the ocean floor is not rectilinear and where bending and torsion effects are also present.

Equivalent linearization of (2.18) is performed by assuming that

$$y(s,t) = y_0(s) + y_1(s,t) \tag{2.65}$$

where

- $y_o(s)$ is the static deflection
- $y_1(s,t)$ is a small dynamic deflection in the vertical direction around the static configuration, given by

$$y_1(s,t) = Re[\bar{y}_1(s)\exp(i\omega t + i\alpha(s))] \tag{2.66}$$

where $\bar{y}_1(s) \geq 0$ is the dynamic motion amplitude in the $\vec{j}$ direction and $\alpha(s)$ is a corresponding phase, related to p, q and r by

$$\bar{y}_1 \exp(i\alpha) = [c^o_{12}, c^o_{22}, c^o_{32}][p,q,r]^T \tag{2.67}$$

which is due to (2.1)

Equation (2.18) can be separated into a static component

$$\vec{F}_{Bo} = \begin{cases} -k^y_e(y_o - h_B)\vec{j} & y_o < h_B \\ 0 & y_o \geq h_B \end{cases} \tag{2.68}$$

and a linearized dynamic component of the form

$$\vec{F}_{B1} = -[\hat{k}^y_e\, y_1 + \hat{c}^y_e\, y_{1t}]\cdot\vec{j} \tag{2.69}$$

where $\hat{k}_e^y$ and $\hat{c}_e^y$ can be found from the following equations

CASE 1: $y_o \leq h_B$ and $y_o + \bar{y}_1 \leq h_B$

$$\hat{k}_e^y = k_e^y,\ \hat{c}_e^y = c_e^y \tag{2.70}$$

CASE 2: $0 \le |y_o - h_B| \le \bar{y}_1$

$$\hat{k}_e^y = k_e^y\left[\frac{1}{2} + \frac{y_o - h_B}{\pi \bar{y}_1}\sqrt{1-\left(\frac{y_o-h_B}{\bar{y}_1}\right)^2} - \frac{1}{\pi}\sin^{-1}\left(\frac{y_o-h_B}{\bar{y}_1}\right)\right] \tag{2.71}$$

$$\hat{c}_e^y = c_e^y\left[\frac{1}{2} - \frac{y_o - h_B}{\pi \bar{y}_1}\sqrt{1-\left(\frac{y_o-h_B}{\bar{y}_1}\right)^2} - \frac{1}{\pi}\sin^{-1}\left(\frac{y_o-h_B}{\bar{y}_1}\right)\right] \tag{2.72}$$

CASE 3: $y_o \ge h_B,\ y_o - \bar{y}_1 \ge h_B$

$$\hat{k}_e^y = \hat{c}_e^y = 0 \tag{2.73}$$

which are, of course, also consistent with our intuition concerning (2.18).

Finally, $\vec{F}_{Bo}$ and $\vec{F}_{B1}$ need to be expressed in the U_o'' system. Using (2.1) and $C_o^{-1} = C_o^T$, we obtain

$$\vec{F}_{Bo} = \begin{cases} -k_e^y(y_o - h_B)[c_{12}^o, c_{22}^o, c_{32}^o]\cdot U_o'' & y_o < h_B \\ 0 & y_o \ge h_B \end{cases} \tag{2.74}$$

$$\vec{F}_{B1} = -\mathrm{Re}\{(\hat{k}_e^y + i\omega\hat{c}_e^y)[c_{12}^o, c_{22}^o, c_{32}^o]\cdot[p,q,r]^T \exp(i\omega t)\}\cdot[c_{12}^o, c_{22}^o, c_{32}^o]\cdot U_o'' \tag{2.75}$$

2.4.2.2 EQUIVALENT LINEARIZATION OF EXTERNAL HYDRODYNAMIC LOADS

To simplify calculations let

$$k' = k(x_o\cos\theta_w + z_o\sin\theta_w) \tag{2.76}$$

$$a' = \omega A_w \frac{\cosh[k(y_o - h_B)]}{\sinh(kH)} \tag{2.77}$$

$$b' = \omega A_w \frac{\sinh[k(y_o - h_B)]}{\sinh(kH)} \tag{2.78}$$

These allow us to write (2.23) to (2.25) and (2.26) to (2.28) as

$$\begin{bmatrix} V^x \\ V^y \\ V^z \end{bmatrix} = (\cos k' - i\sin k') \begin{bmatrix} a'\cos\theta_w \\ ib' \\ a'\sin\theta_w \end{bmatrix} e^{i\omega t} \tag{2.79}$$

$$\begin{bmatrix} V_t^x \\ V_t^y \\ V_t^z \end{bmatrix} = \omega(\sin k' + i\cos k') \begin{bmatrix} a'\cos\theta_w \\ ib' \\ a'\sin\theta_w \end{bmatrix} e^{i\omega t} \tag{2.80}$$

By letting

$$[V_t^{\zeta_o}, V_t^{\xi_o}, V_t^{\eta_o}] = \{[V_{Rt}^{\zeta_o}, V_{Rt}^{\xi_o}, V_{Rt}^{\eta_o}] + i[V_{It}^{\zeta_o}, V_{It}^{\xi_o}, V_{It}^{\eta_o}]\} e^{i\omega t} \tag{2.81}$$

equations (2.38) and (2.80) provide

$$\begin{bmatrix} V_{Rt}^{\zeta_o} \\ V_{Rt}^{\xi_o} \\ V_{Rt}^{\eta_o} \end{bmatrix} + i \begin{bmatrix} V_{It}^{\zeta_o} \\ V_{It}^{\xi_o} \\ V_{It}^{\eta_o} \end{bmatrix} = \omega(\sin k' + i\cos k') \begin{bmatrix} c_{11}^o & c_{12}^o & c_{13}^o \\ c_{21}^o & c_{22}^o & c_{23}^o \\ c_{31}^o & c_{32}^o & c_{33}^o \end{bmatrix} \begin{bmatrix} a'\cos\theta_w \\ ib' \\ a'\sin\theta_w \end{bmatrix} \tag{2.82}$$

which can be analyzed to

$$V_{Rt}^{\zeta_o} = \omega\{a'\sin k'(c_{11}^o\cos\theta_w + c_{13}^o\sin\theta_w) - b'\cos k' c_{12}^o\} \tag{2.83.1}$$

$$V_{It}^{\zeta_o} = \omega\{a'\cos k'(c_{11}^o\cos\theta_w + c_{13}^o\sin\theta_w) + b'\sin k' c_{12}^o\} \tag{2.83.2}$$

$$V_{Rt}^{\xi_o} = \omega\{a'\sin k'(c_{21}^o\cos\theta_w + c_{23}^o\sin\theta_w) - b'\cos k' c_{22}^o\} \tag{2.83.3}$$

$$V_{It}^{\xi_o} = \omega\{a'\cos k'(c_{21}^o\cos\theta_w + c_{23}^o\sin\theta_w) + b'\sin k' c_{22}^o\} \tag{2.83.4}$$

$$V_{Rt}^{\eta_o} = \omega\{a'\sin k'(c_{31}^o\cos\theta_w + c_{33}^o\sin\theta_w) - b'\cos k' c_{32}^o\} \tag{2.83.5}$$

$$V_{It}^{\eta_o} = \omega\{a'\cos k'(c_{31}^o\cos\theta_w + c_{33}^o\sin\theta_w) + b'\sin k' c_{32}^o\} \tag{2.83.6}$$

Similarly, equations (2.39) and (2.79) provide

$$\begin{bmatrix} V_{rel}^{\zeta_o} \\ V_{rel}^{\xi_o} \\ V_{rel}^{\eta_o} \end{bmatrix} = C_o \begin{bmatrix} V_c^x \\ 0 \\ V_c^z \end{bmatrix} + C_o(\cos k' - i\sin k') \begin{bmatrix} a'\cos\theta_w \\ ib' \\ a'\sin\theta_w \end{bmatrix} e^{i\omega t} - i\omega \begin{bmatrix} p \\ q \\ r \end{bmatrix} e^{i\omega t} \quad (2.84)$$

where the real part of the right hand side needs to be taken. To simplify our calculations we let

$$V_{rel}^{\zeta_o} = A + B\sin(\omega t+\theta_1) \quad (2.85)$$

$$V_{rel}^{\xi_o} = C + D\sin(\omega t+\theta_2) \quad (2.86)$$

$$V_{rel}^{\eta_o} = E + F\sin(\omega t+\theta_3) \quad (2.87)$$

where the phases $\theta_1, \theta_2, \theta_3$ are to be chosen so that

$$B,D,F \geq 0 \quad (2.88)$$

In addition we let

$$[p,q,r] = [p_R,q_R,r_R] + i[p_I,q_I,r_I] \quad (2.89)$$

Equations (2.84) to (2.87) provide the components A, C and E due to the current

$$A = c_{11}^o V_c^x + c_{13}^o V_c^z \quad (2.90)$$

$$C = c_{21}^o V_c^x + c_{23}^o V_c^z \quad (2.91)$$

$$E = c_{31}^o V_c^x + c_{33}^o V_c^z \quad (2.92)$$

Similarly equations (2.84) to (2.87) provide

$$-i \begin{bmatrix} B\exp(i\theta_1) \\ D\exp(i\theta_2) \\ F\exp(i\theta_3) \end{bmatrix} = (\cos k' - i\sin k') \begin{bmatrix} c_{11}^o & c_{12}^o & c_{13}^o \\ c_{21}^o & c_{22}^o & c_{23}^o \\ c_{31}^o & c_{32}^o & c_{33}^o \end{bmatrix} \begin{bmatrix} a'\cos\theta_w \\ ib' \\ a'\sin\theta_w \end{bmatrix} - i\omega \begin{bmatrix} p_R+ip_I \\ q_R+iq_I \\ r_R+ir_I \end{bmatrix} \quad (2.93$$

Multiplying (2.93) by i and recognizing the similarity with (2.82) we let

$$V_{Rt}^{\zeta_o} = \omega V_R^{\zeta_o}, \quad V_{It}^{\zeta_o} = \omega V_I^{\zeta_o} \tag{2.94}$$

$$V_{Rt}^{\xi_o} = \omega V_R^{\xi_o}, \quad V_{It}^{\xi_o} = \omega V_I^{\xi_o} \tag{2.95}$$

$$V_{Rt}^{\eta_o} = \omega V_R^{\eta_o}, \quad V_{It}^{\eta_o} = \omega V_I^{\eta_o} \tag{2.96}$$

where $V_R\zeta_o$, $V_I\zeta_o$, etc. are the bracket terms in equations (2.83). Equations (2.83), and (2.93) to (2.96) now provide

$$B\exp(i\theta_1) = \omega p_R + V_R^{\zeta_o} + i(\omega p_I + V_I^{\zeta_o}) \tag{2.97}$$

$$D\exp(i\theta_2) = \omega q_R + V_R^{\xi_o} + i(\omega q_I + V_I^{\xi_o}) \tag{2.98}$$

$$F\exp(i\theta_3) = \omega r_R + V_R^{\eta_o} + i(\omega r_I + V_I^{\eta_o}) \tag{2.99}$$

Using (2.88), B, D and F are the magnitudes of the right hand sides of (2.97) to (2.99). Similarly, θ_1, θ_2 and θ_3 are the phases of the right hand sides of (2.97) to (2.99) which in general belong to the interval

$$-\pi \leq \theta_1, \theta_2, \theta_3 < \pi \tag{2.100}$$

Equations (2.29), (2.35), (2.36) and (2.40) now indicate that the following non-linear terms require equivalent linearization expressed as follows

$$V_{rel}^{\zeta_o} |V_{rel}^{\zeta_o}| \simeq F^{\zeta_o} + C^{\zeta_o} \sin(\omega t + \theta_1) \tag{2.101}$$

$$V_{rel}^{\xi_o} |V_{rel}^{\xi_o}| \simeq F^{\xi_o} + C^{\xi_o} \sin(\omega t + \theta_2) \tag{2.102}$$

$$V_{rel}^{\xi_o} |\vec{V}_{rel}^{\xi_o\eta_o}| \simeq F^{\xi_o\eta_o} + C^{\xi_o\eta_o} \sin(\omega t + \theta_2) \tag{2.103}$$

$$V_{rel}^{\eta_o} |V_{rel}^{\xi_o}| \simeq F^{\eta_o} + C^{\eta_o} \sin(\omega t + \theta_2) \tag{2.104}$$

$$V_{rel}^{\eta_o} |\vec{V}_{rel}^{\xi_o\eta_o}| \simeq F^{\eta_o\xi_o} + C^{\eta_o\xi_o} \sin(\omega t + \theta_3) \tag{2.105}$$

$$V_{rel}^{\xi_o} V_{rel}^{\eta_o} \simeq F_M^{\zeta_o} + C_M^{\zeta_o} \sin(\omega t + \theta_2) \tag{2.106}$$

$$\omega^{\zeta} |\omega^{\zeta}| \simeq C_{fM}^{\zeta_o} \omega^{\zeta} \tag{2.107}$$

where from (2.37)

$$|\vec{V}_{rel}^{\xi_o\eta_o}| = \{[C+D\sin(\omega t+\theta_2)]^2 + [E+F\sin(\omega t+\theta_3)]^2\}^{1/2} \tag{2.108}$$

and from [6] and (2.64)

$$\omega^{\zeta} = \mathrm{Re}[i\omega\beta_{23}\exp(i\omega t)] \tag{2.109}$$

The equivalent linearization coefficients appearing in (2.101) to (2.107) are computed by minimizing the mean square error between the left hand side and the right hand side of these equations over one period of oscillation [17].

Equations (2.101), (2.102), (2.104) and (2.107) are special cases of the following equivalent linearization:

$$[a+b\sin(\tau+\Theta)]|c+d\sin\tau| = f+c_p\sin\tau \tag{2.110}$$

where $\tau = \omega t$ and $b, d \geq 0$. By minimizing

$$\bar{E}^2 = \int_0^{2\pi} d\tau\{f+c_p\sin\tau - [a+b\sin(\tau+\Theta)]|c+d\sin\tau|\}^2 \tag{2.111}$$

we obtain

$$f = \frac{1}{2\pi}\int_0^{2\pi} [a+b\sin(\tau+\Theta)]|c+d\sin\tau|\,d\tau \tag{2.112}$$

$$c_p = \frac{1}{\pi}\int_0^{2\pi} \sin\tau[a+b\sin(\tau+\Theta)]|c+d\sin\tau|\,d\tau \tag{2.113}$$

where $b, d \geq 0$ is assumed. These integrals, although more general than those computed in [17], can be expressed in terms of elementary functions by distinguishing a number of cases.

CASE 1: $|c| \geq d \geq 0$

$$f = \mathrm{sgn}(c)\left(ac + \frac{bd}{2}\cos\Theta\right) \tag{2.114}$$

$$c_p = \mathrm{sgn}(c)\,(ad + bc\cos\Theta) \tag{2.115}$$

where

$$\mathrm{sgn}(c) = \begin{cases} 1 & c > 0 \\ 0 & c = 0 \\ -1 & c < 0 \end{cases} \tag{2.116}$$

CASE 2: $d \geq |c| \geq 0$ with $d > 0$

$$f = \frac{2}{\pi}\,\mathrm{sgn}(c)\{(ac + \frac{bd}{2}\cos\Theta)\sin^{-1}(\frac{|c|}{d}) + \frac{b|c|}{2}\cos\Theta\sqrt{1-(\frac{c}{d})^2}\} + \frac{2}{\pi}\,da\sqrt{1-(c/d)^2} \quad (2.117)$$

$$c_p = \frac{2}{\pi}\,\mathrm{sgn}(c)(ad+bc\cos\Theta)\sin^{-1}(\frac{|c|}{d}) + \frac{2}{3\pi}\{3ac+bd[4-(\frac{c}{d})^2]\cos\Theta\}\sqrt{1-(\frac{c}{d})^2} \quad (2.118)$$

The values of f and c_p are functions of a, b, c, d, Θ

$$f = f(a,b,c,d,\Theta)$$
$$c_p = c_p(a,b,c,d,\Theta) \quad (2.119)$$

and therefore (2.85) to (2.87), (2.101), (2.102), (2.104) and (2.119) allow us to obtain

$$F^{\zeta_o} = f(A,B,A,B,0),\ C^{\zeta_o} = c_p(A,B,A,B,0) \quad (2.120)$$

$$F^{\xi_o} = f(C,D,C,D,0),\ C^{\xi_o} = c_p(C,D,C,D,0) \quad (2.121)$$

$$F^{\eta_o} = f(E,F,C,D,\theta_3-\theta_2),\ C^{\eta_o} = c_p(E,F,C,D,\theta_3-\theta_2) \quad (2.122)$$

Similarly, by letting

$$\beta_{23} = \beta_{23R} + i\beta_{23I} = |\beta_{23}|\exp(i\theta_4) \quad (2.123)$$

we obtain

$$\omega^{\zeta} = \omega|\beta_{23}|\cos(\omega t + \theta_4 + \frac{\pi}{2}) \quad (2.124)$$

and using (2.107), (2.124) and (2.118) we obtain

$$C_{fM}^{\zeta_o} = \frac{8}{3\pi}\,\omega|\beta_{23}| \quad (2.125)$$

and therefore

$$\omega^{\zeta}|\omega^{\zeta}| \simeq C_{fM}^{\zeta_o}\,\mathrm{Re}\{i\omega[\beta_{23R} + i\beta_{23I}]\exp(i\omega t)\} \quad (2.126)$$

Similarly, by minimizing the mean square error over a period of the left hand side minus the right hand side of (2.106) we obtain

$$F_M^{\zeta_o} = CE + \frac{DF}{2}\cos(\theta_3-\theta_2) \tag{2.127}$$

$$C_M^{\zeta_o} = DE + CF\cos(\theta_3-\theta_2) \tag{2.128}$$

Unfortunately, the coefficients in the right hand sides of (2.103) and (2.105) cannot be expressed in terms of elementary functions and, therefore, numerical quadrature will be used to evaluate them from:

$$F^{\xi_o\eta_o} = \frac{1}{2\pi}\int_0^{2\pi} d\tau[C+D\sin(\tau+\theta_2)]\{[C+D\sin(\tau+\theta_2)]^2 + [E+F\sin(\tau+\theta_3)]^2\}^{1/2} \tag{2.129}$$

$$C^{\xi_o\eta_o} = \frac{1}{\pi}\int_0^{2\pi} d\tau\sin(\tau+\theta_2)[C+D\sin(\tau+\theta_2)]\{[C+D\sin(\tau+\theta_2)]^2 + [E+F\sin(\tau+\theta_3)]^2\}^{1/2} \tag{2.130}$$

$$F^{\eta_o\xi_o} = \frac{1}{2\pi}\int_0^{2\pi} d\tau[E+F\sin(\tau+\theta_3)]\{[C+D\sin(\tau+\theta_2)]^2 + [E+F\sin(\tau+\theta_3)]^2\}^{1/2} \tag{2.131}$$

$$C^{\eta_o\xi_o} = \frac{1}{\pi}\int_0^{2\pi} \sin(\tau+\theta_3)[E+F\sin(\tau+\theta_3)]\{[C+D\sin(\tau+\theta_2)]^2 + [E+F\sin(\tau+\theta_3)]^2\}^{1/2} \tag{2.132}$$

This completes the equivalent linearization of the hydrodynamic loads. The expressions for these loads, provided below, have been split into static (subscript o) and dynamic components (subscript 1), the sinusoid time dependence exp[iωt] has been dropped from the dynamic components, while the real part also needs to be taken in the dynamic components.

$$F_{Ho}^{\zeta_o} \simeq 0.5\rho_w p_e^{\xi\eta} C_f F^{\zeta_o} \tag{2.133}$$

$$F_{H1}^{\zeta_o} \simeq [\rho_w(A_b-A_o) + m_a^{\zeta}][V_{Rt}^{\zeta_o}+iV_{It}^{\zeta_o}] + m_a^{\zeta}\omega^2(p_R+ip_I)+0.5\rho_w P_e^{\xi\eta} C_f C^{\zeta_o}[\sin\theta_1-i\cos\theta_1] \tag{2.134}$$

$$F_{Ho}^{\xi_o} \simeq 0.5\rho_w C_D\{(D^{\xi}-D^{\eta})F^{\xi_o} + D^{\eta}F^{\xi_o\eta_o}\} \tag{2.135}$$

$$F_{Hl}^{\xi_o} \simeq [\rho_w A_b + m_a^{\xi}][V_{Rt}^{\xi_o} + iV_{It}^{\xi_o}] + m_a^{\xi}\omega^2(q_R + iq_I)$$

$$+ 0.5\rho_w C_D\{(D^{\xi} - D^{\eta})C^{\xi_o} + D^{\eta}C^{\xi_o\eta_o}\}(\sin\theta_2 - i\cos\theta_2) \qquad (2.136)$$

$$F_{Ho}^{\eta_o} \simeq 0.5\rho_w C_D\{(D^{\xi} - D^{\eta})F^{\eta_o} + D^{\eta}F^{\eta_o\xi_o}\} \qquad (2.137)$$

$$F_{Hl}^{\eta_o} \simeq [\rho_w A_b + m_a^{\eta}][V_{Rt}^{\eta_o} + iV_{It}^{\eta_o}] + m_a^{\eta}\omega^2(r_R + ir_I)$$

$$+ 0.5\rho_w C_D\{(D^{\xi} - D^{\eta})C^{\eta_o}(\sin\theta_2 - i\cos\theta_2) + D^{\eta}C^{\eta_o\xi_o}(\sin\theta_3 - i\cos\theta_3)\} \qquad (2.138)$$

$$M_{Ho}^{\xi_o} \simeq (m_a^{\xi} - m_a^{\eta})\, F_M^{\xi_o} \qquad (2.139.1)$$

$$M_{Hl}^{\zeta_o} \simeq (m_a^{\xi} - m_a^{\eta})C_M^{\zeta_o}(\sin\theta_2 - i\cos\theta_2) + \omega^2 J_a^{\zeta\zeta}(\beta_{23R} + i\beta_{23I})$$

$$-0.5\rho_w C_F^{\xi} p^{\xi\eta} r^3 C_{FM}^{\zeta_o}\omega[-\beta_{23I} + i\beta_{23R}] \qquad (2.139.2)$$

2.4.2.3 STRUCTURAL DAMPING FORCES AND MOMENTS

The following linear expressions for the structural damping forces and moments per unit length are used

$$\Delta^{\zeta} = -\delta^{\zeta} i\omega(p_R + ip_I) \qquad (2.140)$$

$$\Delta^{\xi} = -\delta^{\xi} i\omega(q_R + iq_I) \qquad (2.141)$$

$$\Delta^{\eta} = -\delta^{\eta} i\omega(r_R + ir_I) \qquad (2.142)$$

$$\Theta^{\zeta} = -\theta^{\zeta} i\omega(\beta_{23R} + i\beta_{23I}) \qquad (2.143)$$

where the sinusoid time dependence exp[iωt] has been dropped, the real part needs to be taken in (2.140) to (2.143) and δ^{ζ}, δ^{ξ}, δ^{η}, θ^{ζ} are structural damping coefficients, which may be frequency dependent. The structural damping moments Θ^{ξ} and Θ^{η} are omitted because their effects may be represented by Δ^{ξ} and Δ^{η}. The values δ^{ζ}, δ^{ξ}, δ^{η}, θ^{ζ} are expected to be much larger than those encountered in conventional tensioned steel risers because of the multilayer construction of typical compliant risers.

2.4.3 NON-LINEAR DYNAMIC EQUATIONS FOR MONOCHROMATIC RESPONSE

We now derive the governing dynamic equations by

- incorporating the external forces and moments linearized in Section 2.4.2 for monochromatic response in the structurally linearized riser equations around a static configuration derived in [6];
- eliminating the sinusoid time dependence exp[iωt];
- separating real and imaginary parts in the resulting equations; and
- non-dimensionalizing all forces by the maximum static effective tension T'_{om} and all lengths by the unstretched length L of the riser.

For the reader's convenience, we repeat the definition of the following parameters first introduced in [6]

$$e_{om} = T'_{om}/EA \tag{2.144}$$

$$\varepsilon_e^p = GI_e^p/T'_{om}\,L^2,\ \varepsilon_e^\xi = EI_e^{\xi\xi}/T'_{om}\,L^2,\ \varepsilon_e^\eta = EI_e^{\eta\eta}/T'_{om}\,L^2 \tag{2.145}$$

$$h^\zeta = m_T^\zeta/\bar{m}_T^\xi,\ h^\xi = m_T^\xi/\bar{m}_T^\xi,\ h^\eta = m_T^\eta/\bar{m}_T^\xi \tag{2.146}$$

$$\Sigma = \omega L\,(\bar{m}_T^\xi/T'_{om})^{1/2} \tag{2.147}$$

$$\kappa_i = c\rho_i\,A_i\,(\bar{m}_T^\xi\,T'_{om})^{-1/2} \tag{2.148}$$

$$\lambda_T = L(\bar{m}_T^\xi/J_T^{\zeta\zeta})^{1/2} \tag{2.149}$$

$$\lambda_i^\zeta = cJ_i^{\zeta\zeta}/L^2(\bar{m}_T^\xi\,T'_{om})^{1/2}\quad \lambda_i^\xi = cJ_i^{\xi\xi}/L^2\,(\bar{m}_T^\xi\,T'_{om})^{1/2} \tag{2.150}$$

$$\lambda_i^\eta = cJ_i^{\eta\eta}/L^2(\bar{m}_T^\xi\,T'_{om})^{1/2} \tag{2.151}$$

$$\lambda^\xi = L\,(\bar{m}_T^\xi/J^{\xi\xi})^{1/2}\qquad \lambda^\eta = L\,(\bar{m}_T^\xi/J^{\eta\eta})^{1/2} \tag{2.151}$$

where $\bar{m}_T^\xi$ is the average value of m_T^ξ along the length and

$$m_T^\zeta = m+m_a^\zeta,\ m_T^\xi = m+m_a^\xi,\ m_T^\eta = m+m_a^\eta \tag{2.152}$$

$$J_T^{\zeta\zeta} = J^{\zeta\zeta}+J_a^{\zeta\zeta} \tag{2.153}$$

In addition, we define the following coefficients:

$$C^{i\zeta} = L[\rho_w(A_b-A_o) + m_a^\zeta]/T'_{om} \tag{2.154}$$

$$C^{d\zeta} = 0.5\rho_w p_e^{\xi\eta}\,L\,C_f/T'_{om} \tag{2.155}$$

$$C^{i\xi} = L[\rho_w A_b + m_a^\xi]/T'_{om} \tag{2.156}$$

$$C^{d\xi} = 0.5\rho_w D^{\xi} L\ C_D/T'_{om} \tag{2.157}$$

$$C^{i\eta} = L[\rho_w A_b + m_a^{\eta}]/T'_{om} \tag{2.158}$$

$$C^{d\eta} = 0.5\rho_w D^{\eta} L\ C_D/T'_{om} \tag{2.159}$$

$$C_{MOM} = (m_a^{\xi}-m_a^{\eta})/T'_{om} \tag{2.160}$$

$$\delta^{\zeta'} = \omega\delta^{\zeta} L^2/T'_{om} \tag{2.161}$$

$$\delta^{\xi'} = \omega\delta^{\xi} L^2/T'_{om} \tag{2.162}$$

$$\delta^{\eta'} = \omega\delta^{\eta} L^2/T'_{om} \tag{2.163}$$

$$\Theta^{\zeta'} = \omega\Theta^{\zeta}/T'_{om} \tag{2.164}$$

$$\hat{k}_e^{y'} = \hat{k}_e^{y} \cdot L^2/T'_{om} \tag{2.165}$$

$$\hat{c}_e^{y'} = \omega\ \hat{c}_e^{y}\ L^2/T'_{om} \tag{2.166}$$

$$c_{MOM}^{d\zeta} = 0.5\rho_w\ C_f^{\xi}\ P^{\xi}\eta_r^3\omega/T'_{om} \tag{2.167}$$

Based on the above notation and [6], the governing dynamic equations are:

$$\begin{aligned} T_{1Rs} &= Q_o^{\xi}\Omega_{1R}^{\eta} + \Omega_o^{\eta}Q_{1R}^{\xi} - Q_o^{\eta}\Omega_{1R}^{\xi} - \Omega_o^{\xi}Q_{1R}^{\eta} \\ &+ \beta_{12R}F_2 + \beta_{13R}F_3 - \Sigma^2 h^{\zeta}p_R - \delta^{\zeta'}p_I - C^{d\zeta}C^{\zeta}{}_o \sin\theta_1 \\ &- C^{i\zeta}V_{Rt}^{\zeta_o} + c_{12}^o\ \{\hat{k}_e^{y'}(c_{12}^o p_R + c_{22}^o q_R + c_{32}^o r_R) \\ &- \hat{c}_e^{y'}(c_{12}^o p_I + c_{22}^o q_I + c_{32}^o r_I)\} \end{aligned} \tag{2.168}$$

$$T_{1Is} = Q_o^{\xi}\Omega_{1I}^{\eta} + \Omega_o^{\eta}Q_{1I}^{\xi} - Q_o^{\eta}\Omega_{1I}^{\xi} - \Omega_o^{\xi}Q_{1I}^{\eta}$$

$$+ \beta_{12I}F_2 + \beta_{13I}F_3 - \Sigma^2 h^{\zeta} p_I + C^{d\zeta}C^{\zeta_o}\cos\theta_1 + \delta^{\xi'} D_R$$

$$- C^{i\zeta} V_{It}^{\zeta_o} + c_{12}^o \{\hat{k}_e^{y'}(c_{12}^o p_I + c_{22}^o q_I + c_{32}^o r_I)$$

$$+ \hat{c}_e^{y'}(c_{12}^o p_R + c_{22}^o q_R + c_{32}^o r_R)\} \qquad (2.169)$$

$$Q_{1Rs}^{\xi} = Q_o^{\eta}\Omega_{1R}^{\zeta} + \Omega_o^{\zeta}Q_{1R}^{\eta} - T_o\Omega_{1R}^{\eta} - \Omega_o^{\eta}T_{1R} - \beta_{12R}F_1 + \beta_{23R}F_3$$

$$-\Sigma^2 h^{\xi} q_R - 2\Sigma\kappa_i\beta_{12I} - \delta^{\xi'} q_I - [(C^{d\xi} - C^{d\eta})C^{\xi_o} + C^{d\eta}C^{\xi_o\eta_o}]\sin\theta_2$$

$$-C^{i\xi}V_{Rt}^{\xi_o} + c_{22}^o\{\hat{k}_e^{y'}(c_{12}^o p_R + c_{22}^o q_R + c_{32}^o r_R) - \hat{c}_e^{y'}(c_{12}^o p_I + c_{22}^o q_I + c_{32}^o r_I)\} \qquad (2.170)$$

$$Q_{1Is}^{\xi} = Q_o^{\eta}\Omega_{1I}^{\zeta} + \Omega_o^{\zeta}Q_{1I}^{\eta} - T_o\Omega_{1I}^{\eta} - \Omega_o^{\eta}T_{1I} - \beta_{12I}F_1 + \beta_{23I}F_3$$

$$-\Sigma^2 h^{\xi} q_I + 2\Sigma\kappa_i\beta_{12R} + \delta^{\xi'} q_R + [(C^{d\xi} - C^{d\eta})C^{\xi_o} + C^{d\eta}C^{\xi_o\eta_o}]\cdot\cos\theta_2$$

$$- C^{i\xi}V_{It}^{\xi_o} + c_{22}^o\{\hat{k}_e^{y'}(c_{12}^o p_I + c_{22}^o q_I + c_{32}^o r_I) + \hat{c}_e^{y'}(c_{12}^o p_R + c_{22}^o q_R + c_{32}^o r_R)\} \qquad (2.171)$$

$$Q_{1Rs}^{\eta} = T_o\Omega_{1R}^{\xi} + \Omega_o^{\xi}T_{1R} - Q_o^{\xi}\Omega_{1R}^{\zeta} - \Omega_o^{\zeta}Q_{1R}^{\xi} - \beta_{13R}F_1 - \beta_{23R}F_2$$

$$-\Sigma^2 h^{\eta} r_R - 2\Sigma\kappa_i\beta_{13I} - \delta^{\eta'} r_I - (C^{d\xi} - C^{d\eta})C^{\eta_o}\sin\theta_2$$

$$-C^{d\eta}C^{\eta_o\xi_o}\sin\theta_3 - C^{i\eta}V_{Rt}^{\eta_o} + c_{32}^o\{\hat{k}_e^{y'}(c_{12}^o p_R + c_{22}^o q_R$$

$$+ c_{32} r_R) - \hat{c}_e^{y'}(c_{12}^o p_I + c_{22}^o q_I + c_{32}^o r_I)\} \qquad (2.172)$$

$$Q^{\eta}_{1Is} = T_o\Omega^{\xi}_{1I} + \Omega^{\xi}_{o}T_{1I} - Q^{\xi}_{o}\Omega^{\zeta}_{1I} - \Omega^{\zeta}_{o}Q^{\xi}_{1I} - \beta_{13I}F_1 - \beta_{23I}F_2$$

$$-\Sigma^2 h^{\eta} r_I + 2\Sigma\kappa_i\beta_{13R} + \delta^{\eta'} r_R + (C^{d\xi} - C^{d\eta})C^{\eta o}\cos\theta_2$$

$$+ C^{d\eta}C^{\eta o}\xi_o\cos\theta_3 - C^{i\eta}v^{\eta o}_{It} + c^o_{32}\{\hat{k}^{y'}_e(c^o_{12}p_I + c^o_{22}q_I$$

$$+ c^o_{32}r_I) + \hat{c}^{y'}_e(c^o_{12}p_R + c^o_{22}q_R + c^o_{32}r_R)\} \qquad (2.173)$$

$$\varepsilon^{P}_{e}\Omega^{\zeta}_{1Rs} = -\varepsilon^{P}_{es}\Omega^{\zeta}_{1Rs} - (\varepsilon^{\eta}_{e} - \varepsilon^{\xi}_{e})(\Omega^{\xi}_{o}\Omega^{\eta}_{1R} + \Omega^{\eta}_{o}\Omega^{\xi}_{1R})$$

$$- (\Sigma/\lambda_T)^2\beta_{23R} - \Sigma[\lambda^{\xi}_i(2\Omega^{\zeta}_{1I} - \Omega^{\eta}_{o}\beta_{13I}$$

$$- \Omega^{\xi}_{o}\beta_{12I}) + (\lambda^{\eta}_i - \lambda^{\xi}_i)(\Omega^{\xi}_{o}\beta_{12I} - \Omega^{\eta}_{o}\beta_{13I})]$$

$$- C_{MOM}C^{\zeta o}_{M}\sin\theta_2 - C^{d\zeta}_{MOM}C^{\zeta o}_{fM}\beta_{23I} - \Theta^{\zeta'}\beta_{23I} \qquad (2.174)$$

$$\varepsilon^{P}_{e}\Omega^{\zeta}_{1Is} = -\varepsilon^{P}_{es}\Omega^{\zeta}_{1I} - (\varepsilon^{\eta}_{e} - \varepsilon^{\xi}_{e})(\Omega^{\xi}_{o}\Omega^{\eta}_{1I} + \Omega^{\eta}_{o}\Omega^{\xi}_{1I})$$

$$- (\Sigma/\lambda_T)^2\beta_{23I} + \Sigma[\lambda^{\xi}_i(2\Omega^{\zeta}_{1R} - \Omega^{\eta}_{o}\beta_{13R} - \Omega^{\xi}_{o}\beta_{12R})$$

$$+ (\lambda^{\eta}_i - \lambda^{\xi}_i)(\Omega^{\xi}_{o}\beta_{12R} - \Omega^{\eta}_{o}\beta_{13R})]$$

$$+ C_{MOM}C^{\zeta o}_{M}\cos\theta_2 + C^{d\zeta}_{MOM}C^{\zeta o}_{fM}\beta_{23R} + \Theta^{\zeta'}\beta_{23R} \qquad (2.175)$$

$$\varepsilon_e^{\xi}\Omega_{1Rs}^{\xi} = -\varepsilon_{es}^{\xi}\Omega_{1R}^{\xi} + Q_{1R}^{\eta} - (\varepsilon_e^{p} - \varepsilon_e^{\eta})(\Omega_o^{\eta}\Omega_{1R}^{\zeta} + \Omega_o^{\zeta}\Omega_{1R}^{\eta})$$

$$+ \beta_{12R}M_{Ho}^{\zeta} + (\Sigma/\lambda^{\xi})^2 \beta_{13R} - \Sigma[\lambda_i^{\xi}(2\Omega_{1I}^{\xi}$$

$$+ \Omega_o^{\xi}\beta_{12I} - \Omega_o^{\eta}\beta_{23I}) + (\lambda_i^{\xi} - \lambda_i^{\eta})(\Omega_o^{\xi}\beta_{12I} + \Omega_o^{\eta}\beta_{23I})] \qquad (2.176)$$

$$\varepsilon_e^{\xi}\Omega_{1Is}^{\xi} = -\varepsilon_{es}^{\xi}\Omega_{1I}^{\xi} + Q_{1I}^{\eta} - (\varepsilon_e^{p}-\varepsilon_e^{\eta})(\Omega_o^{\eta}\Omega_{1I}^{\zeta} + \Omega_o^{\zeta}\Omega_{1I}^{\eta})$$

$$+ \beta_{12I}M_{Ho}^{\zeta} + (\Sigma/\lambda^{\xi})^2 \beta_{13I} + \Sigma[\lambda_i^{\xi}(2\Omega_{1R}^{\xi}$$

$$+ \Omega_o^{\xi}\beta_{12R} - \Omega_o^{\eta}\beta_{23R}) + (\lambda_i^{\xi} - \lambda_i^{\eta})(\Omega_o^{\xi}\beta_{12R} + \Omega_o^{\eta}\beta_{23R})] \qquad (2.177)$$

$$\varepsilon_e^{\eta}\Omega_{1Rs}^{\eta} = -\varepsilon_{es}^{\eta}\Omega_{1R}^{\eta} - Q_{1R}^{\xi} - (\varepsilon_e^{\xi}-\varepsilon_e^{p})(\Omega_o^{\xi}\Omega_{1R}^{\zeta} + \Omega_o^{\xi}\Omega_{1R}^{\zeta})$$

$$+ \beta_{13R}M_{Ho}^{\zeta} - (\Sigma/\lambda^{\eta})^2 \beta_{12R} - \Sigma[\lambda_i^{\eta}(2\Omega_{1I}^{\eta} + \Omega_o^{\xi}\beta_{23I}$$

$$+ \Omega_o^{\xi}\beta_{13I}) + (\lambda_i^{\xi} - \lambda_i^{\xi})(\Omega_o^{\xi}\beta_{23I} - \Omega_o^{\xi}\beta_{13I})] \qquad (2.178)$$

$$\varepsilon_e^{\eta}\Omega_{1Is}^{\eta} = -\varepsilon_{es}^{\eta}\Omega_{1I}^{\eta} - Q_{1I}^{\xi} - (\varepsilon_e^{\xi}-\varepsilon_e^{p})(\Omega_o^{\xi}\Omega_{1I}^{\zeta} + \Omega_o^{\xi}\Omega_{1I}^{\zeta})$$

$$+ \beta_{13I}M_{Ho}^{\zeta} - (\Sigma/\lambda^{\eta})^2 \beta_{12I} + \Sigma[\lambda_i^{\eta}(2\Omega_{1R}^{\eta} +$$

$$\Omega_o^{\xi}\beta_{23R} + \Omega_o^{\xi}\beta_{13R}) + (\lambda_i^{\xi}-\lambda_i^{\xi})(\Omega_o^{\xi}\beta_{23R} - \Omega_o^{\xi}\beta_{13R})] \qquad (2.179)$$

$$\beta_{23Rs} = \Omega_{1R}^{\xi} - \Omega_o^{\xi}\beta_{12R} - \Omega_o^{\eta}\beta_{13R} \qquad (2.180)$$

$$\beta_{23Is} = \Omega_{1I}^{\xi} - \Omega_o^{\xi}\beta_{12I} - \Omega_o^{\eta}\beta_{13I} \qquad (2.181)$$

$$\beta_{13Rs} = -\Omega^{\xi}_{1R} + \Omega^{\eta}_{o}\beta_{23R} - \Omega^{\zeta}_{o}\beta_{12R} \tag{2.182}$$

$$\beta_{13Is} = -\Omega^{\xi}_{1I} + \Omega^{\eta}_{o}\beta_{23I} - \Omega^{\zeta}_{o}\beta_{12I} \tag{2.183}$$

$$\beta_{12Rs} = \Omega^{\eta}_{1R} + \Omega^{\zeta}_{o}\beta_{13R} + \Omega^{\xi}_{o}\beta_{23R} \tag{2.184}$$

$$\beta_{12Is} = \Omega^{\eta}_{1I} + \Omega^{\zeta}_{o}\beta_{13I} + \Omega^{\xi}_{o}\beta_{23I} \tag{2.185}$$

$$p_{Rs} = T_{1R}e_{om} - \Omega^{\xi}_{o}r_{R} + \Omega^{\eta}_{o}q_{R} \tag{2.186}$$

$$p_{Is} = T_{1I}e_{om} - \Omega^{\xi}_{o}r_{I} + \Omega^{\eta}_{o}q_{I} \tag{2.187}$$

$$q_{Rs} = (1+e_{o})\beta_{12R} - \Omega^{\eta}_{o}p_{R} + \Omega^{\zeta}_{o}r_{R} \tag{2.188}$$

$$q_{Is} = (1+e_{o})\beta_{12I} - \Omega^{\eta}_{o}p_{I} + \Omega^{\zeta}_{o}r_{I} \tag{2.189}$$

$$r_{Rs} = (1+e_{o})\beta_{13R} - \Omega^{\zeta}_{o}q_{R} + \Omega^{\xi}_{o}p_{R} \tag{2.190}$$

$$r_{Is} = (1+e_{o})\beta_{13I} - \Omega^{\zeta}_{o}q_{I} + \Omega^{\xi}_{o}p_{I} \tag{2.191}$$

Equations (2.168) to (2.191) form a system of twenty-four first order coupled non-linear ordinary differential equations in the following twenty-four unknowns:

$$\vec{w}(s) = [T_{1R}, T_{1I}, Q^{\xi}_{1R}, Q^{\zeta}_{1I}, Q^{\eta}_{1R}, Q^{\eta}_{1I}; \Omega^{\zeta}_{1R}, \Omega^{\zeta}_{1I},$$

$$\Omega^{\xi}_{1R}, \Omega^{\xi}_{1I}, \Omega^{\eta}_{1R}, \Omega^{\eta}_{1I}; \beta_{23R}, \beta_{23I}, \beta_{13R}, \beta_{13I},$$

$$\beta_{12R}, \beta_{12I}; p_{R}, p_{I}, q_{R}, q_{I}, r_{R}, r_{I}]^{T} \tag{2.192}$$

Twenty-four boundary conditions are in addition required to complete the statement of the dynamic problem. In this work, single leg multitube riser configurations with prescribed dynamic displacements and angles at both ends

are studied. These are estimated from the motions and rotations of the supporting platforms in a surface wave given by (2.20). In this calculation the following equations are also useful

$$\beta_{23} = \beta_{13} = \beta_{12} = p = q = r = 0 \quad \text{at } s = 0 \tag{2.193}$$

$$\beta_{23} = \beta'_{23} + i\beta''_{23},\ \beta_{13} = \beta'_{13} + i\beta''_{13},\ \beta_{12} = \beta'_{12} + i\beta''_{12} \quad \text{at } s = 1 \tag{2.194}$$

$$p = p' + ip'',\ q = q' + iq'',\ r = r' + ir'' \quad \text{at } s = 1 \tag{2.195}$$

$$\beta_{23} = \psi_1 - \phi_1 \sin\theta_0 \tag{2.196}$$

$$\beta_{13} = -\phi_1 \cos\theta_0 \sin\psi_0 - \theta_1 \cos\psi_0 \tag{2.197}$$

$$\beta_{12} = \phi_1 \cos\theta_0 \cos\psi_0 - \theta_1 \sin\psi_0 \tag{2.198}$$

3. SOLUTION METHOD

3.1 INTRODUCTION

General methods for the solution of two-point boundary value problems can be found in Keller [19], Ferziger [20] and Pereyra [21]. We start our discussion by considering the following general boundary value problem:

$$\vec{w}' = \vec{f}(s,\vec{w}), \qquad \vec{g}(\vec{w}(0),\vec{w}(1)) = 0 \tag{3.1}$$

where

- ( )' denotes derivative with respect to s
- $\vec{w} = [w_1(s),w_2(s),....,w_N(s)]^T$ is the solution vector
- $\vec{f} = [f_1,f_2,....,f_N]^T$
- $\vec{g} = [g_1,g_2,....,g_N]^T$
- $0 \leq s \leq 1$ and $[\ ]^T$ denotes transpose

Embedding solution methods introduce a continuation of (3.1) to

$$\vec{w}' = \vec{f}(s,\vec{w};\varepsilon), \qquad \vec{g}[\vec{w}(0),\vec{w}(1);\varepsilon)] = 0 \tag{3.2}$$

where ε is a continuation parameter $0 \leq \varepsilon \leq 1$, and when $\varepsilon = 1$ equations (3.1) and (3.2) are identical.

Using the embedding technique, a sequence of problems with values of ε such that $0 = \varepsilon_1 < \varepsilon_2 < ... < \varepsilon_p = 1$ are solved. The solution of the problem involving ε_k uses as initial approximation the solution of the problem involving ε_{k-1}. The non-linear static solutions presented in [2] to [5] and the eigensolutions presented in [6] and [7] for various compliant riser configurations use the above embedding method specialized to the particular situation. It was found that the following two rules in selecting (3.2) make the embedding process robust and very efficient:

- The problem corresponding to $\varepsilon = 0$ should be easier to solve than the initial problem ($\varepsilon = 1$) so that we can start the solution process with no difficulty.
- The problem corresponding to $\varepsilon = 0$ should express the balance of all major external and restoring forces of the original problem correctly everywhere in $0 \leq s \leq 1$.

So in choosing (3.2) for $\varepsilon = 0$, it is advisable to use our intuition about the physics of the problem at hand and then derive initial approximate solutions for $\varepsilon = 0$ using asymptotic techniques or a combination of asymptotic and numerical techniques (for example involving the solution of a small system of non-linear algebraic equations or the solution of a system of linear equations). This is the solution method followed in this work.

3.2 STATIC PROBLEM SOLUTION METHOD

As indicated earlier, the first step in the solution process followed in this work is the solution of the non-linear static problem in the presence of mean forces and moments due to currents and waves possibly involving static riser ocean bottom interaction. The non-linear three-dimensional static equations for a flexible riser were presented in section 2.4.1 (equations 2.42 - 2.54).

The solution of the set of non-linear static equations is obtained using a non-uniform grid finite difference method, Pereyra [21]. The non-uniform grid is necessary to permit an efficient resolution of internal or boundary layers in the riser. The solution of the finite difference equations is based on a modified Newton's iteration method coupled with a deferred correction technique also described in Pereyra [21]. The numerical solution scheme employed to solve the static equations uses the embedding techniques described in the previous section, which require an initial static approximate solution. The numerical scheme uses the approximate solution of the problem and yields a more accurate solution which makes the absolute error less than a prespecified tolerance. During the solution process, additional grid points may be inserted automatically to reduce and equidistribute the error on the final mesh. The computer implementation of this solution scheme uses the NAG Fortran mathematical library [22]. The initial approximations of the solution of the static problem are either analytical (for two-dimensional cases) or numerical.

The analytical approximate solutions of two-dimensional static problems are derived using asymptotic techniques. These analytical solutions correctly account for all major external and restoring forces in a riser equation and, therefore, provide excellent initial approximations of the solution of the non-linear static problem. For this reason fast convergence of the embedding sequence and the associated Newton-Raphson iterations employed in the numerical solution of the non-linear problem is observed in most cases.

References [3] and [4] provide an analytical two-dimensional approximate solution for the case of buoyant risers (risers with small effective weight) in the presence of current, while reference [5] provides an analytical technique to compute the static solution for catenary risers (risers with large effective weight). The above two analytic solutions are used also in the present work. For the buoyant riser in a current case, the major external force is the current force which is balanced with the riser restoring forces to determine the initial approximation. For the catenary riser case, the major external force is the weight of the riser, which is balanced with the riser restoring forces to determine the initial approximation.

An additional asymptotic technique was developed to provide an analytical approximate static solution for the case of a catenary riser experiencing static riser-ocean bottom interaction. In this case the major external forces are

the weight of the riser and the static bottom interaction force over a portion of the riser, both of which need to be balanced with the riser restoring forces to determine the initial static approximation. Appendix I presents an analytical approximate solution for catenary risers experiencing bottom interaction. For the other asymptotic solutions the reader should consult references [3], [4] and [5] for a detailed account.

An alternative to using analytical asymptotic techniques to determine an initial approximation to the static problem is to use an already existing two-dimensional or three-dimensional static solution for different excitation conditions (wave, current or riser motions) and/or different boundary conditions (static displacements at the top, static angles e.t.c.). These different excitation conditions and/or different boundary conditions are modified incrementally with the continuation parameter ε introduced in section 3.1, until they reach the actual excitation conditions and/or actual boundary conditions for the problem at hand. Thus for $\varepsilon=1$ the solution obtained corresponds to the excitation conditions and/or boundary conditions of the actual problem. In this way, we can also march from a two-dimensional static solution to a three-dimensional static solution by embedding on the three-dimensional excitation characteristics and/or boundary conditions, [2], [3] and [5].

The initial approximation to the static solution is the single most important factor for fast convergence of the Newton Raphson iteration and care should be exercised for the rational selection of the form of the approximate solution to use in each case. An example of a special, relatively difficult, static problem and the best approach to solve it follow. For the case of a buoyant riser in a weak or zero current, the "buoyant riser in a current" analytic approximation is not valid and Newton's iteration may break down if such an initial approximation is used. In this case it is preferable to analyze first the buoyant riser in an artificial moderate current, using the buoyant riser initial approximation, and then use the numerical solution for the artificial moderate current as an initial approximation to solve for the buoyant riser in the weak or zero current using embedding. This methodology was found to provide fast convergence of the Newton Raphson iterations.

The final element in the static solution technique implemented is that once the static solution and then the dynamic solution is obtained for a particular excitation, the dynamic riser motions are determined. Then the mean static forces and moments due to current, waves and the riser dynamic motions can be estimated more accurately in equations 2.133, 2.135, 2.137 and 2.139. These more accurate forces and moments can then be used to solve the non-linear static problem and improve the static solution. This iteration step can be repeated, until a satisfactory converged solution is obtained. This technique allows us to account more accurately for the mean configuration of compliant risers in the presence of waves and small dynamic motions.

3.3 DYNAMIC PROBLEM SOLUTION METHOD

After the static riser problem is solved, the structural part of the non-linear dynamic riser equations is linearized around the static configuration assuming small dynamic motions and rotations. Then the non-linear drag forces and moments as well as the non-linear riser-ocean bottom interaction forces are harmonically linearized for the solution of the dynamic riser problem. This results in a non-linear boundary value problem. The formulation of the dynamic compliant riser problem was already presented in detail in Chapter 2 of this report.

The solution of the set of dynamic equations is obtained using a non-uniform grid finite difference method, Pereyra [21]. The non-uniform grid is necessary to permit efficient resolution of internal or boundary layers in the riser response. The solution of the finite difference equations is based on a modified Newton's iteration method coupled with a deferred correction technique also described in Pereyra [21]. This method uses an approximate solution of the dynamic problem and yields a more accurate solution which makes the absolute error less than a prespecified tolerance. During the solution process, additional grid points may be inserted automatically to reduce and to equidistribute the error on the final mesh. The computer implementation of this solution technique uses the NAG Fortran library [22].

The numerical technique used for the dynamic problem is similar to the technique used for the static problem. Again the initial approximation is the most important factor in ensuring fast convergence of the Newton iterations. For the estimation of the hydrodynamic forces and moments the local wave and current characteristics are evaluated on the static riser configuration. The procedure followed to solve the non-linear dynamic problem is as follows.

First the non-linear drag forces and moments and bottom interaction forces are approximately linearized and the resulting linear dynamic equations are solved using a non-uniform grid finite difference technique for solving a system of linear ordinary differential equations. The above approximate linearization of the drag forces and moments, replaces the product $|V_{rel}|\cdot V_{rel}$ by $A\cdot V_{rel}$ where A is a local approximate relative velocity using an estimate for the riser dynamic motions. In the first iteration the riser dynamic motions are assumed to vary linearly along the length of the riser from the given riser top dynamic motions to the given riser bottom dynamic motions. In the second and following iterations the approximate linear riser problem is solved using as an approximation for the riser dynamic motions the resulting motions of the previous iteration of the approximate linear riser problem. In this initial approximation, the effect of bottom interaction in the dynamic problem is only accounted in the region of static riser-ocean bottom interaction.

This linear dynamic problem is solved a few times, improving each time the approximation to the riser motions and also improving the overall initial approximation to the non-linear dynamic problem. Once a satisfactory linear

solution is obtained, it is used as an initial approximation to solve the complete non-linear problem using the complete equivalent linearization technique for the drag forces and the riser-bottom interaction forces and using the Newton Raphson technique as was outlined before.

4. COMPARISON WITH OTHER THEORIES

The solution techniques described above have been implemented in general computer codes for the static and dynamic analysis of single leg multitude flexible risers. In this chapter, comparisons of the results of our theoretical formulation with other theories for the analysis of the static and dynamic response of flexible risers will be presented in order to validate the proposed formulation.

4.1 COMPARISON WITH CABLE STATICS AND DYNAMICS TECHNIQUES

The proposed formulation was compared with the cable static and dynamic analysis techniques developed by Triantafyllou et al [8] for a catenary riser using a cable idealization. The characteristics of the riser system analyzed are presented in Table 4.1. Initially the cable static solution was determined to obtain the static angles at the bottom and at the top of the riser to use as boundary conditions in our riser static solution. This is required, since the riser static formulation assumes fixed (clamped) boundary conditions with prescribed static angles in the riser ends while a cable formulation allows only for pin-supported boundary conditions (bending effects are not modelled). Such choice of the end angle boundary conditions is likely to reduce bending effects in the comparison of the riser and cable idealizations. Using the above static angles at the riser ends, the riser static and dynamic solutions were determined. The riser analyzed has a length of 140 m, in water depth of 90 m. The static boundary conditions for our riser solution are:

$x(L) = 115$ m
$y(L) = 60$ m
$x(0) = y(0) = 0$ m
$\phi(0) = -13.6°$
$\phi(L) = 62.7°$

The static excitation conditions used in this comparison correspond to linear current varying from 1.03 m/s at the bottom end of the riser (y=0) to 1.5 m/s at the top of the riser. The dynamic excitation consisted of top end dynamic motions in the x and y directions with an amplitude of 1 m and zero phase between the motions ($|x_1(L)| = 1$ m, $|y_1(L)| = 1$ m and zero phase angle). Two excitation frequencies equal to 0.6 and 0.8 rad/s were used. All other riser dynamic motions and rotations at the ends were assumed to be zero, and no waves were present. The resulting configuration is two-dimensional in the x-y plane.

Figure 4.1 presents the static riser configuration for the above conditions, while Table 4.2 presents the comparisons for the effective tension at the top and bottom of the riser from the static and dynamic solutions using the riser and cable formulations. The agreement for the static effective tension at the riser ends is very good. The agreement of the dynamic results is also very good both in the amplitude of the dynamic tension at the top as well as in the phase of the dynamic tension at the top. No comparison of curvatures was performed, because the cable idealization does not include the effects of the actual clamped boundary conditions on the curvature.

Table 4-1: Characteristics of Compliant Riser

L	= 140 m
$D_o=D^{\xi}$	= 0.3048 m
D_i	= 0.269 m
$P^{\xi\eta}$	= 0.9576 m
m_T	=119.6 kg/m
m_a^{ξ}	= 74.79 kg/m
W_a	= 439.35 N/m
EA	= 4.882×10^8 N
$EI^{\eta\eta}$	= 3.6×10^4 Nm^2 (for riser formulation only)
C_D	= 1.0
C_f	= 0.05

Figure 4-1: Static Configuration of Catenary Compliant Riser Using Riser and Cable Idealizations

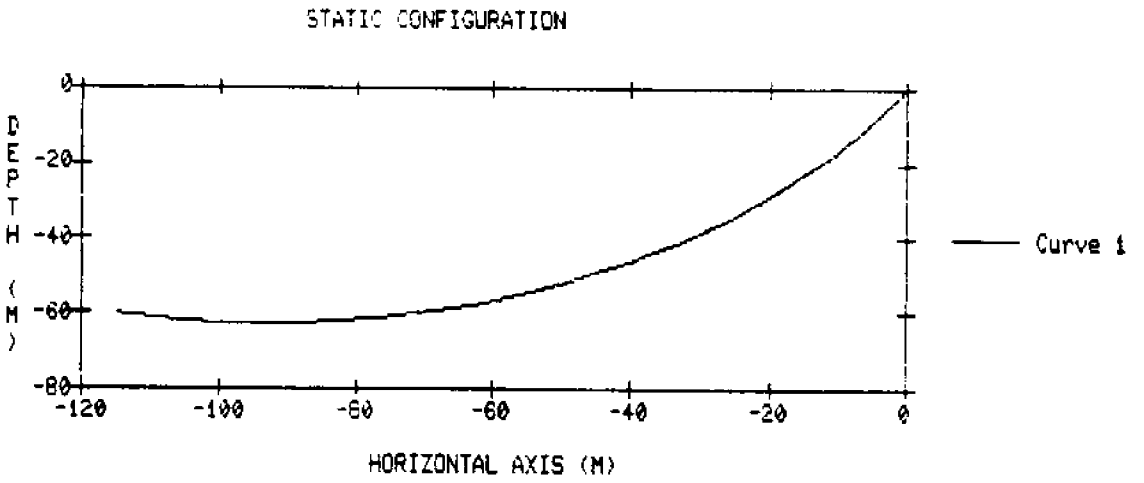

4.2 COMPARISON WITH A HYBRID FINITE ELEMENT TECHNIQUE, [23]

The present formulation was also compared with the two-dimensional non-linear static and dynamic analysis presented in reference [23]. McNamara et al, [23], used a time domain hybrid finite element formulation to analyze the static and dynamic performance of flexible risers. This formulation uses the usual beam-column equations of the Bernoulli-Euler bending theory extended for large deformations and introduces the inextensibility condition as a geometric constraint on the axial deformations leading to a hybrid or mixed formulation of the resulting equations. Thus the axial force is independently interpolated and only combined with the corresponding axial displacements via

Table 4-2: Static and Dynamic Comparison for Catenary Compliant Riser Using Riser and Cable Idealization

L=140 m $\phi_o(L)$=62.6° $\phi_o(0)$=-13.6° x_{top}=115 m y_{top}=60 m
$V_c(y=0)$=1.03 m/s $V_c(y=60)$=1.5 m/s

STATIC COMPARISON

CABLE	RISER
T(L) = 65 kN	T(L) = 65.07 kN
T(0) = 40.5 kN	T(0) = 41.7 kN

$|x_1(L)| = |y_1(L)|$ = 1 m Phase = 0°

DYNAMIC COMPARISON

	CABLE		RISER	
ω	$T_1(L)$	Phase	$T_1(L)$	Phase
0.6	16.40	122.2	18.87	117.3
0.8	27.61	128.8	30.58	124.2
rad/s	kN	deg	kN	deg

a Lagrangian constraint [23].

Results will be compared for the motions and forces on a flexible catenary riser connecting a tanker to a subsea tower. The characteristics of the riser are presented in Table 4.3. The riser has a length of 350 m and is supported at a subsea tower point at a depth of 150 m and at a surface platform displaced horizontally by 150 m The water depth is equal to 350 m. It is assumed that the riser is full of sea water. No external current is present.

McNamara et al, [23], assumed a pin-supported riser in contrast to the present formulation which assumes the more usual clamped boundary conditions. For the present analysis the static riser angles at the two ends were selected equal to the static riser angles determined from the hybrid finite element technique to approximate the pin-supported configuration and minimize bending effects in the comparison. The above difference, however affects the prediction of bending moments in the riser particularly close to the riser ends (difference between pin-support and fixed support). The static boundary conditions are as follows in this case:

x(L) = 150 m
y(L) = 150 m
x(0) = y(0) = 0 m
$\phi(0)$ = -71.18°
$\phi(L)$ = 82.81°

The dynamic excitation for this comparison consisted of top riser motion due to a sinusoid surge motion of the supporting vessel with amplitude of 2.01 m with an excitation period of 14 s. The resulting configuration is two-dimensional in the x-y plane. Figure 4.2 presents the static configuration for the riser analyzed. Both the present formulation prediction (continuous line) and the hybrid finite element method prediction (circle symbol) are shown. The agreement is very good. Table 4.4 presents a comparison of the horizontal and vertical projections of

the static effective tensions at the top and bottom of the riser predicted from the two techniques. Table 4.4 also presents a comparison of the maximum dynamic vertical projection of the effective tension at the top and bottom of the riser predicted from the two techniques. As can be seen from Table 4.4 the agreement is very good in all cases. The agreement with the static moment predicted by the two techniques was also very good except close to the riser ends where the different boundary conditions affected the static riser bending moments. There was no sufficient information in [23] to compare the predictions from the two methodologies for the dynamic bending moments in the riser.

Table 4-3: Characteristics of a Catenary Riser adapted from [23]

L	= 350 m
$D_o=D^{\xi}$	= 0.26 m
D_i	= 0.20 m
$P^{\xi\eta}$	= 0.8168 m
m_T	= 89.7 kg/m
m_a^{ξ}	= 54.42 kg/m
W_a	= 346.1 N/m
EA	= 1.538×10^9 N
$EI^{\eta\eta}$	= 2.096×10^4 Nm^2
C_D	= 1.0
C_f	= 0.0 (no information was available from [23])

Figure 4-2: Static Configuration of Catenary Riser from [23]

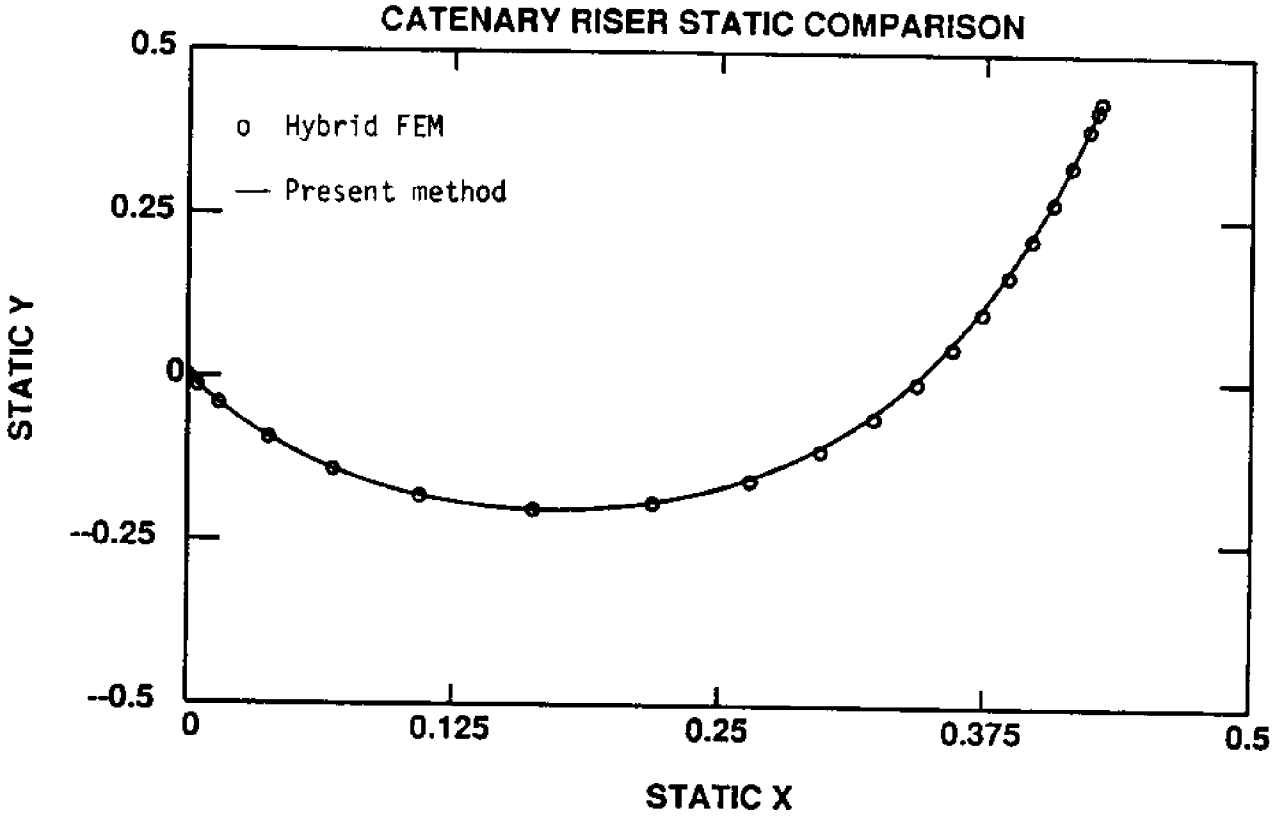

Table 4-4: Static and Dynamic Comparison for Catenary Riser from [23]

L=350 m, $\phi_o(L)$=82.81°, $\phi_o(0)$=-71.18°, x_{top}=150 m, y_{top}= 150 m, V_c = 0 m/s

STATIC COMPARISON

HYBRID FEM	RISER
V(L) = 91.45 kN	V(L) = 87.1 kN
V(0) = 35.83 kN	V(0) = 34.5 kN
H(L) = 11.57 kN	H(L) = 11.4 kN
H(0) = 11.92 kN	H(0) = 11.42 kN

$|x_1(L)|$ = 2.01 m Phase = 0° Period = 14 s

DYNAMIC COMPARISON

HYBRID FEM	RISER
$V_1(L)$ = 1.5 kN	$V_1(L)$ = 1.532 kN
$V_1(0)$ = 0.20 kN	$V_1(0)$ = 0.173 kN

V = vertical force
H = horizontal force

4.3 COMPARISON WITH TIME DOMAIN FINITE ELEMENT RISER DYNAMIC SOLUTION

Comparisons with the two-dimensional static and dynamic analysis of flexible risers presented in references [24] and [25] will be presented next. References [24] and [25] used a general purpose non-linear finite element program to analyze large amplitude dynamic response of flexible risers. Results will be compared for the motions and forces on a flexible steep-wave riser configuration. The flexible riser system is located at 320 meters water depth. The upper point of the riser is connected to a floater 22 meters below the water surface and follows the motion of the platform. The system is exposed to current and waves. The lower end point is located 9 meters above the sea floor. The characteristics of the riser are presented in Table 4.5. The riser has a length of 420 meters. It is composed of two bare sections and two buoyancy sections. The bare sections are uniform in characteristics. The first buoyancy section starts 30 m away from the lower end of the riser and is 60 m long. The second buoyancy section starts 90 m away from the lower end of the riser and is 30 m long. The two buoyancy sections provide a smoother curvature in the lower region of the riser.

The static offset of the floater for the condition analyzed was 225.7 m in the direction of the current flow. The current profile used is piecewise linear and has the following characteristics:

Water Depth (m)	0	25	50	100	200	317
Current (m/s)	1.71	1.42	1.25	0.85	0.70	0.50

References [24] and [25] assumed a pin-supported riser in contrast to the present methodology which assumes

clamped riser support. For the present analysis the static riser angles at the two riser ends were selected to be approximately equal to the static riser angles determined from the finite element technique. The difference in the boundary conditions for the two techniques, however, affects significantly only the prediction of the curvature close to the riser ends. The static boundary conditions for the case analyzed are as follows:

$x(L) = 225.7$ m
$y(L) = 289.0$ m
$x(0) = y(0) = 0$ m
$\phi(0) = 65°$
$\phi(L) = 80°$

For the dynamic comparison, a regular surface wave with amplitude of 15.5 m and period of 16 seconds (circular frequency 0.392 rad/s) was used. In addition, the top end of the riser was excited by a heave motion amplitude of 8.99 m with zero phase angle and a surge motion amplitude of 10.37 m with -90 degrees phase angle relative to the wave crest at the top end of the riser. The resulting configuration is two-dimensional in the x-y plane.

Figure 4.3 presents the static configuration for the riser analyzed. Both the present formulation prediction (continuous line) and the finite element technique prediction (circle symbol) from [24] and [25] are shown. As can be seen the agreement is very good. Figure 4.4 compares the static effective tension for the two formulations along the length of the riser. The continuous line corresponds to our solution, while the square symbol corresponds to the finite element technique solution. The maximum effective static tension is about 150 kN, at about 25 m from the lower end of the riser. The agreement is very good, except near the riser ends where the effect of the different boundary conditions is more significant, although still relatively small.

Figure 4.5 presents a comparison for the two formulations for the predictions of the dynamic effective tension along the length of the riser. Since the result from the time domain non-linear finite element analysis is not sinusoid in time, the maximum, minimum and average dynamic effective tension in one cycle of oscillation from the finite element analysis is plotted (circle, square and triangle symbols respectively). Our definition of the average dynamic effective tension from the time domain program is to take the mean of the absolute values of the maximum and minimum dynamic effective tension. Two curves from our analysis are also shown. The first corresponds to the dynamic effective tension based on a static configuration in which wave and dynamic riser motion effects are not included, while the second corresponds to the dynamic effective tension based on a corrected static configuration accounting for waves and dynamic riser motion. Both curves from the present formulation are in fair agreement with the average dynamic effective tension (square symbol) predicted by the finite element technique except near the top end of the riser where the present methodology overpredicts the average dynamic effective tension.

Since it is difficult to determine from the time domain finite element technique a single dynamic tension

amplitude, Figure 4.6 was prepared to compare the maximum total effective tension (static + dynamic) from the two formulations. Again two curves from our analysis are shown, corresponding to the corrected static configuration accounting for waves and riser dynamic motions and to the initial static configuration without wave and riser motion effects. The square symbol corresponds to the finite element method prediction. As can be seen the agreement between the two methodologies is very good. The corrected dynamic result is more accurate than the initial dynamic result from our methodology. The present methodology overpredicts the total effective tension at the top of the riser (177 kN as compared to 165 kN for the finite element technique at the top of the riser) and underpredicts the total effective tension at the lower part of the riser (167 kN as compared to 173 kN for the finite element technique at about 25 m from the lower point of the riser). Again these differences may be partly attributed to the different boundary conditions used by the two methodologies. The non-linear terms employed in the time domain finite element solution do not appear to significantly affect the response even under extreme excitation conditions. It is noteworthy that our linearized frequency domain formulation reproduces the results of time domain non-linear formulations to the degree seen in Figure 4.6. Such a favorable comparison is, however, expected to be valid when the dynamic effective tension is relatively small compared to the local static effective tension at all points along the length. There were no data available to compare the dynamic bending moment predictions from the two formulations.

Table 4-5: Characteristics of Steep-Wave Riser adapted from [24] and [25]

L	= 420 m
$D_o=D^{\xi}$	= 0.2755 m
D_i	= 0.2008 m
D_b	= 0.9 m (in buoyancy sections)
EA	= 9.6×10^6 N
$EI^{\eta\eta}$	= 3.417×10^4 Nm^2
C_D	= 1.0
C_f	= 0.0 (no information was available from [24],[25])
$p^{\xi\eta}$	= 0.8655 m (in bare section) = 2.827 m (in buoyancy sections)

Riser sections from lower point

30 m	60 m	30 m	300 m
Bare	Buoyancy I	Buoyancy II	Bare

	Bare	Buoyancy I	Buoyancy II
m =	112.4 kg/m	334.8 kg/m	241.7 kg/m
m_a^{ξ} =	61.1 kg/m	652.1 kg/m	652.1 kg/m
W =	503.2 N/m	-2285.0 N/m	-1118.0 N/m

Figure 4-3: Static Configuration Comparison for Steep-Wave Riser

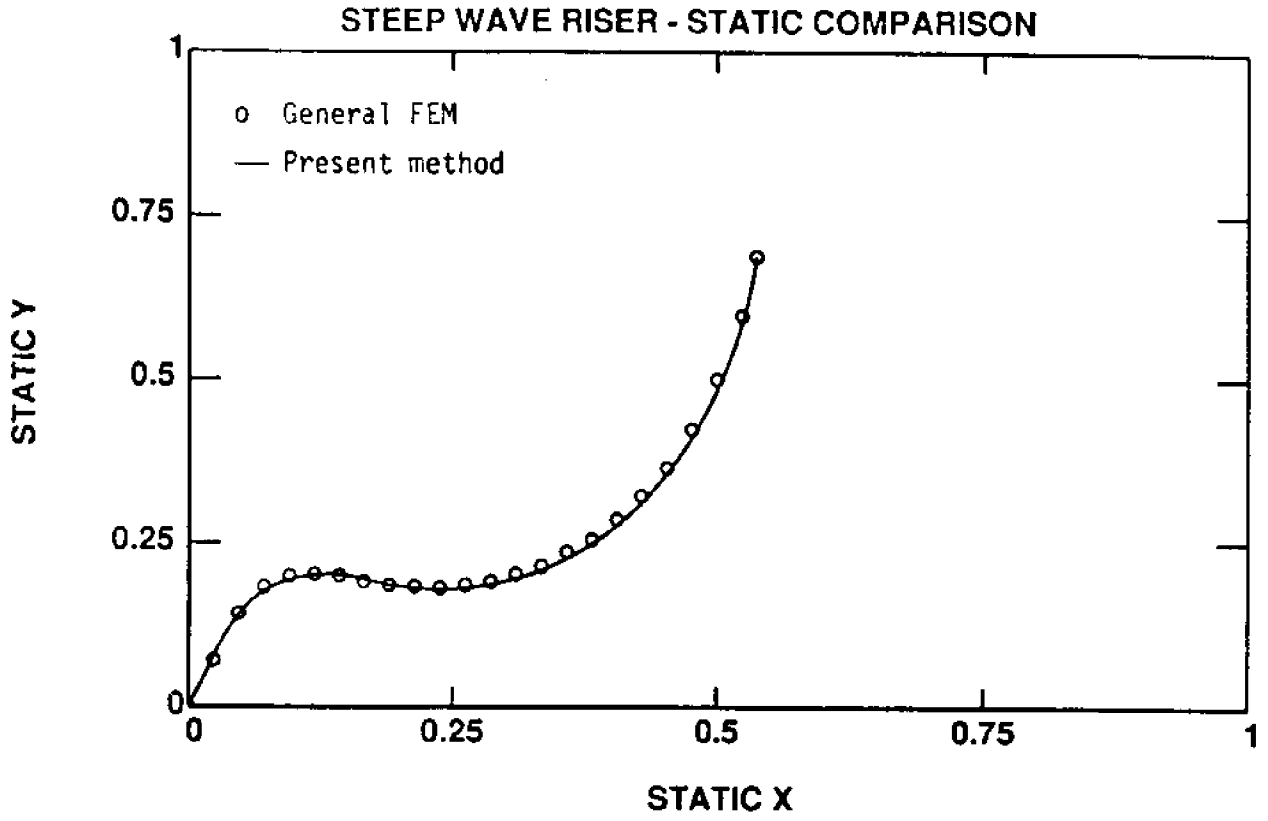

4.4 SUMMARY OF COMPARISONS

The proposed methodology for the analysis of the static and dynamic response of flexible risers was shown to be in good agreement with three independent analyses, the cable analysis of reference [5], the hybrid finite element analysis of reference [23] and the general finite element analysis of references [24] and [25]. Some additional riser examples will be treated in the following section. We could not locate data to compare the proposed methodology for the case of a catenary riser experiencing ocean bottom interaction.

All the configurations compared assumed pin-supported conditions in contrast to the more used fixed (clamped) boundary conditions for flexible risers. Clamped boundary conditions may result in boundary layers at the ends of the riser. Such layers require a large number of finite elements to analyze accurately the response. The proposed solution method using an adaptive non-uniform grid finite difference technique allows resolution of these boundary layers in an efficient manner.

Comparisons with experimental results are still required to verify the validity of our methodology in predicting riser motions, effective tension and bending moments. The authors could not, however, locate appropriate

Figure 4-4: Comparison for Static Effective Tension

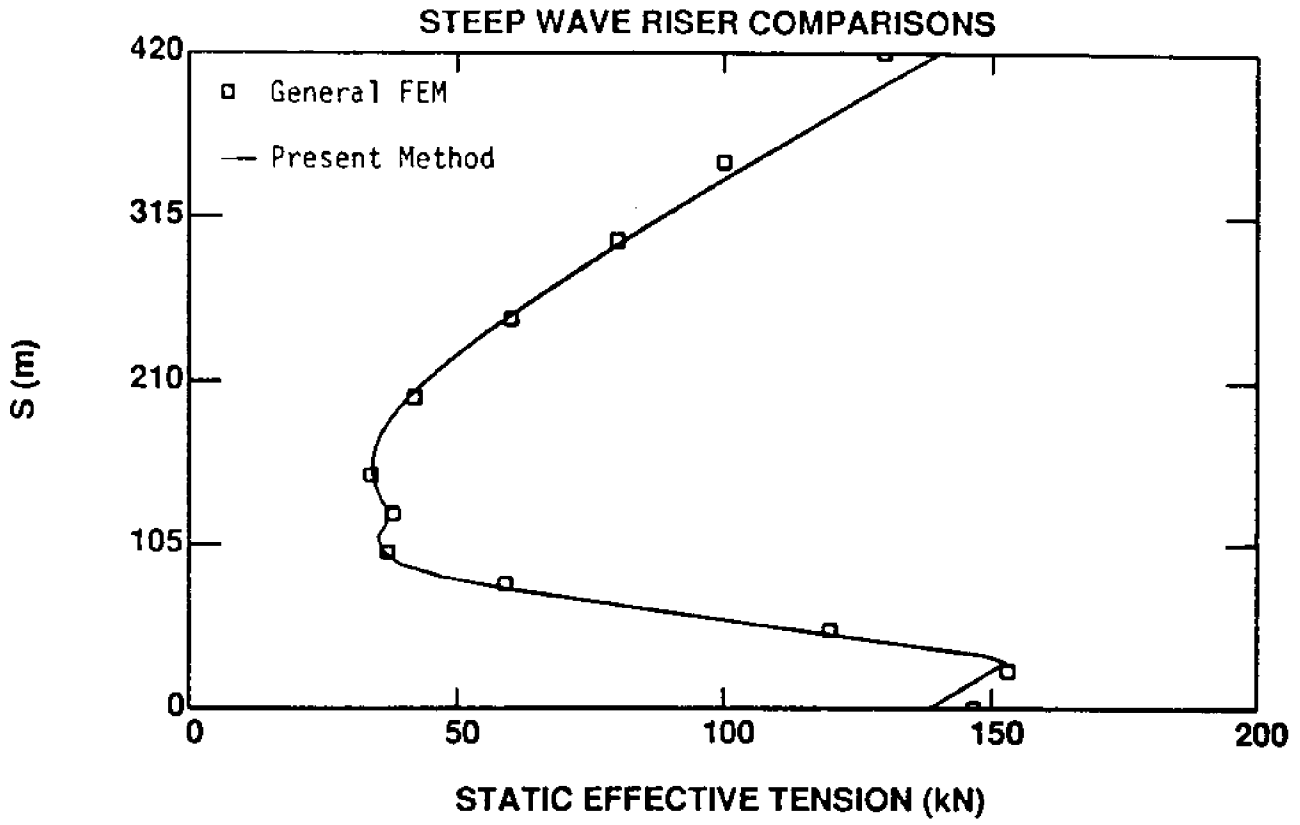

experimental data needed in such a comparison.

Figure 4-5: Comparison for Dynamic Effective Tension
A_w=15.5 m, T=16 s, $|x_1|$=10.37 m, phase -90°, $|y_1|$=8.99 m and phase 0°

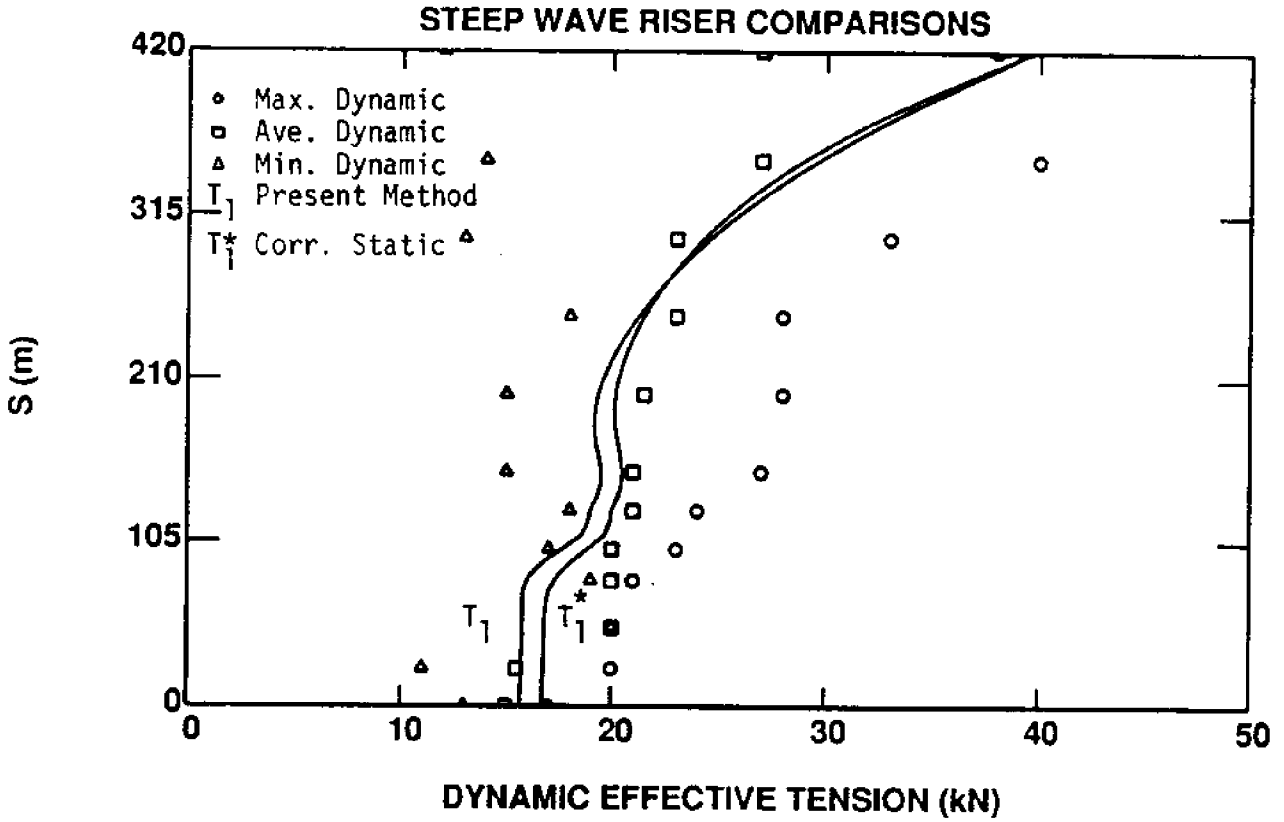

Figure 4-6: Comparison for Total Effective Tension from the Two Formulations

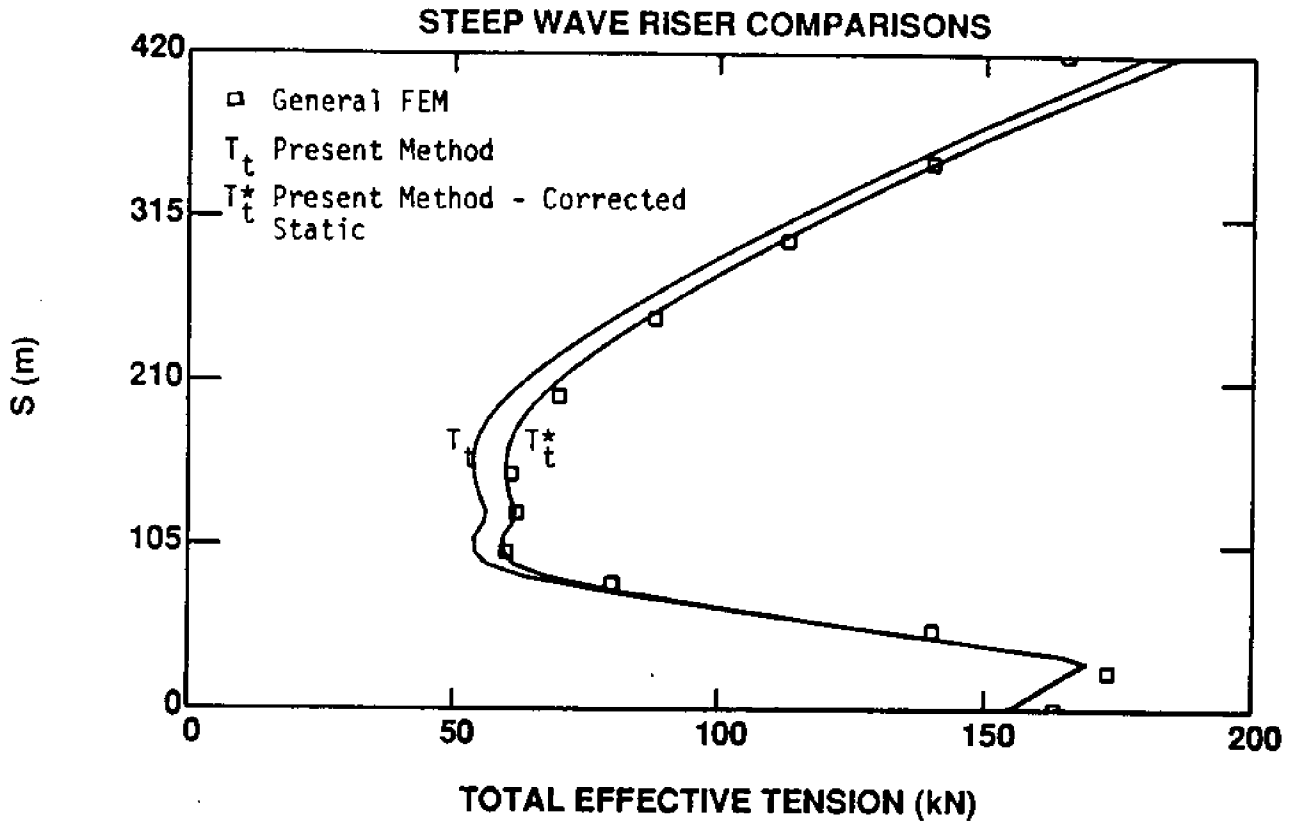

5. ADDITIONAL NUMERICAL EXAMPLES

In this chapter, some additional and more detailed results will be presented from the dynamic analysis of flexible risers. Three riser systems were analyzed, a shallow water buoyant riser, a shallow water catenary riser in a two-dimensional and a three-dimensional configuration and a deep water catenary riser experiencing riser ocean-bottom interaction.

5.1 SHALLOW WATER BUOYANT RISER

The first case analyzed is a buoyant flexible riser in the presence of current and top dynamic excitation. The static configuration for this riser has been analyzed in reference [3]. The structural design details for this buoyant riser can be found in reference [26]. The characteristics of this riser are presented in Table 5.1. The riser analyzed in this section is made up of two flexible tubes with inner diameter of 85.7 mm and outer diameter of 122.9 mm clamped together. The riser has a length of 88.392 m and is located in water depth of 80.77 m. The lower end of the riser is located 7.62 m from the ocean bottom. The value of the effective weight of the riser is taken constant because it is assumed that buoyancy is provided by small uniformly distributed modules. Due to the presence of strain relief units at the ends of the riser, the following values of bending and torsional rigidities at s=0 and s=L are used: $EI^{\eta\eta}$= 6.6 kN.m^2, $EI^{\xi\xi}$= 22.4 kN.m^2, GI^{p}= 1.164 MN.m^2. These rigidities are assumed to decay linearly to the values in Table 5.1 within 10 m from s=0 and s=L. The static boundary conditions used in this case are:

$x(L) = x(0) = y(0) = 0$
$y(L) = 70.1$ m
$\phi(0) = 90°$
$\phi(L) = 90°$
$\theta(L) = 0°$
$z(L) = 0$

The condition analyzed involves two-dimensional excitation (no torsion) by a unidirectional linear current with $V_x(0) = 1.03$ m/s and $V_x(h_w) = 1.55$ m/s. The dynamic excitation consists of top end dynamic motion of the riser in heave and surge. The heave amplitude (x_1) is 1 m and the surge amplitude (y_1) is also 1 m with zero phase angle between the two motions. The exciting frequency is 0.77 rad/s close to the second natural frequency for this riser configuration as was presented in reference [6], where the natural modes for this riser have been analyzed.

Figure 5.1, adapted from [3], present the static results for this riser configuration. The static configuration and the static angle along the length of the riser are shown in the top figure in Figure 5.1, while the static effective tension and static curvature in the η direction along the length of the riser are shown in the bottom figure in Figure 5.1. Figure 5.2 presents the dynamic results for this particular excitation. In the top graph of Figure 5.2, the dimensional p and q dynamic riser motions are shown as a function of the non-dimensional arc length. In the left lower graph in Figure 5.2 the non-dimensional dynamic effective tension (continuous line) and the non-dimensional dynamic shear

force in the ξ direction (dotted line) are shown as a function of the non-dimensional arc length. In the right lower graph in Figure 5.2, the non-dimensional dynamic curvature in the η direction is shown as a function of the riser arc length.

An important result to note, is that there are sharp boundary layers close to the riser ends and the values of curvature and shear are larger at these points and particularly at the top of the riser (inherent buoyant riser weakness at these points). The maximum static effective tension for this case is estimated to be 7.974 kN, while the maximum dynamic effective tension is 2.4 kN at the top of the riser. The dynamic shear force at the top is also significant 3.8 kN.

Since buoyant risers have a small static effective tension, dynamic effects are potentially very important. For relatively small dynamic excitations, the dynamic tension is large and can exceed the small static effective tension. This means that the total effective tension can become negative over a part of the cycle and the length of the riser and may lead to partial effective compression of the riser possibly causing "dynamic buckling" in the riser tubes and very large bending stresses.

An additional concern in this case is that one of the basic assumptions of the structural linearization used in our methodology concerning small dynamic quantities compared to the static quantities may be violated (e.g. dynamic vs static efective tension). As a result for buoyant risers, the proposed methodology might reach the limit of its acceptability with smaller dynamic excitations than in a catenary riser case.

5.2 SHALLOW WATER CATENARY RISER

The second case analyzed is a shallow water catenary riser in the presence of currents, waves and dynamic excitation in a two-dimensional or three-dimensional configuration. The static configuration for this riser has been analyzed in reference [5].

The heavy riser with catenary configuration analyzed consists of a single uniform flexible pipe with inner diameter of 269 mm and outer diameter of 304.8 mm. The overall riser characteristics are given in Table 5.2. The riser has a length of 140 m and is located in water depth of 90 m. The lower end of the riser is located 30 m from the ocean bottom. Due to the presence of strain relief units at the riser ends, the following values of bending and torsional rigidities at s=0 and s=L are used: $EI^{\xi\xi} = 72x10^3$ Nm^2, $EI^{\eta\eta} = 72x10^3$ Nm^2, $GI^p = 23.28x10^5$ Nm^2. These rigidities are assumed to decay linearly to the values given in Table 5.2 within 10 m from s=0 and s=L.

The two-dimensional and three-dimensional static boundary conditions used in this case were
$x(0) = y(0) = 0$

Table 5-1: Characteristics of Buoyant Riser from [3]

L	= 88.392 m
D_o	= 0.1229 m (of single tube)
D_i	= 0.0857 m (of single tube)
D^{ξ}	= 0.31 m (of tube bundle)
D^{η}	= 0.20 m (of tube bundle)
$P_e{}^{\xi\eta}$	= 0.93 m
A^o	= 237.4 cm^2
A^i	= 115.4 cm^2
m_T	= 49.93 kg/m
m^{ζ}	= 40.47 kg/m
$m_a{}^{\xi}$	= 82.44 kg/m
$m_a{}^{\eta}$	= 50.32 kg/m
W	= 2.92 N/m
EA	= 2.67×10^8 N
$EI^{\eta\eta}$	= 3.3×10^3 Nm^2
$EI^{\xi\xi}$	= 1.22×10^4 Nm^2
GI^p	= 5.82×10^5 Nm^2
ρ_i	= 820 kg/m^3
p	= 3.45 MPa
c	= 0 m/s
C_D	= 1.0
C_f	= 0.05
$C_f{}^{\zeta}$	= 0.05

Figure 5-1: Static Results for Buoyant Riser from [3]

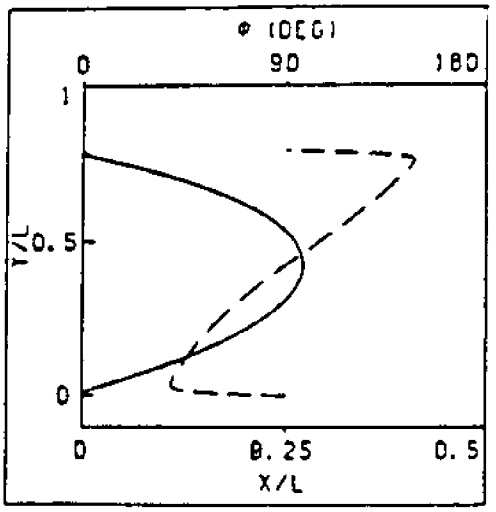

x_0, ϕ_0 Versus y_0

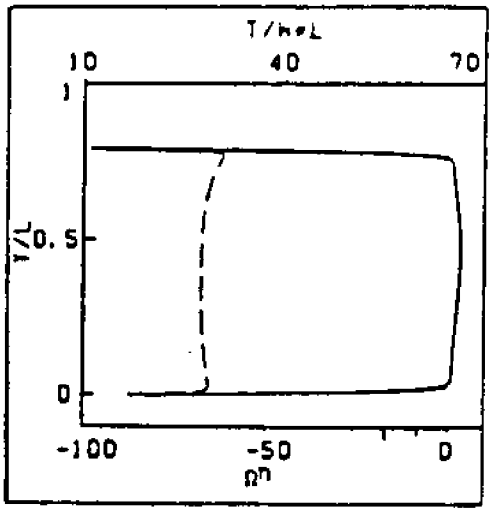

Ω_0^{η}, T_0 Versus y_0

Figure 5-2: Dynamic Results for Buoyant Riser

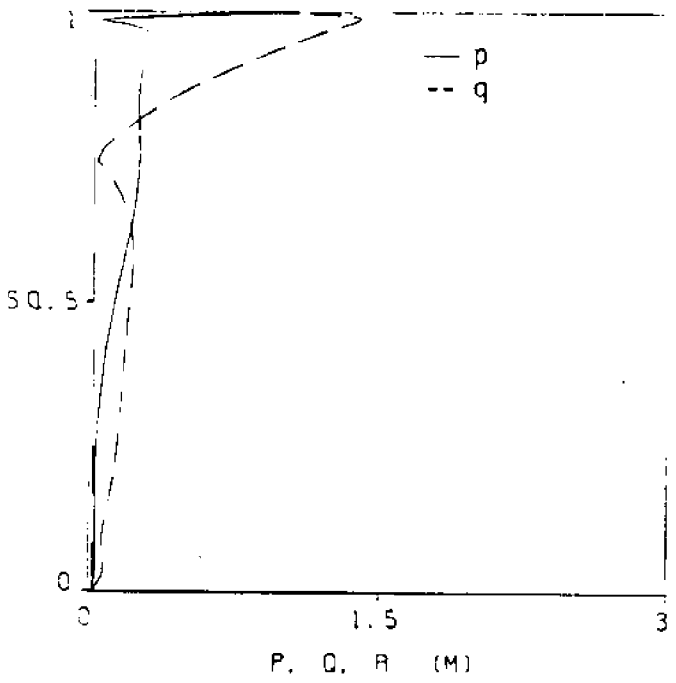

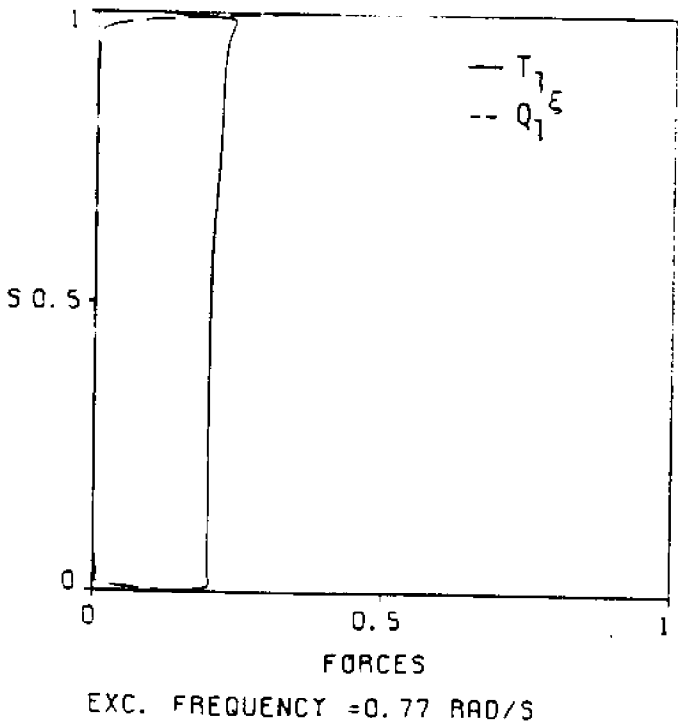

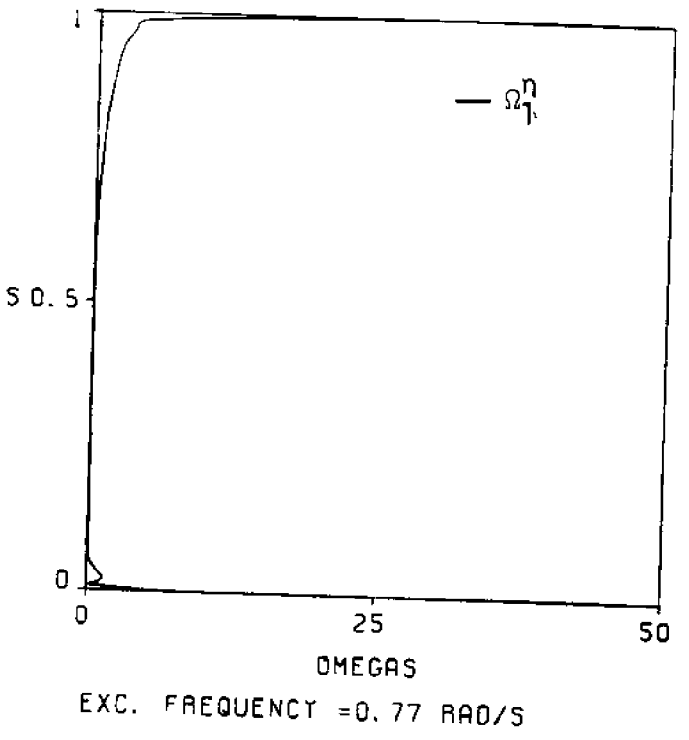

$x(L) = 60$ m
$y(L) = 60$ m
$\phi(0) = -90°$
$\phi(L) = 90°$
3-d additional boundary conditions
$\theta(L) = \theta(0) = \psi(0) = z(0) = 0$
$\psi(L) = 25°$
$z(L) = 15$ m

The cases analyzed are the following:

1. Two-dimensional excitation
   Linear current velocity with $V_x(0)$=1.03 m/s and $V_x(h_w)$=1.5 m/s
   Riser top dynamic excitation, excitation frequency = 0.6 rad/s $|x_1| = 3$ m, $|y_1| = 3$ m and zero phase between these motions
   No waves

2. Two-dimensional excitation
   Current and top dynamic excitation are the same as above
   Wave amplitude = 3 m with wave angle = 0° and the same excitation frequency. The phase of the dynamic motions of the riser is measured with respect to the wave elevation at x=0 and z=0.

3. Three-dimensional excitation
   The same current profile is used but is rotated by 22.5 degrees about the y-axis from the +x direction to the +z direction,
   $V_x(0) = 0.952$ m/s, $V_z(0) = 0.394$ m/s
   $V_x(h_w) = 1.386$ m/s, $V_z(h_w) = 0.574$ m/s
   Top dynamic excitation was also rotated by 22.5°
   $|x_1| = 2.77$ m, $|y_1| = 3$ m, $|z_1| = 1.15$ m, with zero phase with respect to the wave elevation at x=0, z=0
   Wave amplitude = 3 m, wave frequency = 0.6 rad/s and wave angle = 22.5° with respect to the positive x direction.

Figure 5.3 adapted from [5], presents the static configuration, static effective tension and curvature for static cases I and II (no account for wave and dynamic motion static effects). The maximum static effective tension is estimated to be 45.16 kN with location close to the upper end of the riser. The presence of the boundary layer can be seen in these figures. The minimum static bending radius is 3.34 m and occurs at the lower end of the riser.

Figures 5.4, 5.5 and 5.6 present the dynamic results for case 1, while Figures 5.7, 5.8 and 5.9 present the dynamic results for case 2 using an initial static configuration which does not account for static effects of wave and riser dynamic motions. Figures 5.10, 5.11 and 5.12 present the dynamic results for case 2 again using the corrected static configuration accounting for static effects of wave and riser dynamic motions. Figures 5.4, 5.7 and 5.10 present the non-dimensional dynamic effective tension and dynamic shear in the ξ direction as a function of the non-dimensional arc length, while Figures 5.5, 5.8 and 5.11 present the non-dimensional curvature in the η direction as a function of the non-dimensional arc length and Figures 5.6, 5.9 and 5.12 present the dimensional p and q motions of the riser as a function of the non-dimensional arc length.

Comparing Figures 5.4, 5.5 and 5.6 with Figures 5.7, 5.8 and 5.9, the effect of the wave on the dynamic response of the riser can be measured. This effect is important only in the upper part of the riser where direct wave effects are

more significant. The maximum dynamic tension, the maximum dynamic shear and the maximum dynamic curvature at the top of the riser increase under the presence of the wave; the maximum dynamic tension from 14.4 kN to 15.3 kN, the maximum dynamic shear from 13.1 kN to 23.1 kN and the maximum dynamic curvature from 0.21 m^{-1} to 0.36 m^{-1}. The dynamic motions near the top of the riser increase also in the presence of waves, particularly the q motions.

Comparing Figures 5.7, 5.8 and 5.9 with Figures 5.10, 5.11 and 5.12 the effect of the improvement of the static solution accounting for waves and riser dynamic motions can be seen on the predicted dynamic response of the riser. This effect is only minor. The maximum dynamic tension at the top decreases from 15.3 kN to 14.2 kN, the maximum dynamic shear at the top increases from 23.1 kN to 24.0 kN and the maximum dynamic curvature in the η direction increases from 0.36 m^{-1} to 0.38 m^{-1}. The dynamic motions at the top of the riser increase also in the corrected dynamic solution.

Figures 5.13 and 5.14, adapted from [5], present some of the static results for the three-dimensional riser configuration in case III. The static configuration, the static effective tension, static shear in the ξ and η directions and the static curvatures in the ξ and η directions are shown as a function of the arc length. The maximum static effective tension is 45 kN, while the maximum static shear in the ξ direction is 11.54 kN. Figures 5.15 (dynamic forces), 5.16 (dynamic curvatures) and 5.17 (dynamic motions) summarize our dynamic results for this static configuration. For the excitation conditions which are the conditions of case 2 rotated by 22.5 degrees the following maximum dynamic quantities at the top of the riser are obtained; Maximum dynamic effective tension of 15.63 kN, maximum dynamic shear in the ξ direction of 15.29 kN, maximum shear in the η direction of 17.03 kN, maximum dynamic curvature in the η direction of 0.257 m^{-1}, maximum dynamic curvature in the ξ direction of 0.247 m^{-1} while the dynamic torsion in the ζ direction is negligible.

5.3 DEEP WATER CATENARY RISER WITH BOTTOM INTERACTION

The catenary riser with bottom interaction analyzed in this section consists of the same uniform flexible pipe used in the previous section except for the total length and the strain relief units at the riser ends. The total length of the riser is L=1000 m and the length of the strain relief units near the ends is 20 m from s=0 and s=L. The water depth is 300 m. The spring and damping bottom interaction coefficients are taken equal to K_e^y = 5000 Pa and C^y = 5000 Kg/ms respectively. The static boundary conditions for this configuration are:

$x(0) = y(0) = 0$
$x(L) = 800$ m
$y(L) = 300$ m
$\phi(0) = 0°$
$\phi(L) = 90°$

Table 5-2: Characteristics of Shallow Water Catenary Riser from [5]

L	= 140 m
D_i	= 0.269 m
D^{ξ}	= 0.3048 m
D^{η}	= 0.3048 m
$P_c^{\xi\eta}$	= 0.9576 m
A^o	= 729.7 cm^2
A^i	= 506.7 cm^2
m_T	= 119.6 kg/m
m^{ζ}	= 78.05 kg/m
m_a^{ξ}	= 74.79 kg/m
m_a^{η}	= 74.79 kg/m
W	= 439.35 N/m
EA	= 4.88×10^8 N
$EI^{\eta\eta}$	= 3.6×10^4 Nm^2
$EI^{\xi\xi}$	= 3.6×10^4 Nm^2
GI^P	= 1.164×10^6 Nm^2
ρ_i	= 820 kg/m^3
p	= 3.45 MPa
c	= 0 m/s
C_D	= 1.0
C_f	= 0.05
C_f^{ζ}	= 0.05

Figure 5-3: Static Results for a 2-D Catenary Riser, adapted from [5]

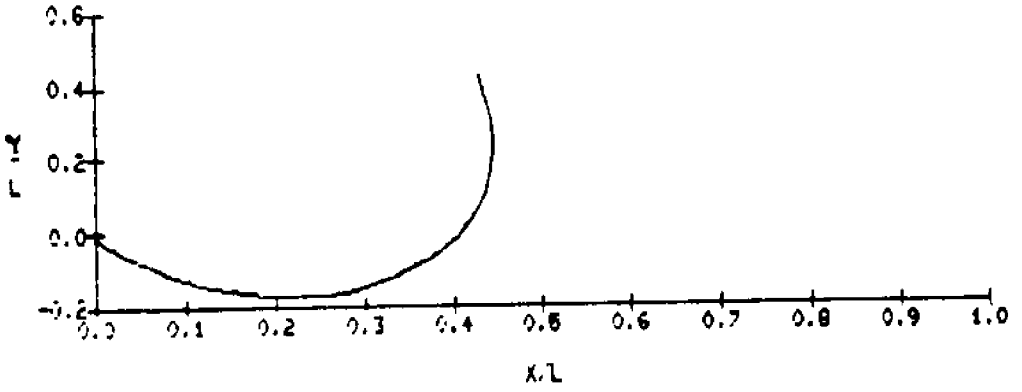

x Versus y, 2-D Case With Current

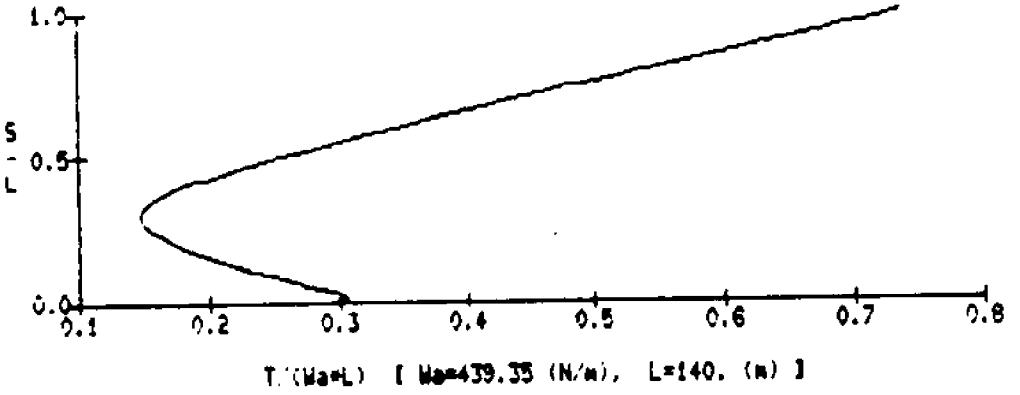

T Versus s, 2-D Case With Current

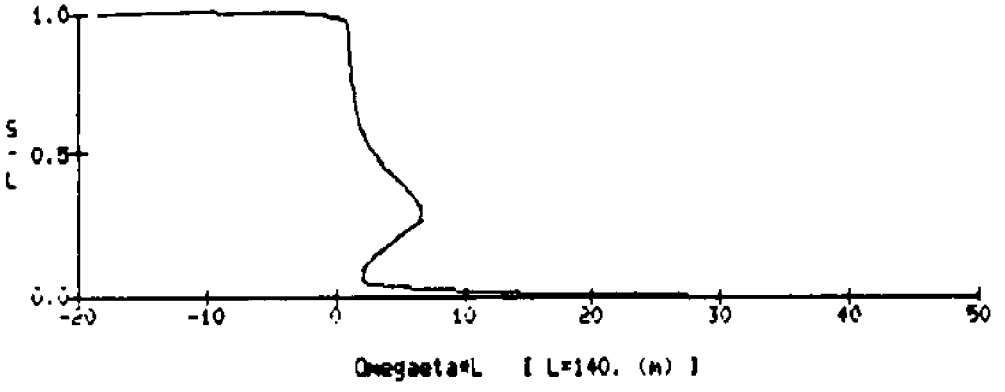

Ω^n Versus s, 2-D Case With Current

Figure 5-4: Dynamic Forces for 2-D Catenary Riser, Case 1

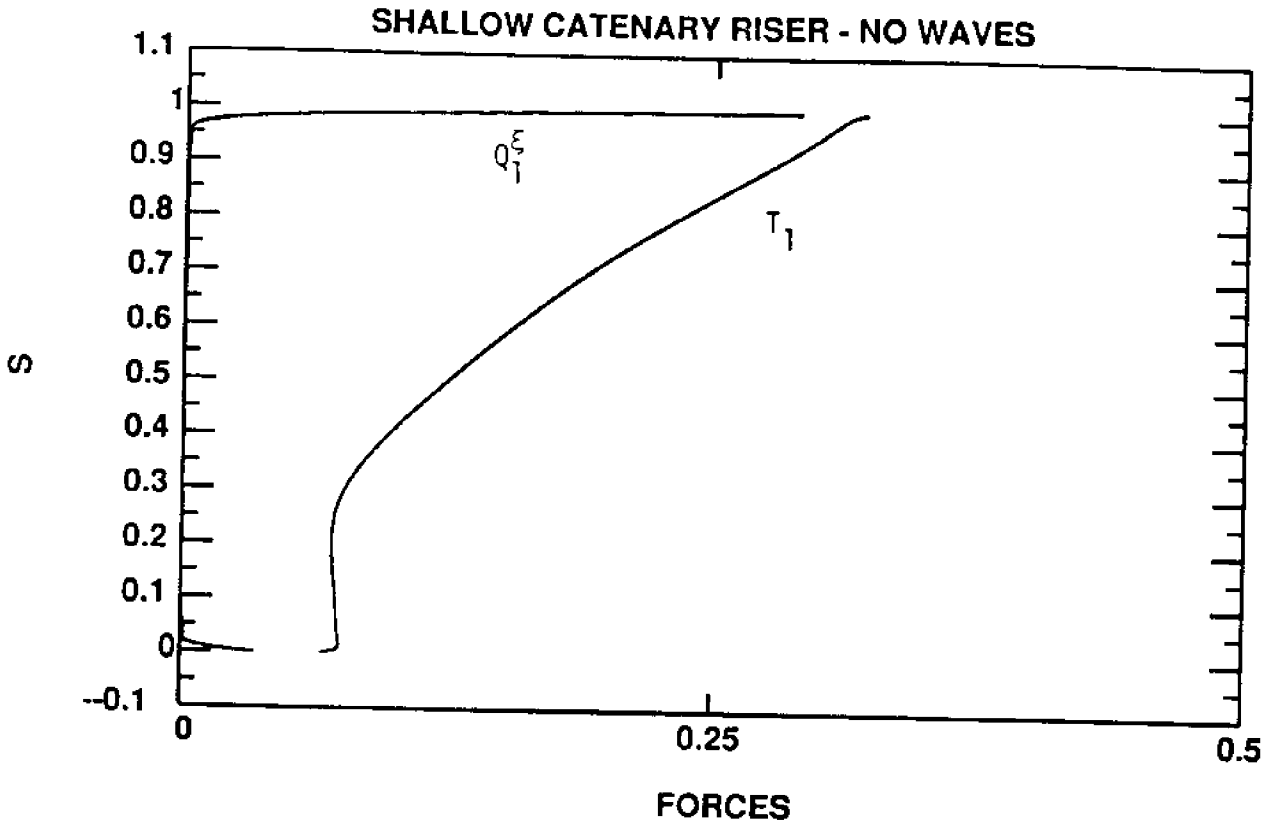

The excitation characteristics used in this case include a linear current profile with riser bottom velocity of 1.03 m/s and riser top velocity of 1.5 m/s. The dynamic excitation frequency is 0.6 rad/s and the riser is excited by top motion in the heave direction (y_1) with amplitude 3 m and in the surge direction (x_1) with amplitude 3 m and zero phase between the motions.

Figures 5.18, 5.19 and 5.20 present the static configuration, the static effective tension and the static curvature in the η direction respectively for this riser configuration as a function of the non-dimensional arc length. Approximately 60% percent of the length of this riser lies on the ocean bottom. The static effective tension is constant for the riser part lying on the bottom and increases linearly for the upper part of the riser. The maximum effective tension is of the order of 192 kN mostly attributed to the weight of the catenary riser. The static shear force is very small (about 1.5 kN) and cannot be seen in Figure 5.19. From Figure 5.20 it can be seen that there is an internal layer in the boundary between the riser part lying on the bottom and the rest of the riser where curvature changes rapidly. Overall the maximum static curvature is very small and of the order of 0.015 m^{-1}.

Figures 5.21, 5.22 and 5.23 present the dynamic forces, the dynamic curvature and the dynamic motions respectively as a function of the arc length for this riser configuration. The maximum dynamic effective tension is

Figure 5-5: Dynamic Curvatures for 2-D Catenary Riser, Case 1

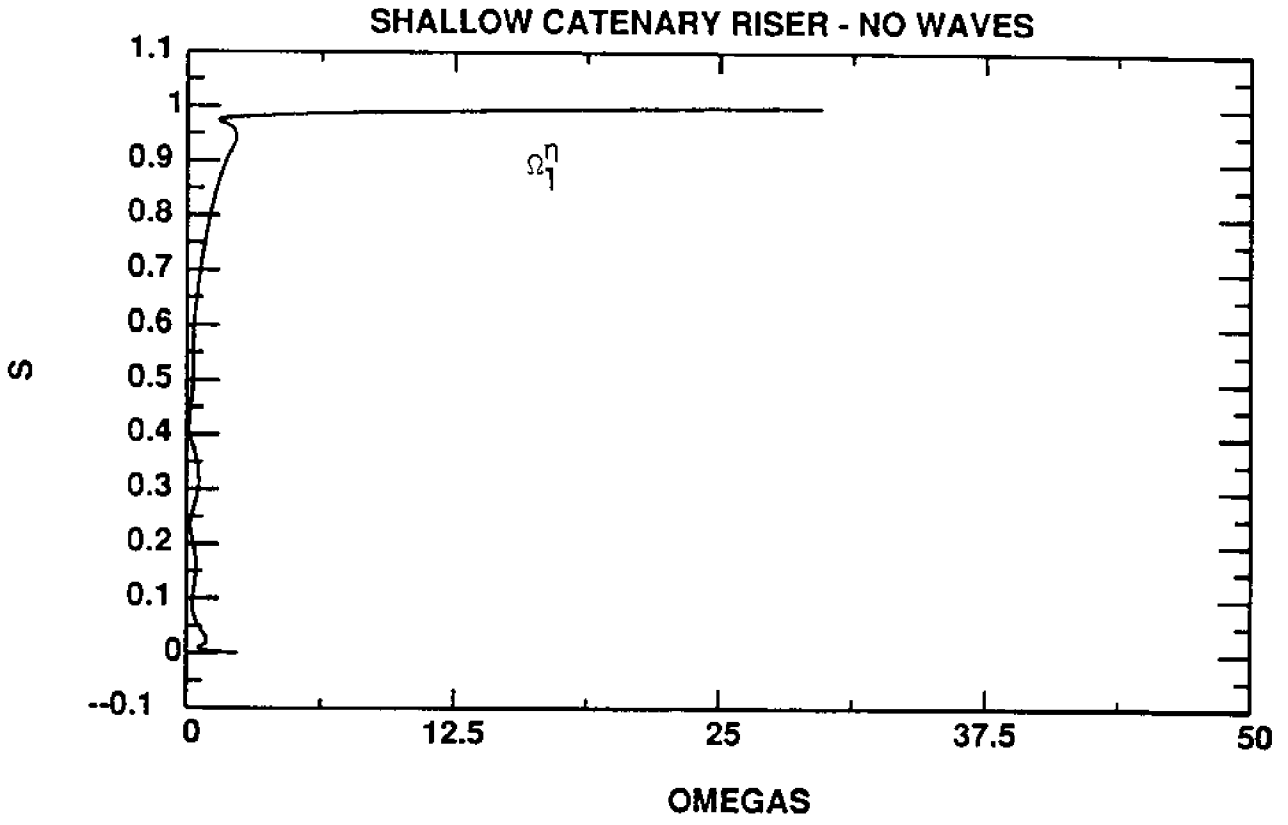

114 kN (59% of the top static effective tension) and the maximum dynamic shear force is 27 kN at the top of the riser. The maximum dynamic curvature is of the order of 0.225 m^{-1} which is comparable to the curvatures for the shallow water catenary riser (previous example). For the deep water catenary riser the total effective tension is very large. The riser weight is the most significant contributing factor increasing the magnitude of the static effective tension. The large dynamic tension is primarily due to the large heave acceleration imposed at the top end. This was verified by artificially reducing the heave amplitude to zero. In this case the dynamic tension reduced to 3.9 kN (only 2% of the top static effective tension), while the dynamic shear reduced to 22.6 kN.

Figure 5-6: Dynamic Motions for 2-D Catenary Riser, Case 1

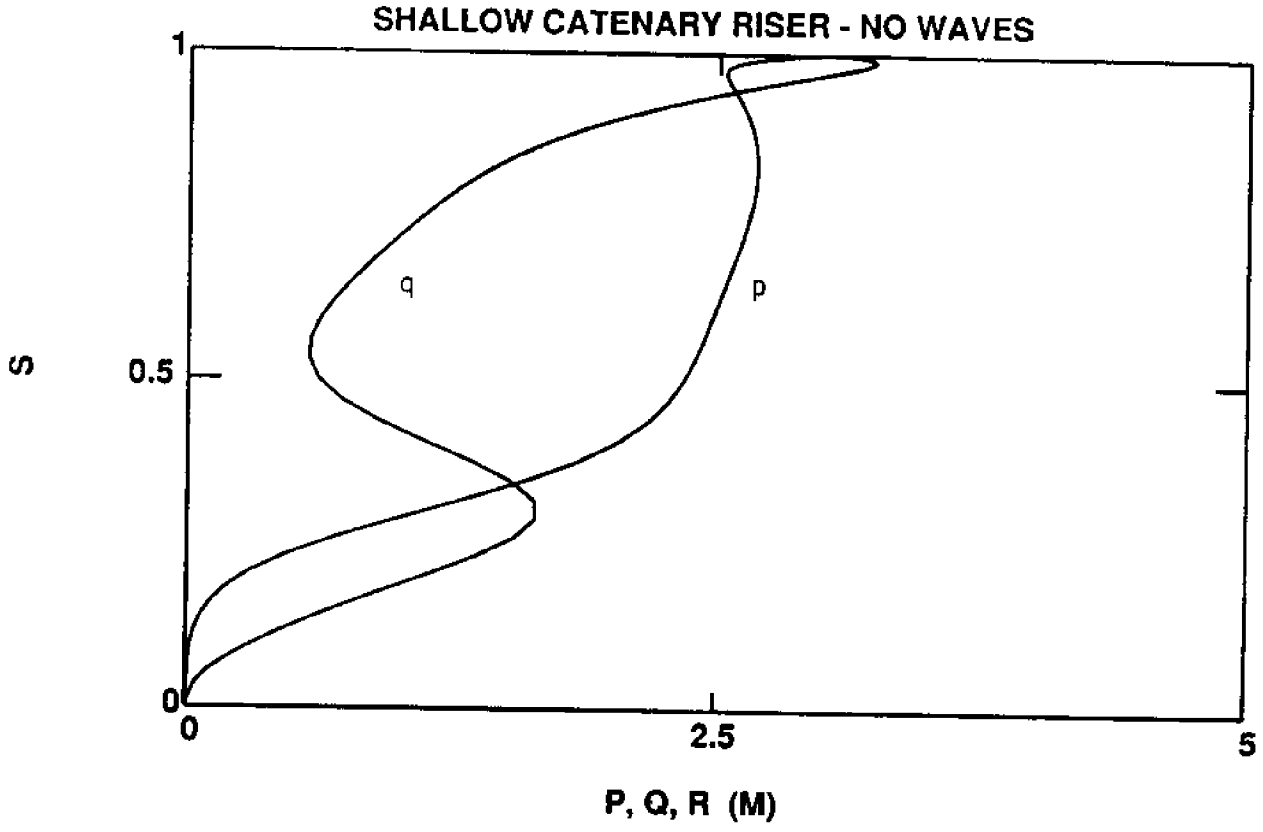

Figure 5-7: Dynamic Forces for 2-D Catenary Riser, Case 2
Initial Static Configuration

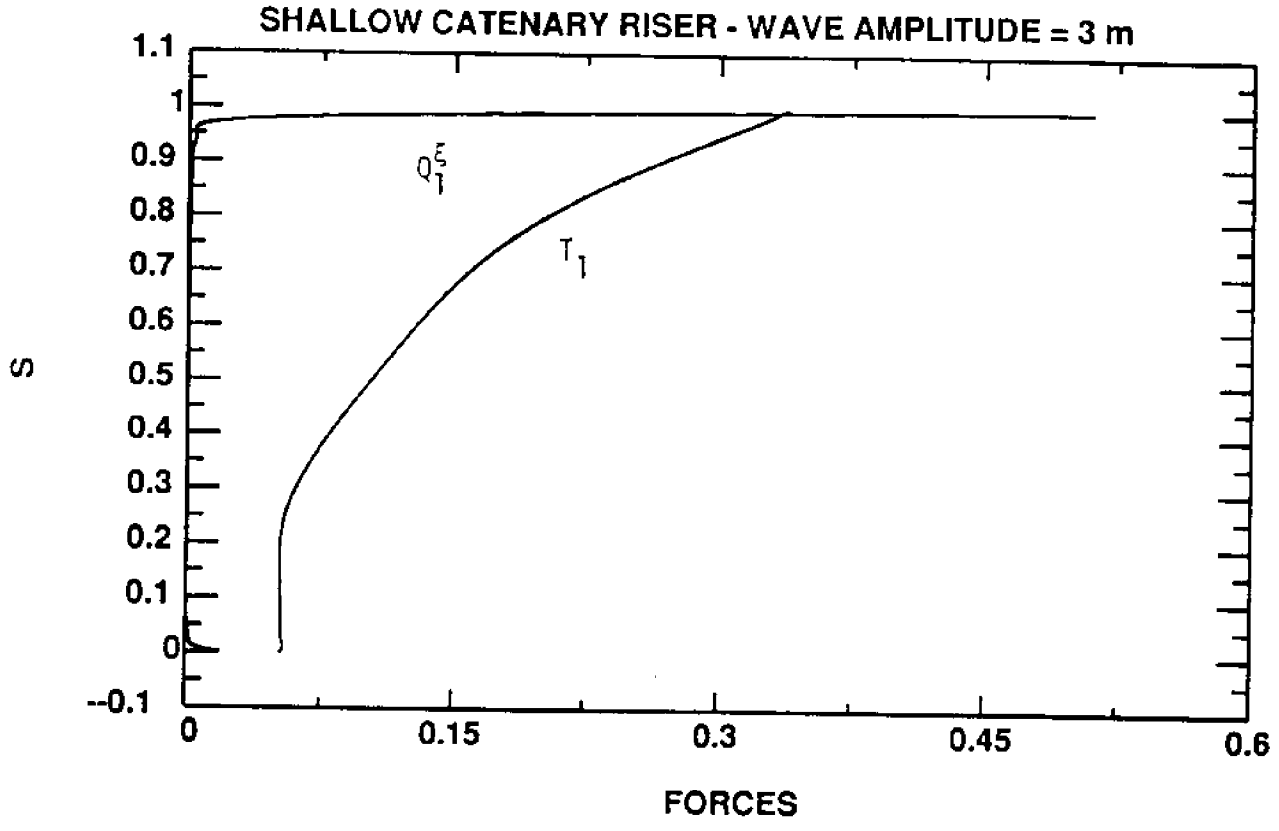

Figure 5-8: Dynamic Curvatures for 2-D Catenary Riser, Case 2
Initial Static Configuration

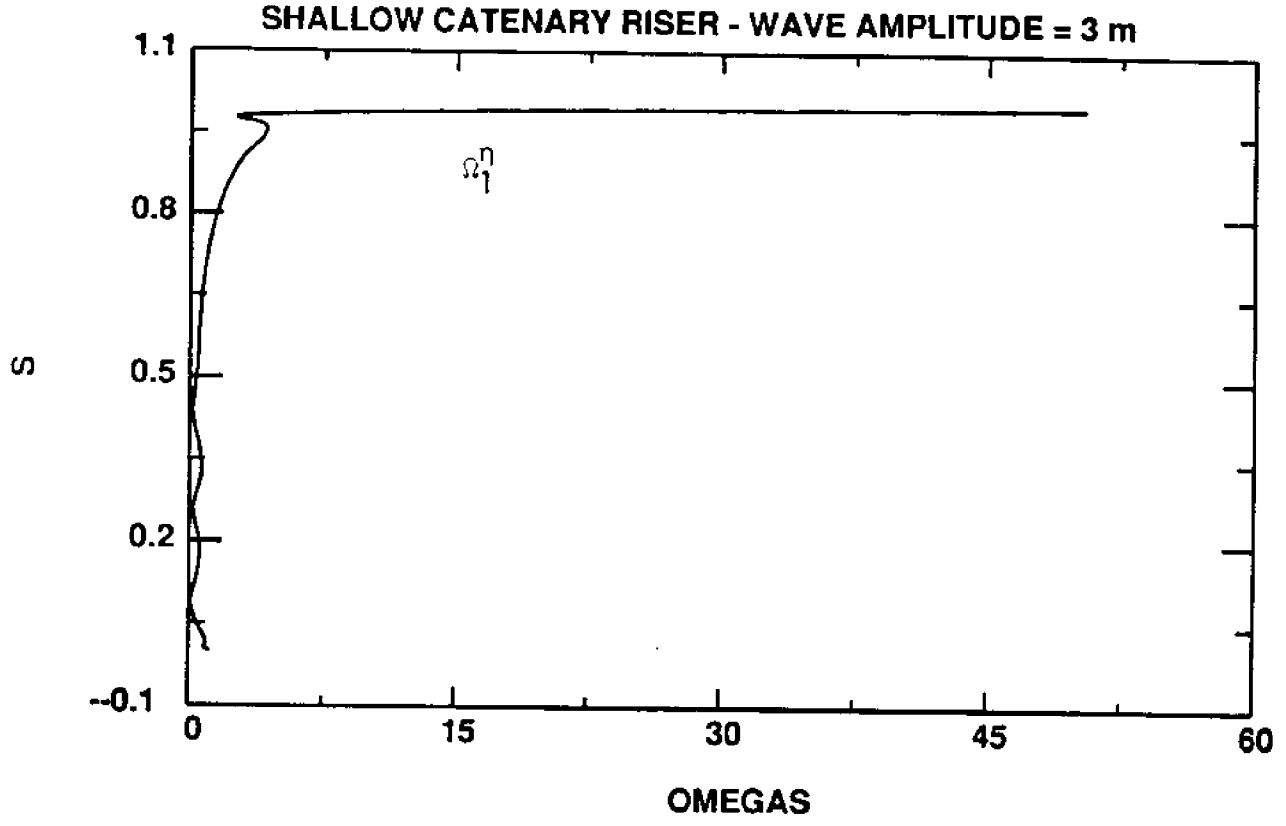

Figure 5-9: Dynamic Motions for 2-D Catenary Riser, Case 2
Initial Static Configuration

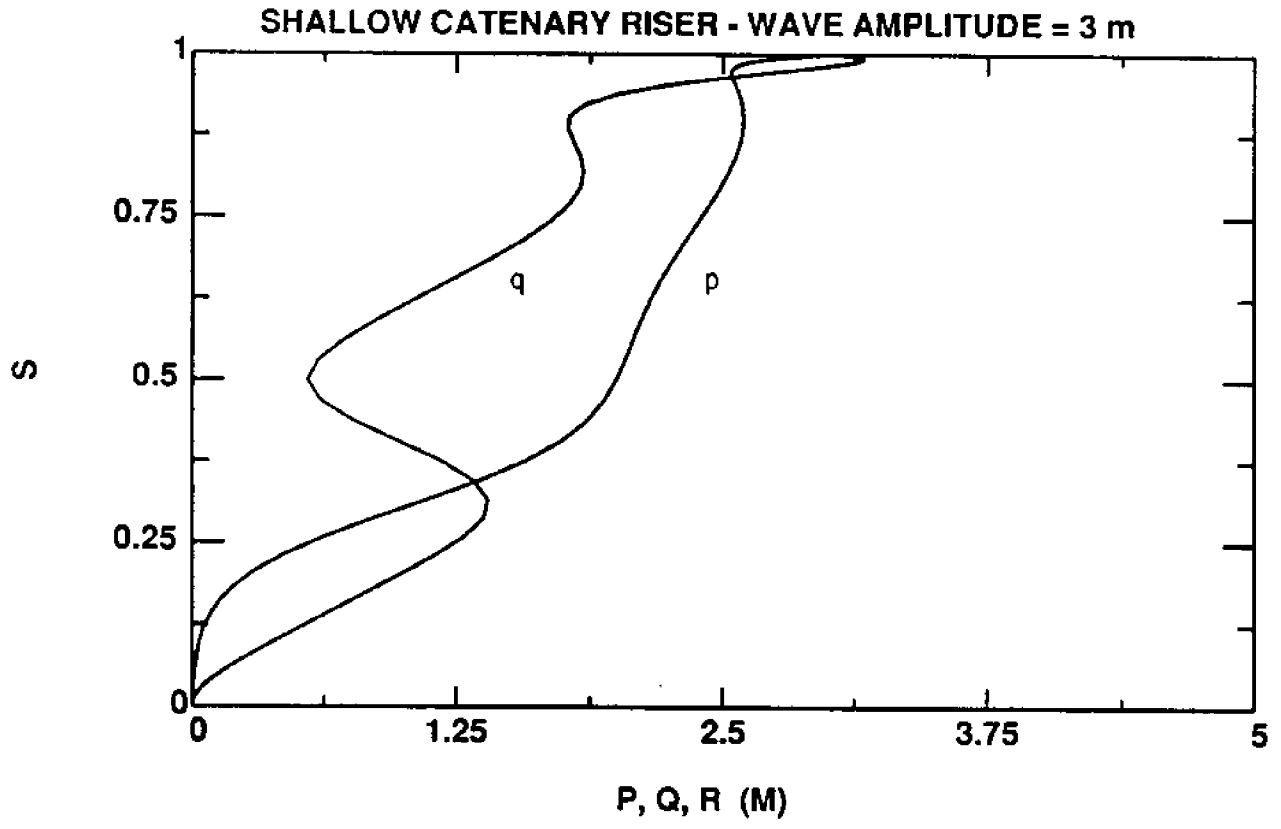

Figure 5-10: Dynamic Forces for 2-D Catenary Riser, Case 2
Corrected Static Configuration

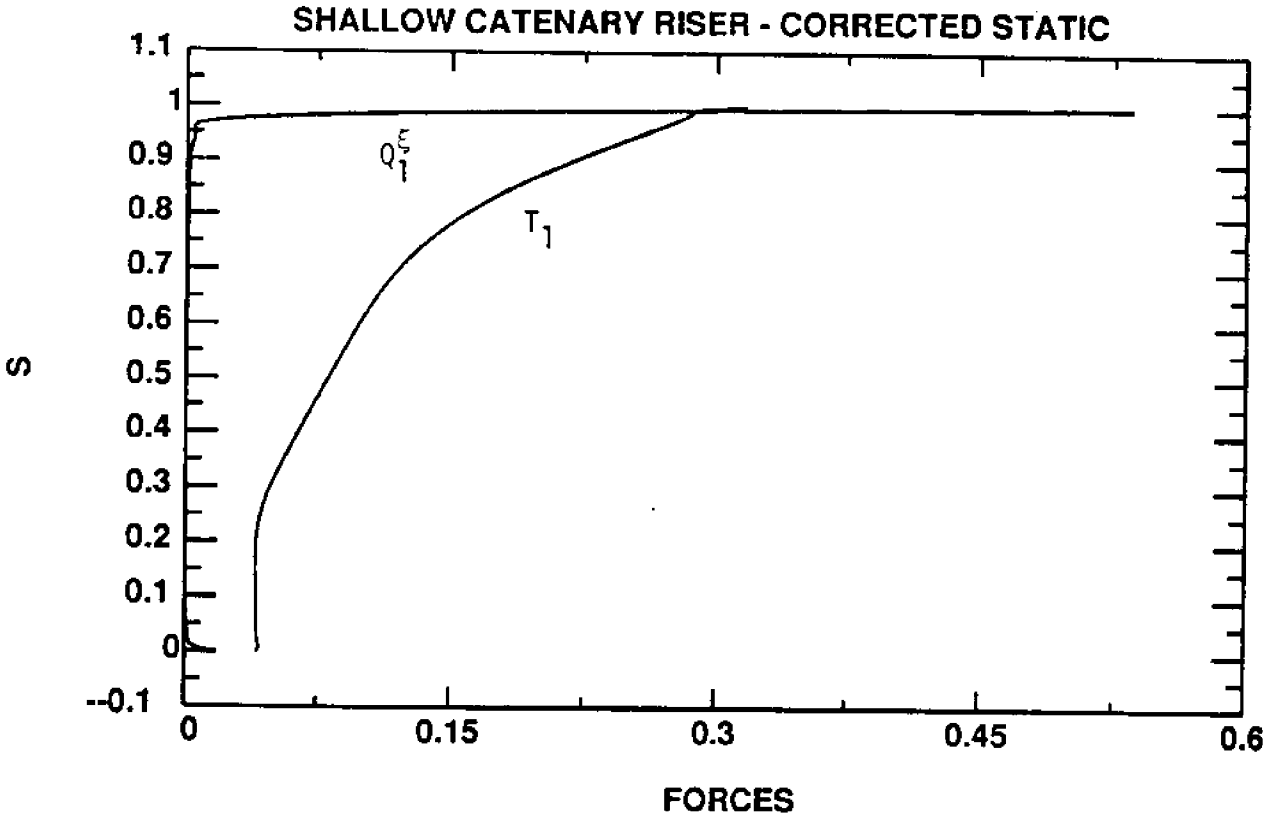

Figure 5-11: Dynamic Curvatures for 2-D Catenary Riser, Case 2
Corrected Static Configuration

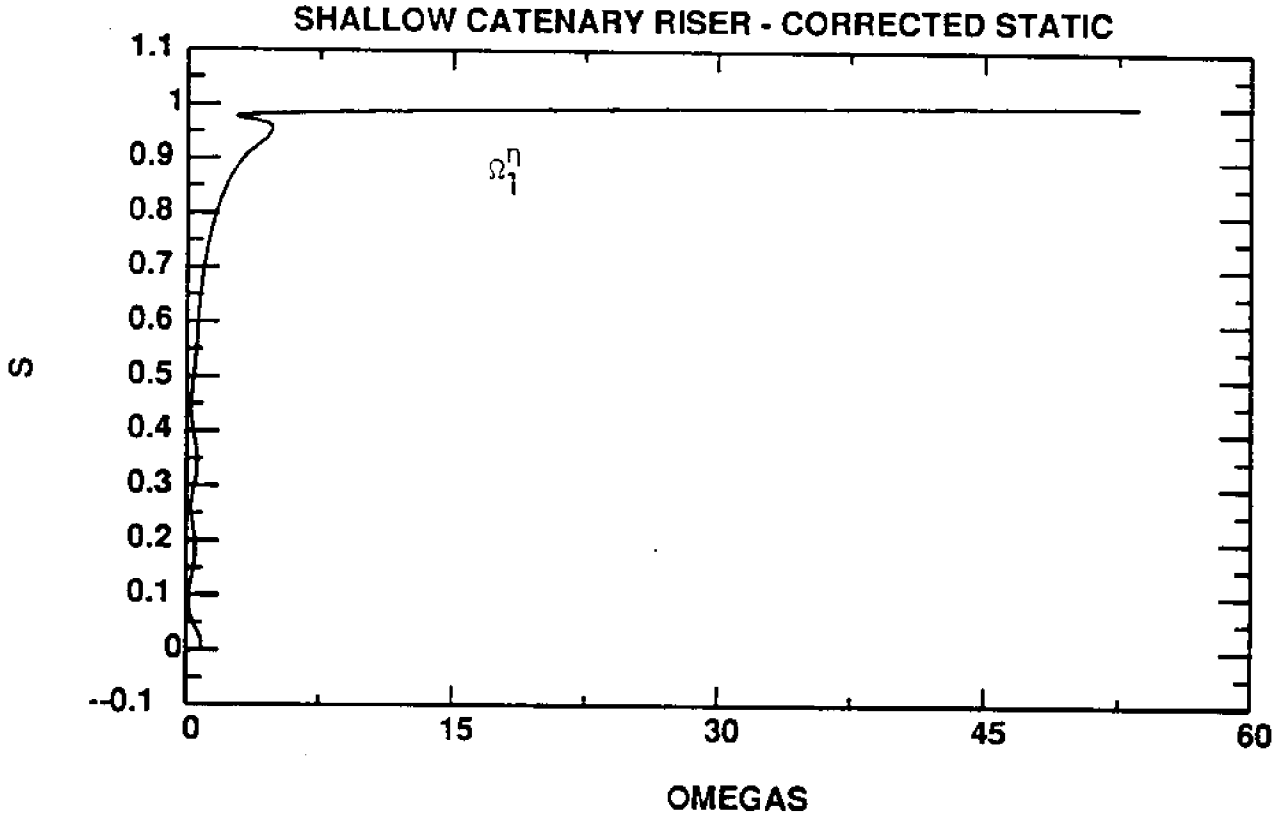

Figure 5-12: Dynamic Motions for 2-D Catenary Riser, Case 2
Corrected Static Configuration

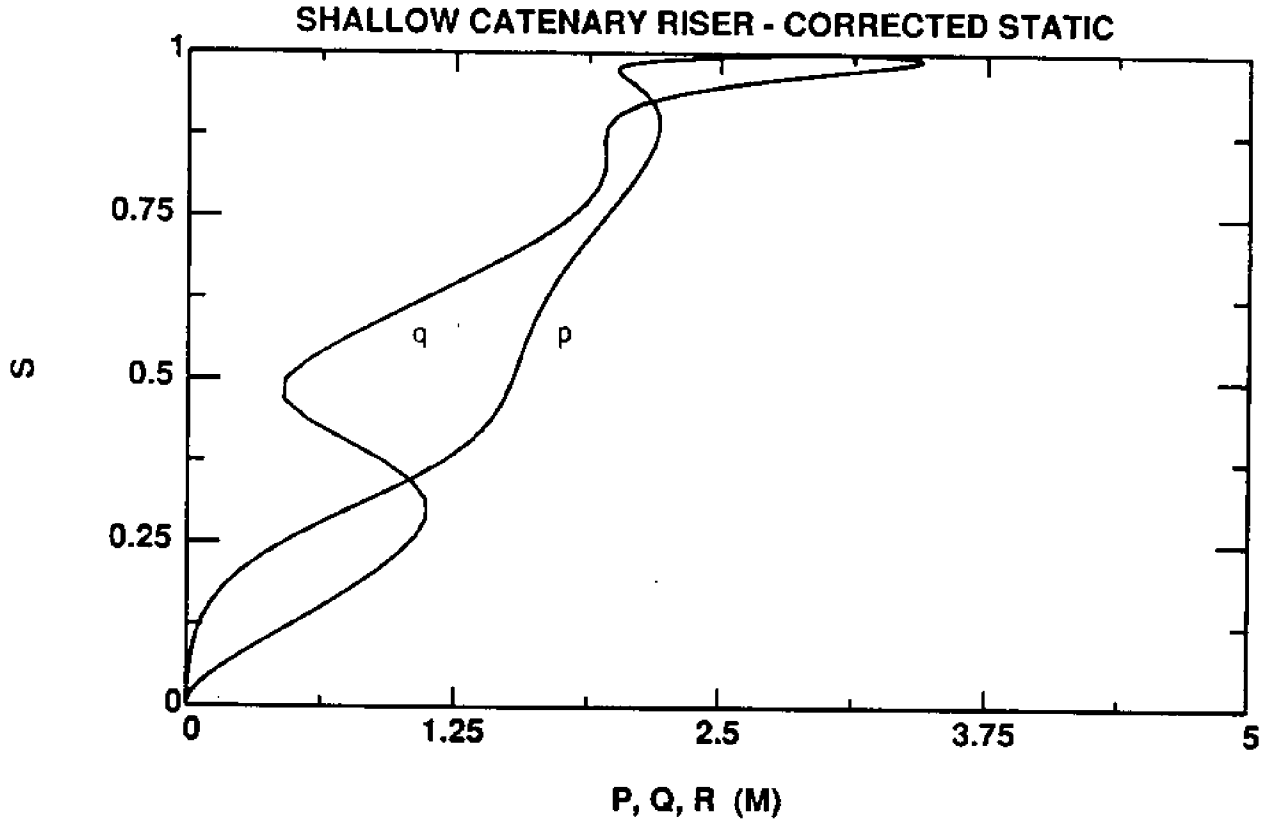

Figure 5-13: Static Results for 3-D Catenary Riser, from [5]

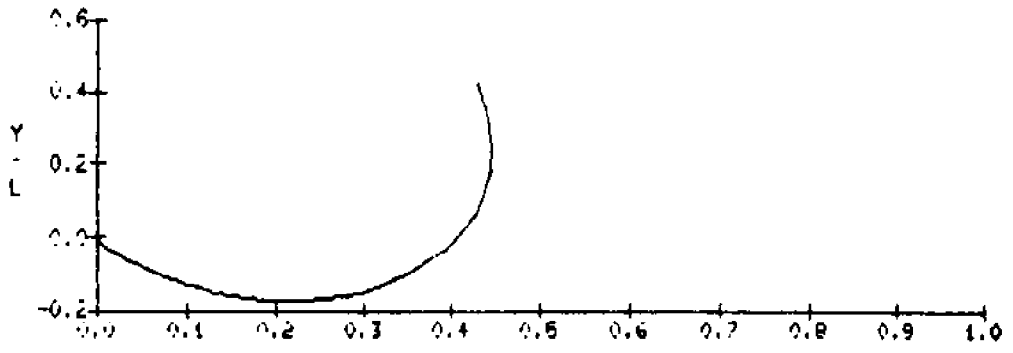

x Versus y, 3-D Case With $\theta_c = 0$

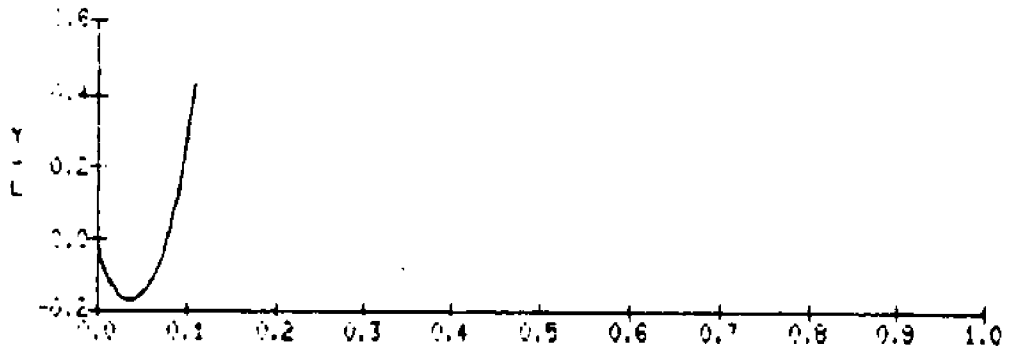

z Versus y, 3-D Case With $\theta_c = 0$

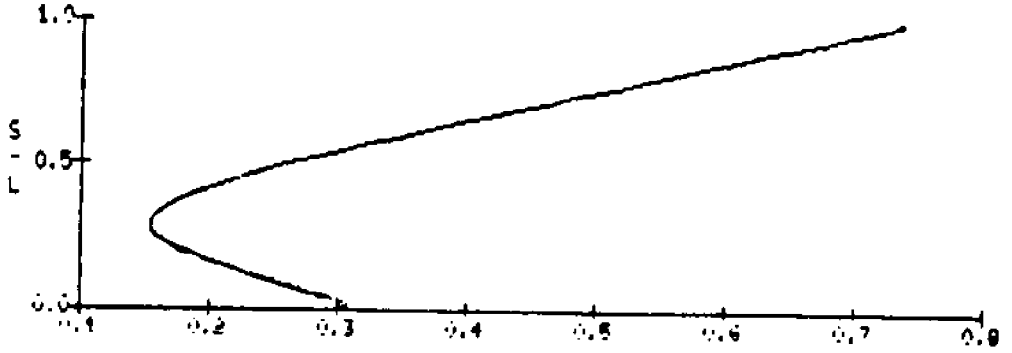

T Versus s, 3-D Case With $\theta_c = 0$

Figure 5-14: Static Results for 3-D Catenary Riser, from [5] continued

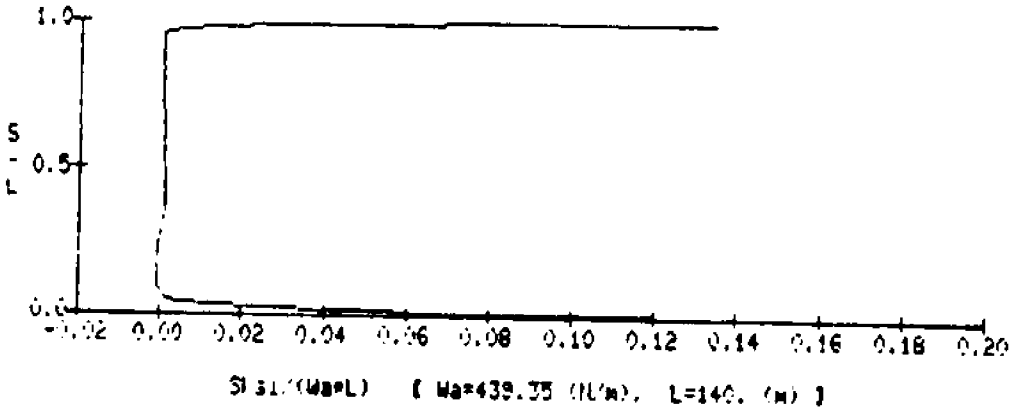

Q^{ξ} Versus s, 3-D Case With $\theta_c = 0$

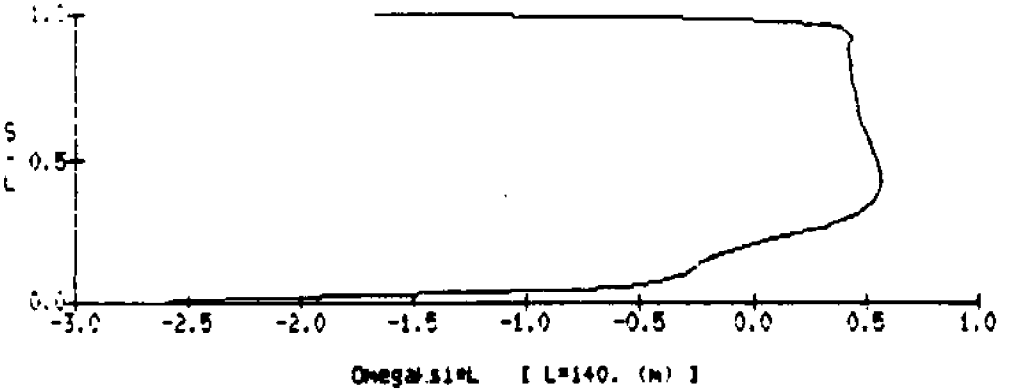

Ω^{ξ} Versus s, 3-D Case With $\theta_c = 0$

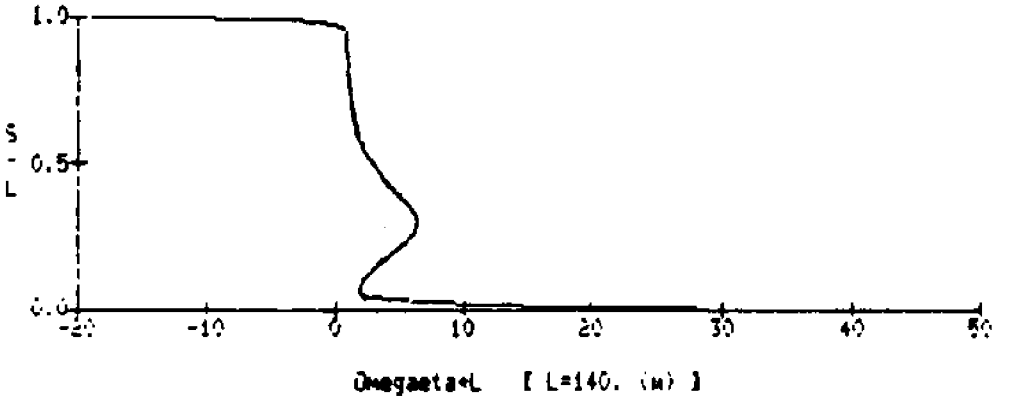

Ω^{η} Versus s, 3-D Case With $\theta_c = 0$

Figure 5-15: Dynamic Forces for 3-D Catenary Riser, Case 3

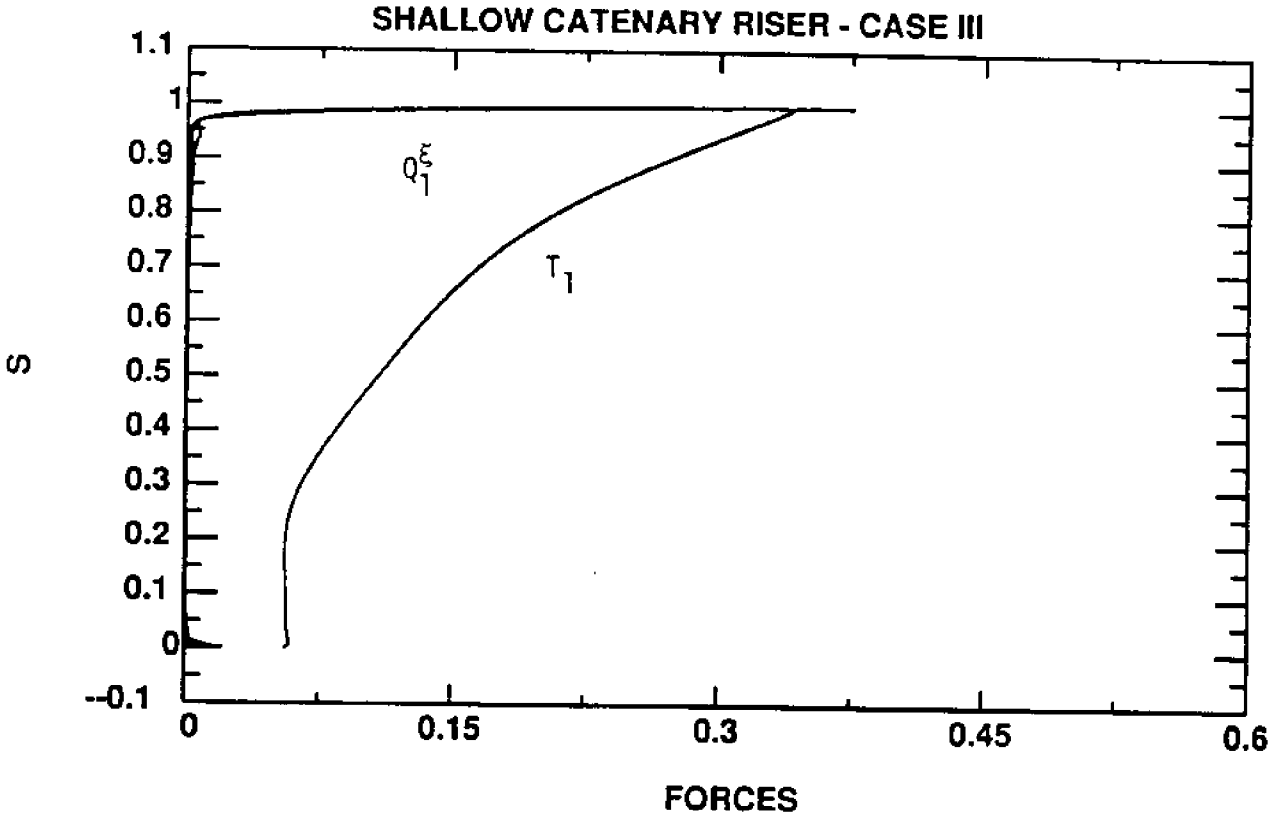

Figure 5-16: Dynamic Curvatures for 3-D Catenary Riser, Case 3

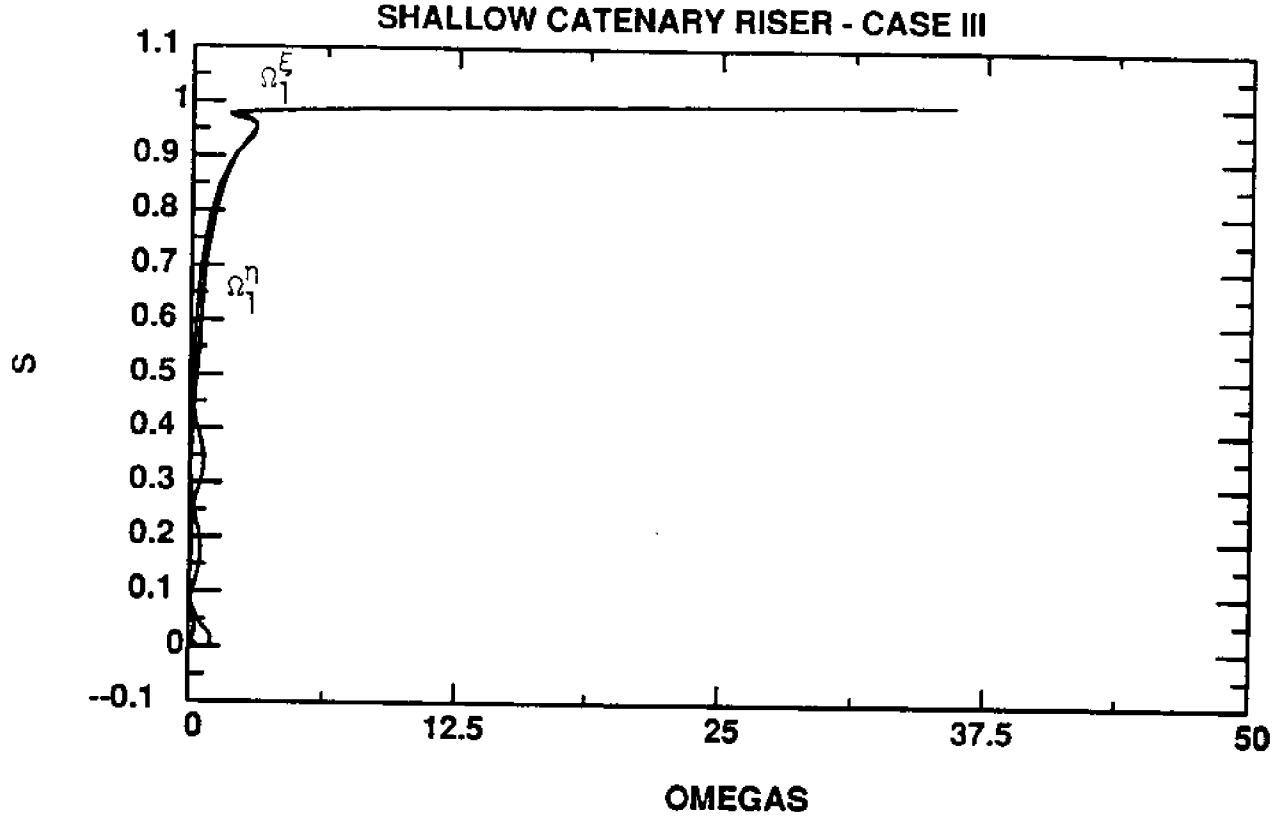

Figure 5-17: Dynamic Motions for 3-D Catenary Riser, Case 3

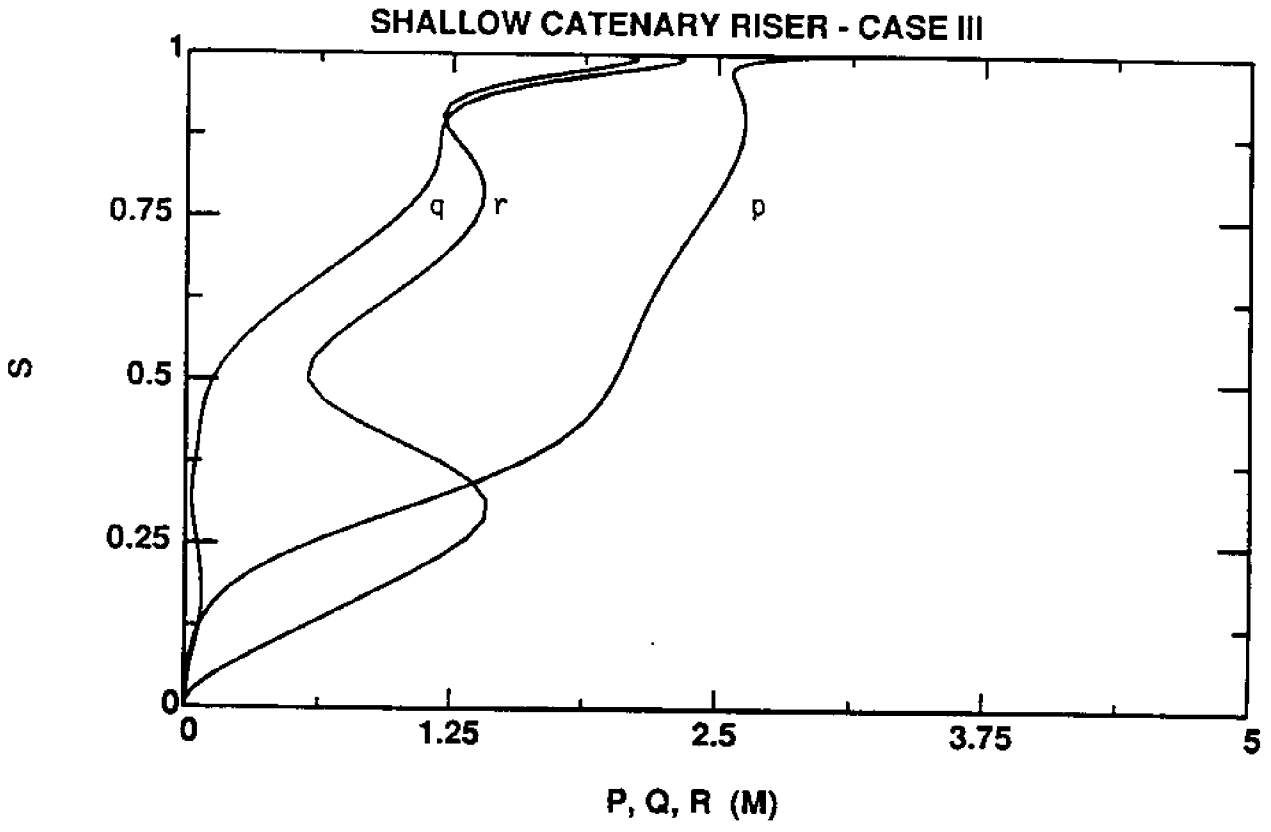

Figure 5-18: Static Configuration of Catenary Riser Experiencing Bottom Interaction

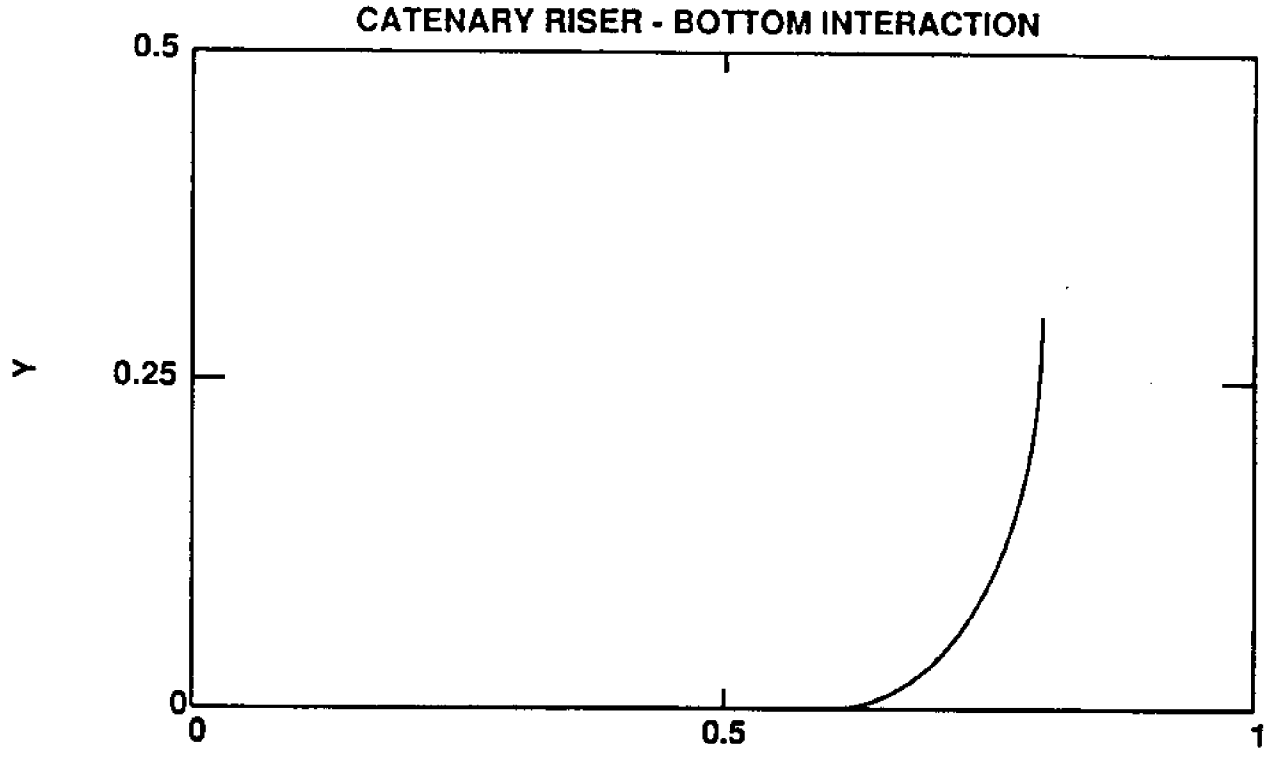

Figure 5-19: Static Effective Tension for Catenary Riser Experiencing Bottom Interaction

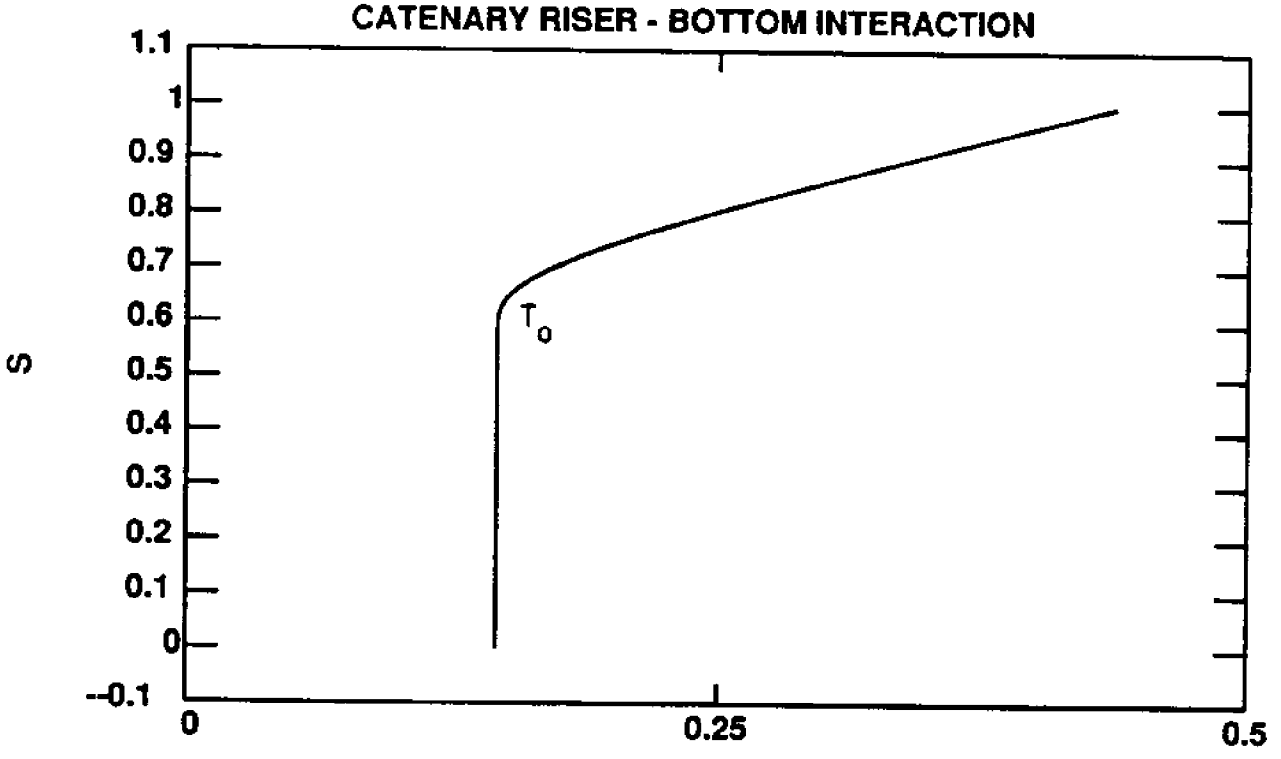

Figure 5-20: Static Curvature for Catenary Riser Experiencing Bottom Interaction

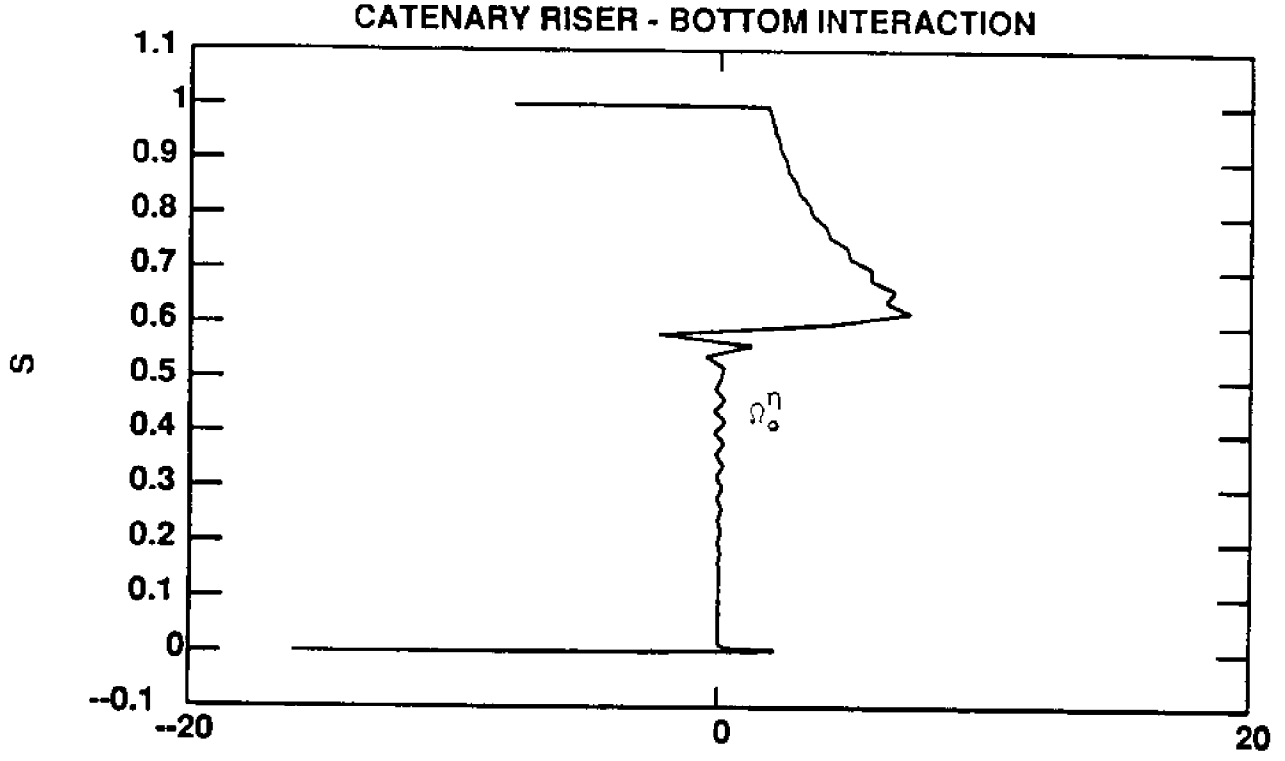

Figure 5-21: Dynamic Forces for Catenary Riser Experiencing Bottom Interaction - Excitation Frequency = 0.6 rad/s

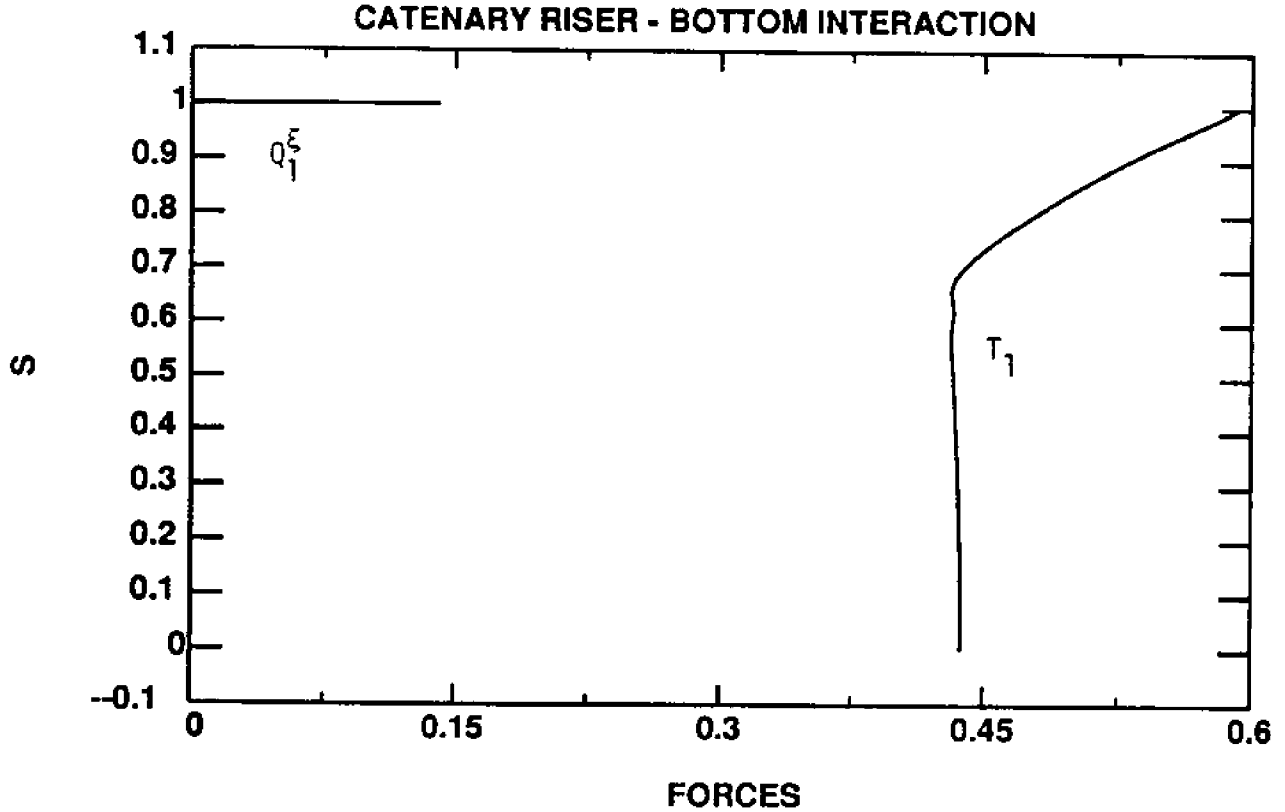

Figure 5-22: Dynamic Curvature for Catenary Riser Experiencing Bottom Interaction - Excitation Frequency = 0.6 rad/s

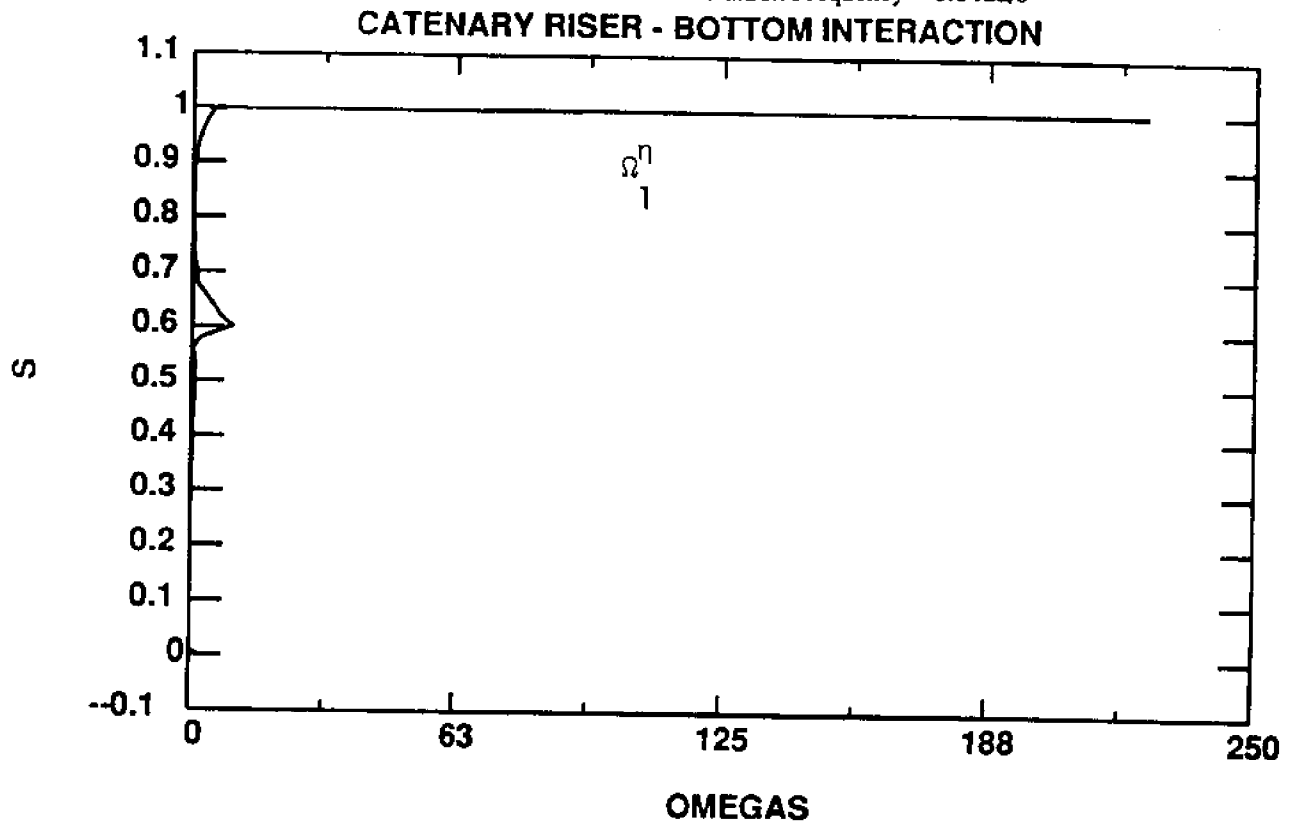

Figure 5-23: Dynamic Motions for Catenary Riser Experiencing Bottom Interaction - Excitation Frequency = 0.6 rad/s

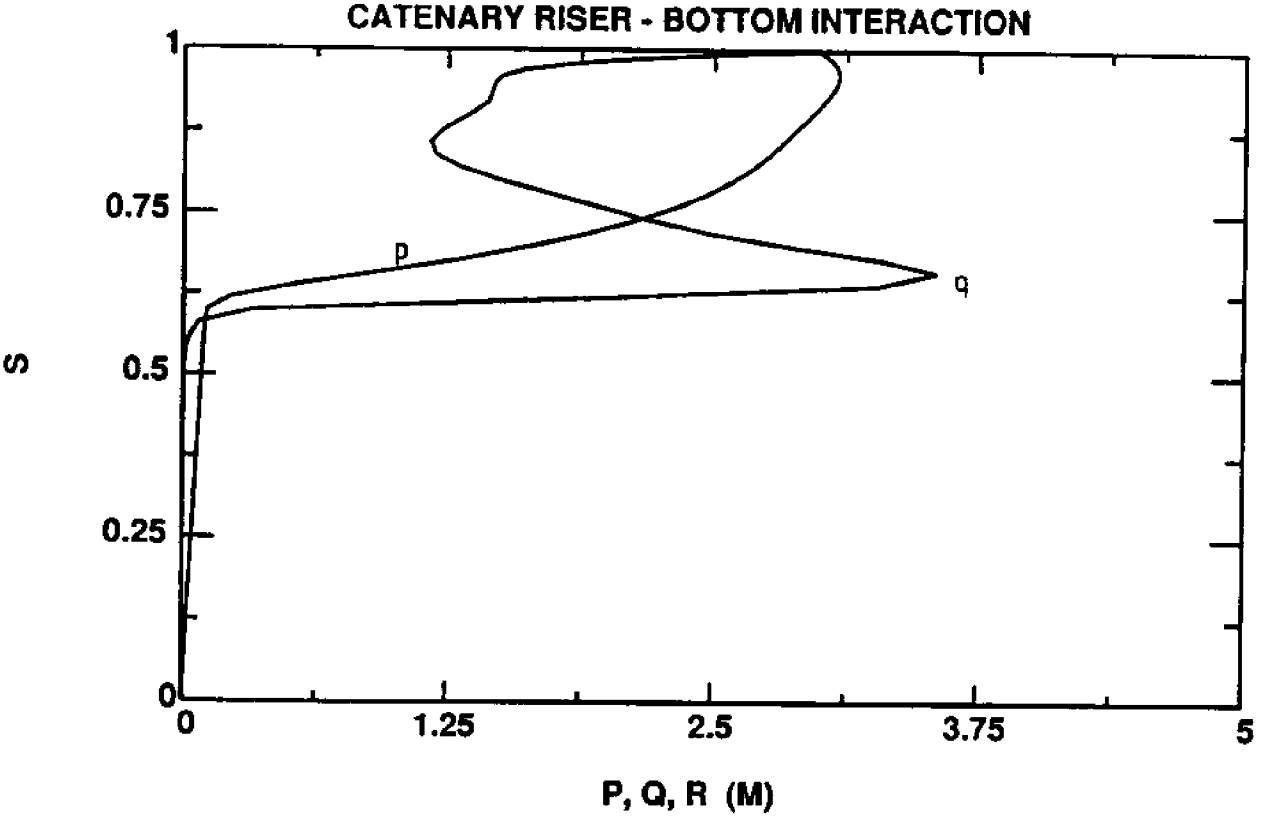

6. CONCLUSIONS AND RECOMMENDATIONS

The research described in this report allows us to analyze global non-linear three-dimensional statics and dynamics of single leg multitube compliant risers in the presence of currents and monochromatic waves and motions and rotations applied at both ends.

The dynamic solutions are based on linearization of the structural part of the equations of motion around a non-linear static configuration and equivalent linearization of non-linear drag and ocean riser bottom interaction forces.

The results of our method have been compared with other idealizations, such as the cable idealization, and other solution techniques such as non-linear time domain methods addressing the full beam problem. Comparisons with appropriate cable idealizations, revealed that, as long as the dynamic tension is small compared to the static tension, the maximum dynamic tension based on a cable idealization is close to the tension predicted by the Euler beam equations. The comparisons with time domain independent non-linear codes for flexible risers using finite element methods confirmed the usefulness of the frequency domain method developed allowing rapid and reliable computations of the response even under extreme excitation. The comparisons were good for the cases studied but are expected to deteriorate when the dynamic tension exceeds the static tension. In such cases the structural linearization ceases to be valid and a non-linear time domain solution is needed.

In the sequel some of the more important observations from our research are summarized.

The results of this work indicate that the effects of dynamic motion on the static forces and solution are relatively small and therefore may be neglected to a first approximation.

The solution method developed based on an adaptive non-uniform grid finite difference technique is successful in efficiently resolving sharp gradients of the solution present either near the supports or at the ends of large buoyancy modules.

Dynamic curvature and tension may be significant in comparison to the static quantities and, therefore, dynamic effects should be considered in preliminary design of compliant risers.

Based on the present research the following recommendations for further work may be made

1. Develop a frequency domain fatigue program for compliant risers in the presence of direct wave and platform motion excitation. The effect of vortex induced oscillations should also be investigated. Such a capability is necessary because of the small oscillatory bending radii and large dynamic tensions possible in compliant risers, especially for deeper waters. Reliable laboratory experiments to determine the fatigue characteristics of flexible riser constructions are needed to make the results of fatigue programs useful to the practicing designer.

2. Extend the present methodology for statics and dynamics to multileg configurations. This can be accomplished efficiently because the present method allows incorporation of the effects of compliance at the ends of a single leg system.

3. Investigate the effects of dynamic tension exceeding the static tension and bottom interaction effects (particularly when impact is possible) using a non-linear time domain solution technique.

4. Compare the results of theoretical analysis with measured data.

7. REFERENCES

1. N. M. Patrikalakis and C. Chryssostomidis, A Mathematical Model for Compliant Risers. Cambridge, Mass.: MIT Sea Grant Report No. 85-17, 1985.

2. N. M. Patrikalakis, 'Three-Dimensional Compliant Riser Analysis', Proceedings of the 5th International Symposium on Offshore Mechanics and Arctic Engineering, Tokyo, Japan, April 1986, V. III, pp. 458-465. NY: ASME, 1986.

3. N. M. Patrikalakis and C. Chryssostomidis, Non-Linear Statics of Non- Rotationally Uniform Rods with Torsion. Cambridge, Mass.: MIT Sea Grant Report No. 85-18, 1985.

4. C. Chryssostomidis and N. M. Patrikalakis, 'Compliant Riser Analysis', Proceedings of the International Symposium on Ocean Space Utilization, Tokyo, Japan, 1985. V.1, pp. 401-410. NY: Springer, 1985.

5. Gursoy, H. N., Non-Linear Statics of Non-Rotationally Uniform Rods with Torsion. M.S. Thesis, Cambridge, Mass.: MIT Department of Ocean Engineering, 1985.

6. N. M. Patrikalakis and C. Chryssostomidis, Linear Dynamics of Compliant Risers. Cambridge, Mass.: MIT Sea Grant Report No. 85-19, 1985.

7. N. M. Patrikalakis and G. A. Kriezis, 'Linear Dynamics of Flexible Risers', Proceedings of the 1st Offshore Mechanics and Arctic Engineering Specialty Symposium on Offshore and Arctic Frontiers, New Orleans, Louisiana, Feb. 1986, pp. 327-336. NY: ASME, 1986.

8. M. S. Triantafyllou, et al., Mooring Dynamics for Offshore Applications, Part I: Theory. Cambridge, Mass.: MIT Sea Grant Report No. 86-1, 1986.

9. S. H. Crandall, et al., Dynamics of Mechanical and Electromechanical Systems. NY: McGraw-Hill, 1968.

10. F. E. Richart, Jr., J. R. Hall, Jr. and R. D. Woods, Vibrations of Soils and Foundations. Englewood Cliffs, N.J.: Prentice Hall, 1970.

11. M. S. Triantafyllou, et al., 'Dynamic Analysis as a Tool for Open-Sea Mooring System Design', SNAME Transactions, Vol. 93, pp. 303-324. NY: SNAME, 1985.

12. N. M. Patrikalakis, Theoretical and Experimental Procedures for the Prediction of the Dynamic Behavior of Marine Risers, Ph.D. Thesis, Cambridge, Mass.: MIT Department of Ocean Engineering, 1983.

13. N. M. Patrikalakis and C. Chryssostomidis, 'Vortex Induced Response of a Flexible Cylinder in a Constant Current'. Journal of Energy Resources Technology, ASME Trans., Vol. 107, pp. 244-249, 1985.

14. N. M. Patrikalakis and C. Chryssostomidis, 'Vortex Induced Response of a Flexible Cylinder in a Sheared Current'. Journal of Energy Resources Technology, ASME Trans., Vol. 108, pp. 59-64, 1986.

15. T. Sarpkaya and M. Isaackson, Mechanics of Wave Forces on Offshore Structures. NY: Van Nostrand, 1981.

16. J. N. Newman, Marine Hydrodynamics. Cambridge, Mass.: M.I.T. Press, 1977.

17. J. R. Paulling, 'Frequency Domain Analysis of OTEC CW Pipe and Platform Dynamics', Proceedings of the 11th Offshore Technology Conference, 1979, V.III, Paper OTC 3543, pp. 1641-1651, Houston: OTC, 1979.

18. L. P. Krolikowski and T. A. Gay, 'An Improved Linearization Technique for Frequency Domain Riser Analysis', Proceeding of the 12th Offshore Technology Conference, 1980, V.II, Paper OTC 3777, pp. 341-353. Houston: OTC, 1980.

19. H. B. Keller, Numerical Methods for Two-Point Boundary Value Problems. Waltham, Mass.: Blaisdell, 1968.

20. J. H. Ferziger, Numerical Methods for Engineering Application. NY: J. Wiley and Sons, 1981.

21. V. Pereyra, 'PASVA3: An Adaptive Finite Difference Fortran Program for First Order Non-linear Ordinary Boundary Value Problems'. Codes for Boundary Value Problems in Ordinary Differential Equations. Edited by B. Child, et al. Lecture Notes in Computer Science, Vol. 76, pp. 67-88. NY: Springer, 1979.

22. NAG. Numerical Algorithms Group FORTRAN Library. Oxford, England: NAG, 1985.

23. McNamara J.F., O'Brien P.J., Gilroy S.G., 'Non-Linear Analysis of Flexible Risers Using Hybrid Finite Elements', Proceedings of the 5th International Symposium on Offshore Mechanics and Arctic Engineering, Tokyo, Japan, April 1986, V. III, pp.371-377, NY:ASME, 1986.

24. Mathisen K.M., Bergan P.G., 'Non-Linear Static Analysis of Flexible Risers', Proceedings of the 5th International Symposium on Offshore Mechanics and Arctic Engineering, Tokyo, Japan, April 1986, V. III, pp.337-345, NY:ASME, 1986.

25. Hansen H.T., Bergan P.G., 'Non-Linear Dynamic Analysis of Flexible Risers During Environmental Loading', Proceedings of the 5th International Symposium on Offshore Mechanics and Arctic Engineering, Tokyo, Japan, April 1986, V. III, pp.346-353, NY:ASME, 1986.

26. de Oliveira J.G., Morton A.W., "Floating Production Systems With Vertical Flexible Risers", Proceedings of the Indonesian Petroleum Association 13th Annual Convention, 1984, Djakarta, Indonesia: IPA, 1984.

27. Powell M.J.D., "A Hybrid Method for Nonlinear Algebraic Equations", Numerical Methods for Nonlinear Algebraic Equations, Edited by P.Rabinowitz, pp. 87-161. NY: Gordon and Breach, 1970.

I. Approximate Analytical Static Solution For Catenary Risers With Ocean Bottom Interaction

In this section, an approximate analytical solution of the two-dimensional static problem corresponding to a catenary riser in calm water, experiencing riser-ocean bottom interaction is presented. This analytical solution is similar to the catenary riser approximate solution presented in reference [5].

For simplicity we use the mean effective weight and assume that $\gamma=0$ in the static equations, because the extensional rigidity of the riser is very large. With these assumptions the resulting governing static non-dimensional equations without bottom interaction are:

$$T_{os} = \sin\phi_o + Q_o^{\xi}\Omega_o^{\eta}$$

$$Q_{os}^{\xi} = \cos\phi_o - T_o\Omega_o^{\eta}$$

$$\Omega_{os}^{\eta} = -\beta^{\eta}[Q_o^{\xi} + (\frac{1}{\beta^{\eta}})_s\ \Omega_o^{\eta}]$$

$$\phi_{os} = \Omega_o^{\eta}$$

$$X_{os} = \cos\phi_o$$

$$y_{os} = \sin\phi_o$$

A uniform leading order approximation for $\phi_o(s)$ can be found by simple boundary layer theory [5]

$$\phi_o(s) = \phi_{oo}(s) + \phi_{o1}(s) + \phi_{o2}(s)$$

where $\phi_{oo}(s)$ denotes the cable solution and $\phi_{o1}(s)$ and $\phi_{o2}(s)$ are the boundary layer terms possibly important at the lower and upper end of the riser, respectively. Using the catenary cable solution the following non-dimensional results are obtained.

$$T_{oo}(s) = \{H^2+[V-(1-s)]^2\}^{1/2}$$

$$\phi_{oo}(s) = \sin^{-1}\ \{\frac{[V-(1-s)]}{[H^2+(V-(1-s))^2]^{1/2}}\}$$

$$x_{oo}(s) = H\{\sinh^{-1}[\frac{(V-(1-s))}{H}] - \sinh^{-1}[\frac{(V-1)}{H}]\}$$

$$y_{oo}(s) = H\{[1+[\frac{(V-(1-s))}{H}]^2]^{1/2} - [1+[\frac{(V-1)}{H}]^2]^{1/2}\}$$

where V and H are the non-dimensional top end reaction forces in vertical and horizontal directions respectively.

Imposing the boundary conditions on the top motions of the riser we obtain:

$$x_T = H\{\sinh^{-1}(\frac{V}{H}) - \sinh^{-1}[\frac{V-1}{H}]\}$$

$$y_T = H\{[1+(\frac{V}{H})^2]^{1/2} - [1+[\frac{(V-1)}{H}]^2]^{1/2}\}$$

Figure I-1: Catenary riser with bottom interaction configuration

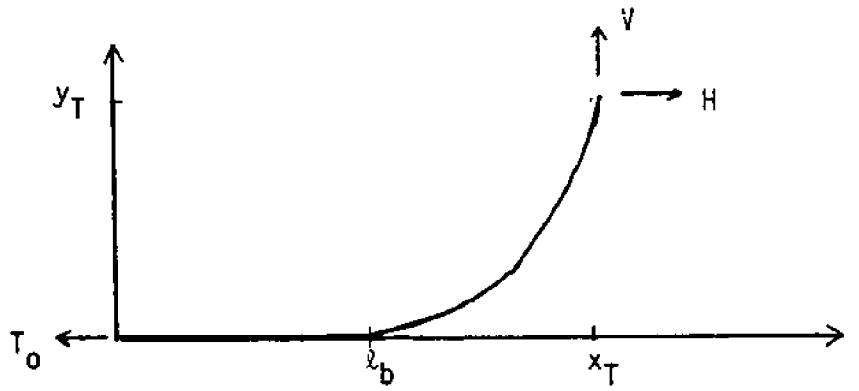

Up to this point the approximate solution is identical to the simple catenary riser case as was also presented in [5]. The above two equations can be solved to determine V and H. Now, if y=0 corresponds to the ocean bottom which is the usual case for catenary, lazy wave and lazy S configurations and if V < 1 from the catenary cable solution we have

$$y_{os} = \sin\phi_o = \frac{s + V-1}{H\sqrt{1+(\frac{s+V-1}{H})^2}} \qquad y_{os}(0) = \sin\phi_o(0) = \frac{\frac{V-1}{H}}{\sqrt{1+(\frac{V-1}{H})^2}} < 0$$

Thus in this case $y_s(0)<0$ and there is riser-ocean bottom interaction and the above cable solution needs to be modified. Figure I.1 presents a two-dimensional riser configuration with bottom interaction where the important parameters are identified. In this case from the vertical force equilibrium,

$$V = 1-\ell_b \quad \Rightarrow \quad \ell_b = 1-V$$

where l_b corresponds to the non-dimensional length of the static bottom interaction region. For the catenary cable solution in this case we need to distinguish two regions:

Region A

$$\text{For } 0 \le s \le \ell_b = 1 \qquad \begin{cases} \phi_{oo}(s) = \frac{\pi}{2}\,[1-\mathrm{sgn}(x_T)] \\ T_{oo}(s) = |H| \\ x_{oo}(s) = \mathrm{sgn}(x_T)\cdot s \\ y_{oo}(s) = -\frac{w(s)}{K_y} \end{cases}$$

Region B

$$\text{For } \ell_b \le s \le 1 \Rightarrow \qquad \begin{cases} \phi_{oo}(s) = \tan^{-1}\frac{s+V-1}{H} + \frac{\pi}{2}\,[1-\mathrm{sgn}(x_T)] \\ T_{oo}(s) = \sqrt{H^2+(s+V-1)^2} \\ x_{oo}(s) = \mathrm{sgn}(x_T)(1-V) + |H|\,\sinh^{-1}\left(\frac{s+V-1}{H}\right) \\ y_{oo}(s) = \sqrt{H^2+(s+V-1)^2} - |H| \end{cases}$$

where K_y is the bottom interaction spring coefficient and w is the riser effective weight per unit length. Applying the boundary conditions at the top of the riser we obtain the following equations to solve for V and H.

$$x_T = \mathrm{sgn}(x_T)(1-V) + |H|\,\ln\left\{\frac{V}{H} + \sqrt{1+\left(\frac{V}{H}\right)^2}\right\}$$

$$y_T = \sqrt{H^2+V^2} - |H|$$

These equations are solved by Powell's hybrid method [22], [27]. Once V and H are determined the cable solution can be determined. Then the leading order aproximations for $T_o(s)$, $Q_o^{\xi}(s)$, $\Omega_o^{\eta}(s)$, $x_o(s)$ and $y_o(s)$ can be also determined by taking account of the boundary layer at the top of the riser. There is no significant boundary layer in the lower end of the riser, but there may be an internal layer in the interface between the bottom interaction and no bottom interaction region which is neglected in this initial approximation. The boundary layer correction for $\phi_o(s)$ at the top of the riser is

$$\phi_{o2}(s) = [\phi_T - \phi_o(1)] \exp[-(1-s)\sqrt{\beta^\eta(1)\ T_{oo}(1)}]$$

$\Omega_o(s)$ is calculated from $\Omega_o = \phi_{os}$ and Q_o^ξ is calculated from $Q_o^\xi = -(1/\beta^\eta)\Omega_{os}^\eta$.